Title
Chemical tools to design and study microbial communities

Author
Smith, Matthew Jordan

Publication Date
2018

Peer reviewed|Thesis/dissertation

Chemical tools to design and study microbial communities

by

Matthew Jordan Smith

A dissertation submitted in partial satisfaction of the

requirements for the degree of

Doctor of Philosophy

in

Chemistry

in the

Graduate Division

of the

University of California, Berkeley

Committee in charge:

Professor Matthew B. Francis, Chair
Professor Evan W. Miller
Professor Michi E. Taga

Spring 2018

Chemical tools to design and study microbial communities

By: Matthew Jordan Smith

Abstract

Chemical tools to design and study microbial communities

by

Matthew Jordan Smith

Doctor of Philosophy in Chemistry
University of California, Berkeley
Professor Matthew B. Francis, Chair

Techniques for the design and study of microbial cocultures may enable the development of bioproductions from more sustainable feedstocks. Furthermore, designed microbial communities could enable insights into a variety of fields including environmental bioremediation, microbial bioproductions or the microbiome. Each chapter of this dissertation describes the development of microbial cocultures or chemical tools to study microbial cocultures. In Chapter One, the development of a microbial coculture where one partner ensnares the other in a secreted biopolymer is described and characterized. In Chapter Two, a microbial coculture that produces the bioplastic polyhydroxybutyrate with no fixed carbon or nitrogen inputs is described. A strategy to improve the performance of this coculture using a spatially-constrained hydrogel is also discussed. Chapter Three delves into various strategies that have been developed to pattern microbes via DNA-based hybridization. This includes the description of a new oxidative coupling strategy that has been developed to pattern DNA on surfaces and its application towards the study of specific microbes and microbial communities.

Table of Contents

Acknowledgments

I would like to thank the following people who have guided, accompanied and supported me through my time as a graduate student at UCB. I am very appreciative of:

Matt Francis, I have enjoyed working in your lab immensely. You have been a supportive advisor and I have learned a great deal working in your lab.

Current and former Francis lab members, I would not have been able to complete my dissertation without your support. Many of the people I have met in this lab have become not just respected colleagues, but, hopefully, lifelong friends. I am excited to follow the progress of the current group of Francis lab members.

Friends and family, I have been lucky to be surrounded by a group of people who encourage me to pursue my passions. I am particularly grateful for the support of my parents and sister. I cannot thank them enough.

Chapter 1

Cooperative, multispecies cellular aggregates between a cyanobacterium and a diazotroph

Abstract

Mutualistic interactions between bacteria often depend critically on the degree of physical interaction between microbial partners, and this dependence complicates the design of cocultures for use in bioproductions. Herein, we report a new microbial mutualism between *Azotobacter vinelandii* and *Synechocystis PCC6803* that forms free-floating, aggregated, multispecies communities in unshaken cultures. These communities form in minimal media and are based on an alginate-based extracellular gel produced by *Azotobacter vinelandii* that ensnares *Synechocystis PCC6803*. In the presence of light and *A. vinelandii*, *Synechocystis* grows to higher optical densities and produces more chlorophyll than the monoculture, demonstrating the ability of this coculture to use nutrients more effectively than the *Synechocystis* monoculture. The reported coculture forms close cellular contacts in solution and serves as a proof-of-principle for the design of spatially-localized microbial communities. This coculture can also be extended to other cyanobacteria.

Key words: coculture, cyanobacteria, diazotroph

1.1. Introduction

1.1.1. Importance of microbial interactions

Multispecies microbial interactions have important implications for the evolution of life on earth[1,2] and the understanding of bacterial behavior in natural ecosystems.[3–7] In addition, they are underutilized in industrial bioproductions, where cocultures could allow the more effective utilization of nutrients.[8,9] A variety of strategies for studying and evolving multicellular communities has resulted from recent, renewed interest in microbial multicellularity.[10,11] This interest has led to the study of multiple phenotypes within a single microbial species[12,13] or between multiple microbial species in structured environments.[14]

Microbial biofilms can exist as surface-attached or aggregated communities.[15] An example of an aggregated community is *Pseudomonas fluorescens*, which produces an adhesive cellulose-like polymer that allows the bacteria greater access to oxygen at the air-water interface.[12] Amyloid fibers have been implicated in the formation of *Bacillus subtilis*, *Staphylococcus aureus* and *Pseudomonas aeruginosa* surface-attached biofilms.[16] A variety of different fimbria or pili have also been implicated in the assembly of surface-attached biofilms.[17,18] In *Pseudomonas aeruginosa* biofilms the role of alginate has been extensively characterized, and alginate lyase has been found to increase the effectiveness of antibiotic treatments of *P. aeruginosa* infections.[19,20]

1.1.2. Strategies to study physical contact in microbial communities

We became interested in using chemical biology tools[21] to design multispecies biofilms for the investigation of chemical bioproduction and the role that physical contact plays. Experiments that can elucidate the role of physical contact in cocultures are not straightforward to design, but there has been some recent progress. For example, Hom and Murray report a coculture between *S. cerevisiae* and *C. reinhardtii* that grows best when not shaken, presumably due to increased cell-cell contacts.[22] Similarly, Christensen et al. report a microbial coculture that grows to drastically different cell ratios when allowed to form biofilms as opposed to in suspended culture, likely due to the ability of the biofilm to form close physical contacts that enable more efficient metabolite sharing.[23] In contrast, Kim et. al. report a microbial community

including *A. vinelandii* that could not survive in the same "well" as its coculture partners or in the absence of its coculture partners; instead, the bacteria could only survive when grown in spatially separated "microwells" in which water-soluble nutrient and signal sharing was still possible.[24]

There are a variety of bioengineering strategies for creating spatially separated or mixed communities of cells. A common and relatively straightforward strategy for mammalian cells is to encapsulate them in Ca^{2+}-alginate gels: a strategy that maintains cell function.[25,26] This technique has also been used with an algae, *Chlamydomonas reinhardtii*, that exhibits increased levels of nitrite uptake and ammonium photoproduction when encapsulated in an alginate gel.[27]

1.1.3. Summary of reported work

Herein, we tested the hypothesis that growing *A. vinelandii* in minimal media would lead to the production of an alginate polymer that could then ensnare a mutualism partner, leading to a more effective coculture and the creation of a multispecies biofilm for the production of biopolymers and ammonia. *Azotobacter vinelandii* has a high metabolism,[28] fixes nitrogen gas[29] and produces the polymers alginate and PHB.[30,31] Alginate production in *A. vinelandii* has been found to aid in the transition to the cyst state.[32–34] *Synechocystis PCC6803* fixes carbon dioxide, does not fix nitrogen, can grow both autotrophically and heterotrophically,[35,36] and has been developed for the production of a variety of chemicals.[37] In this report, we detail a previously unreported microbial mutualism between these two organisms, where *A. vinelandii* produces an alginate-based gel in minimal media that then ensnares *Synechocystis* if grown without shaking. This coculture grows best if not agitated and generates greater biomass than the corresponding monocultures.

1.2. Materials and Methods

Materials. Alginate lyase was obtained from Sigma Aldrich (Product number: A1603). Alpha-chymotrypsin and alpha-chymotrypsin from bovine pancreas type II and bacterial type VIII protease from *Bacillus licheniformis* were also obtained from Sigma Aldrich.

Cell culture. Azotobacter vinelandii was cultured in modified Burke's medium[38] at room temperature at 22 °C with continual shaking at 150 rpm and passaged every 2 d with 1:100 fold dilution. *Synechocystis* PCC6803, *Anabaena cylindrica* (ATCC 27893) and *Synechococcus elongatus* were cultured in BG-11 medium[39] with continual shaking at 150 rpm at 22 °C with 8 W/m^2 irradiance from a 3000 K fluorescent bulb and split once a week with a 1:2 fold dilution. The *Azotobacter vinelandii* and cyanobacteria cocultures were cultured in SAV media with or, for *A. cylindrica*, without glutamate at 22 °C under constant 8 W/m^2 irradiance from a 3000 K fluorescent bulb. For the following SAV media preparation instructions: solution 1 contains 0.2 g/L KH_2PO_4 and 0.8 g/L K_2HPO_4; solution 2 contains 0.09 g/L $CaCl_2*2H_2O$, 0.2 g/L $MgSO_4*7H_2O$ and 0.005 g/L $FeSO_4*7H_2O$; 1000X Burke's micronutrient solution contains 2.8 g/L H_3BO_3, 1.592 g/L $MnSO_4*H_2O$, 0.752 g/L $Na_2MoO_4*2H_2O$, 0.24 g/L $ZnSO_4*7H_2O$, 0.04 g/L of $CuSO_4*5H_2O$ and $NiCl*6H_2O$ and 0.056 g/L $CoSO_4*7H_2O$; 100X BG-11 micronutrient solution contains 0.3 g/L H_3BO_3, 0.2 g/L $MnCl_2*4H_2O$, 0.048 g/L $Na_2MoO_4*2H_2O$, 0.023 g/L $ZnSO_4*7H_2O$, 0.01 g/L $CuSO_4*5H_2O$, 0.028 g/L $NaVO_3$ and 0.011 g/L of $CoSO_4*7H_2O$. SAV media was prepared as follows: for a 1 L solution, start with 700 mL of DI water. From BG-11 media add 5 mL of 15 g/L $MgSO_4$ for a 304 µM final concentration, 4 mL of 9 g/L $CaCl_2$ stock for a 245 µM final concentration, 4 mL of 1.5 g/L citric acid stock for a 31 µM final concentration, 5 mL of 0.2 g/L EDTA stock for a 3 µM final concentration, 4 mL of a 5 g/L Na_2CO_3 stock for a 189 µM final concentration and 10 mL of a 100X BG-11 micronutrients

stock. From Burke's media add 200 mL of 5X solution 2 for 612 µM $CaCl_2$, 811 µM $MgSO_4$, 18 µM $FeSO_4$ in the final solution, 50 mL of 20X solution 1 for a 6 mM KPO_4 final concentration and 1 mL of 1000X Burke's micronutrients solution. Then add 0.338 g of monosodium glutamate for a final concentration of 2 mM. Fill to 1 L. Autoclave the solution and let cool. Then, add 12 mL of sterile 0.5 mg/mL iron (II) citrate to the SAV media. The final concentration of $MgSO_4$ is 1.115 mM, $CaCl_2$ is 857 µM and Fe^{2+} is 42 µM.

A. vinelandii and *Synechocystis* were grown to mid log phase growth over 2 and 4 d, respectively, and 150 uL of washed *A. vinelandii* and 300 uL of washed *Synechocystis* were added to 20 mL of SAV media and grown at 22 °C with 8 W/m^2 irradiance from a 3000 K fluorescent bulb with shaking at 150 rpm and without shaking (Figure 1.2). The *A. vinelandii* and *Synechocystis* cells were washed thoroughly with SAV media to remove any excess sucrose or nitrate. It was found that variations in the relative amounts of cells used to start the coculture had little effect on coculture growth. Optical densities of non-shaking cultures were determined after vortexing the solutions so as to homogenize them. Each optical density reading was its own experiment. The *A. cylindrica* and *S. elongatus* cocultures were prepared in similar fashion.

Dialysis experiments. Dialysis experiments were performed with dialysis bags from Sigma-Aldrich (MWCO = 12,000 Da, Product # D6066-25EA). A 10 mL portion of sterile PBS was added to an Erlenmeyer flask. Then, a dialysis bag was filled with either ten milliliters of *S. elongatus* or *A. vinelandii* in SAV media. Then an additional dialysis bag was filled with either the coculture partner or 10 mL of sterile SAV media. PBS buffer was used to keep the optical densities within a suitable range for the UV/Vis spectrometer. Dialysis bags were sterilized by soaking in 70% ethanol for 2 h and then washed with sterile water.

Chlorophyll analysis. Chlorophyll analysis was performed by first extracting the chlorophyll into an 85% methanol and 1 mM sodium dithionite solution. Then, the concentration was determined based on a previously published method utilizing UV/Vis spectroscopy (Porra, 2012). Chlorophyll measurements were taken with 10 mL of culture media after 10 days in solution.

Fluorescent Microscopy. Microscopy experiments were performed on a Zeiss LSM 710 AxioObserver.

Scanning Electron Microscopy. SEM images were taken at the electron microscope laboratory at UC Berkeley following the standard protocol for cell staining with osmium tetroxide and dehydrating with ethanol. The SEM images were taken on a Hitachi S-5000 SEM.

Optical density (OD) measurements. All optical density time points are individual experiments. To ensure aggregation did not affect the optical density measurements, each sample for OD analysis was vortexed to break up aggregates before OD analysis at 750 nm. Each time point measurement was an individual experiment. Error bars (+/- Standard deviation) were reported with 95% confidence intervals.

Ammonia detection measurements. All ammonia time points are individual experiments. Samples for ammonia analysis were filtered through a DURAPORE – PVDF 0.22 µm filter prior to analysis to remove whole cells whose lipid membranes could compromise the integrity of the ion selective electrode (ISE) membrane. One culture flask/tube was used for each time point measurement. An ammonia ion selective electrode (ISE, Thermo Scientific) was used to detect ammonia concentrations. Prior to each ammonia sample analysis, an ammonia concentration curve was created with 0.01 ppm to 12.0 ppm NH_3 standards in water. The calibration curves reproducibly had an R^2 value above 0.986. The standard and sample volumes used for each analysis was 10 mL. All standards and samples were thermally equilibrated using a room

temperature water bath. The ionic strength of each sample was adjusted through the addition of 200 µL of pH adjusting Ionic Strength Adjustor solution (from Thermo Scientific).

Flow cytometry. All flow cytometry experiments were performed on a BD Bioscience LSR Fortessa X20. The percent of autofluorescent *Synechocystis* cells in the coculture was determined by plotting the Texas Red channel with the forward scatter channel and determining the percent of red fluorescent cells in the total population. A carboxyfluorescein diacetate dye was used to distinguish between *A. vinelandii* live cells and cellular debris in order to properly voltage gate the samples. (+/- SD, N=2)

Light Microscopy. Microscopy experiments were performed on a Zeiss LSM 710 AxioObserver. Instrument settings (gain, laser intensity, pinhole size) were kept the same for all images. For aggregation studies the pinhole was opened all the way to minimize any field-of-view bias.

Scanning Electron Microscopy. Cocultures were fixed with 2.5% glutaraldehyde in 0.1 M cacodylate buffer pH 7.2. The samples were then dehydrated in ethanol, starting with 30% ethanol and slowly increasing to 100 % ethanol. The samples were then critical point dried at the UC Berkeley Electron Microscope laboratory. Samples were then mounted onto stainless steel stubs, covered with carbon dot paper and then coated using a sputter coater before imaging on a Hitachi S-5000 Scanning Electron Microscope.

1.3. Results and Discussion

1.3.1. *A. vinelandii* entraps cyanobacteria in a free-floating biofilm

Initial experiments confirmed that *A. vinelandii* forms a gel-like free-floating biofilm in minimal media.[33] When placed in minimal SAV (*Synechocystis*/*A. vinelandii*) media and grown without shaking, *A. vinelandii* formed free-floating aggregates in the hundreds of micrometers to millimeter size range (Figure 1.1B) that were absent when *A. vinelandii* was grown in modified Burke's media (Figure 1.1A). *Synechocystis* grown in SAV media without shaking did not form free floating celllular aggregates, resulting in minimal aggregates no larger than 100 µm in diameter (Figure 1.1C). SAV media contains 2 mM glutamate as its only nitrogen and carbon source.

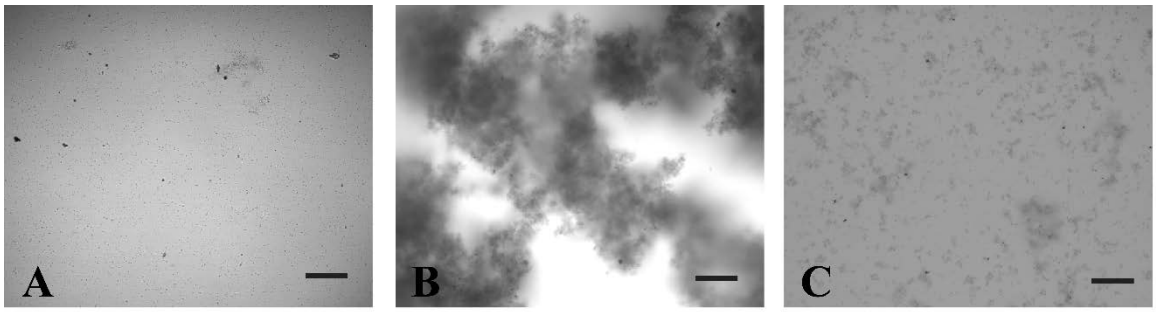

Figure 1.1. *Azotobacter vinelandii* aggregates in minimal media. (A) *A. vinelandii* grown for 2 d without shaking in Burke's growth media. (B) *A. vinelandii* grown for 2 d without shaking in SAV media (minimal media). (C) *Synechocystis* PCC6803 in SAV media grown without shaking. Scale bars are 100 µm. 2

The next set of experiments demonstrated that *A. vinelandii* entraps *Synechocystis* and forms a persistent multispecies free-floating biofilm. When a coculture of these organisms was grown without shaking in SAV media, white aggregates formed between 1 and 2 days. These aggregates slowly turned green between 3 and 4 days (Figure 1.2), suggesting the increasing

presence of *Synechocystis*. When grown with shaking, free-floating aggregates did not form (Figure 1.2).

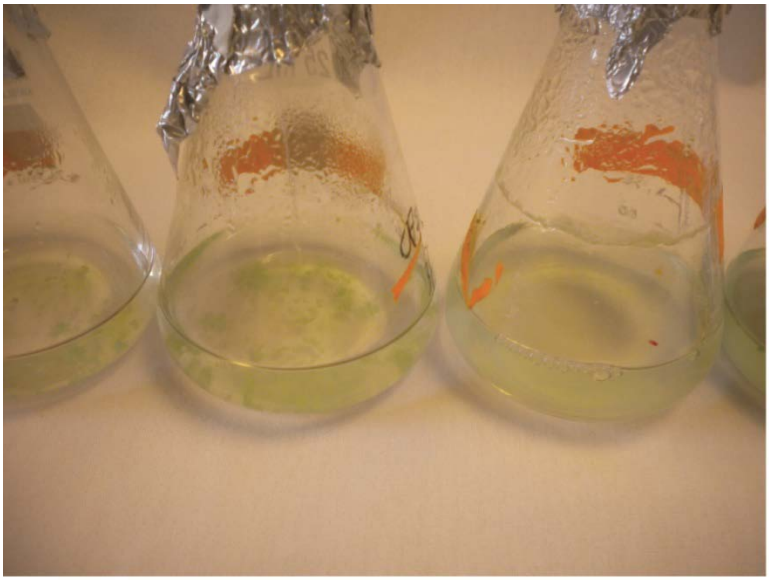

Figure 1.2. Unshaken flask contains free-floating bacterial aggregates. Shown above is an unshaken (leftmost flask) and shaken (rightmost flask) SAV coculture after 9 d.

Fluorescence microscopy confirmed that the red autofluorescent *Synechocystis* cells were trapped throughout the aggregates (Figure 1.3A-D). As further verification, *A. vinelandii* was incubated with carboxyfluorescein diacetate (CFDA) before starting the coculture. After 3 days, imaging of the cell filaments with fluorescence microscopy confirmed the presence of both *A. vinelandii* and *Synechocystis* in the same cellular aggregates (Figure 1.3E). To confirm that the cellular aggregates contained viable *A. vinelandii* cells, a 10 d coculture of the unlabeled cellular aggregates was incubated with the viability dye CFDA (Figure 1.3F). The resulting green-fluorescent cellular aggregates indicated that the cells in these aggregates possessed active esterase activity. The free-floating aggregates persisted in solution for over two weeks (Figure 1.3A-D).

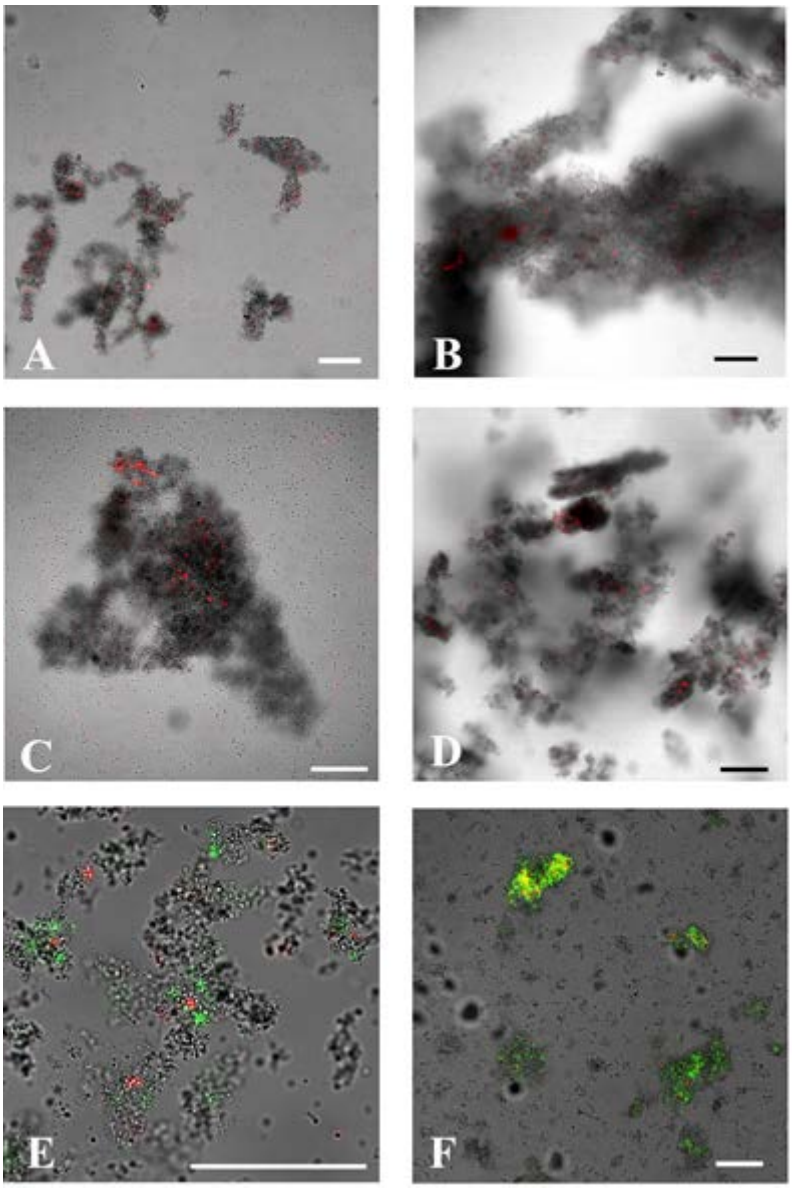

Figure 1.3. A designed, multispecies biofilm. *Azotobacter vinelandii* and *Synechocystis* PCC6803, which autofluoresces red, form multispecies aggregates that persist for over two weeks in unshaken cultures. (A) 5 d, (B) 7 d, (C) 11 d, (D) 15 d coculture timepoints depicting multispecies aggregates were imaged. Each timepoint was taken from a separate biological replicate. The presence of *Synechocystis* clusters in the cellular aggregates suggests that *Synechocystis* becomes entrapped in the cellular aggregates and then proceeds to divide within them. Shown in (E) is a coculture grown for 3 d where the *A. vinelandii* was incubated with the cell tracker dye CFDA before adding the *A. vinelandii* to the coculture. Shown in (F) is a 10 d coculture that was incubated with 200 μM of CFDA, a viability dye, for 5 min, washed, and then imaged. All scale bars are 100 μm.

This coculture strategy can be applied to other types of cyanobacteria. Both *Anabaena cylindrica* and *Synechococcus elongatus* form biofilms with *A. vinelandii* in SAV media (Figure 1.4). This suggests, as expected, that the multispecies cellular aggregation detailed herein is

somewhat general. *A. cylindrica* grows in long filaments containing red autofluorescent cylindrical cells that fix carbon dioxide and non-autofluorescent spherical heterocysts that fix nitrogen.[13] Both of these cell types can be observed in the low-center inset of the *A. cylindrica* coculture image in Figure 1.4.

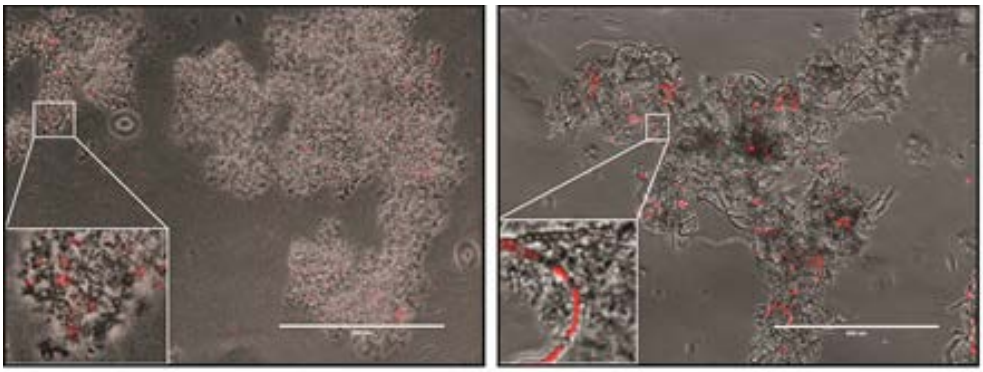

Figure 1.4. SAV coculture forms biofilm with a variety of cyanobacteria. On the left is a 6 d coculture containing both *A. vinelandii* and the red fluorescent *Synechococcus elongatus*. On the right is a 6 d coculture containing both *A. vinelandii* and *Anaebaena cylindrica* (the chain-like red flourescent cells) grown in SAV media without any fixed carbon or nitrogen. The scale bar is 400 μm.

1.3.2. Biofilm composed of alginate produced as a starvation response

Common strategies to dissociate biofilms failed to disrupt the *A. vinelandii*/*Synechocystis* aggregates. Several general strategies for the disruption of biofilms have been reported in the literature. Particular interest was given to strategies that were effective at disrupting *Pseudomonas aeruginosa*[16,17,40] due to its relatively close relationship to *A. vinelandii*.[41] The addition of iron salts,[40] D-amino acids,[16] and alpha-methyl D-mannoside[17] failed to disrupt the SAV biofilm (Figure 1.5). Similarly, the addition of a variety of proteases to degrade the biofilm, a strategy that has been used to inhibit multispecies biofilms,[42,43] did not degrade the *Synechocystis*/*A. vinelandii* aggregates (Figure 1.6B). After treatment with proteases the aggregates not only remained intact, but also still contained *Synechocystis* (Figure 1.7).

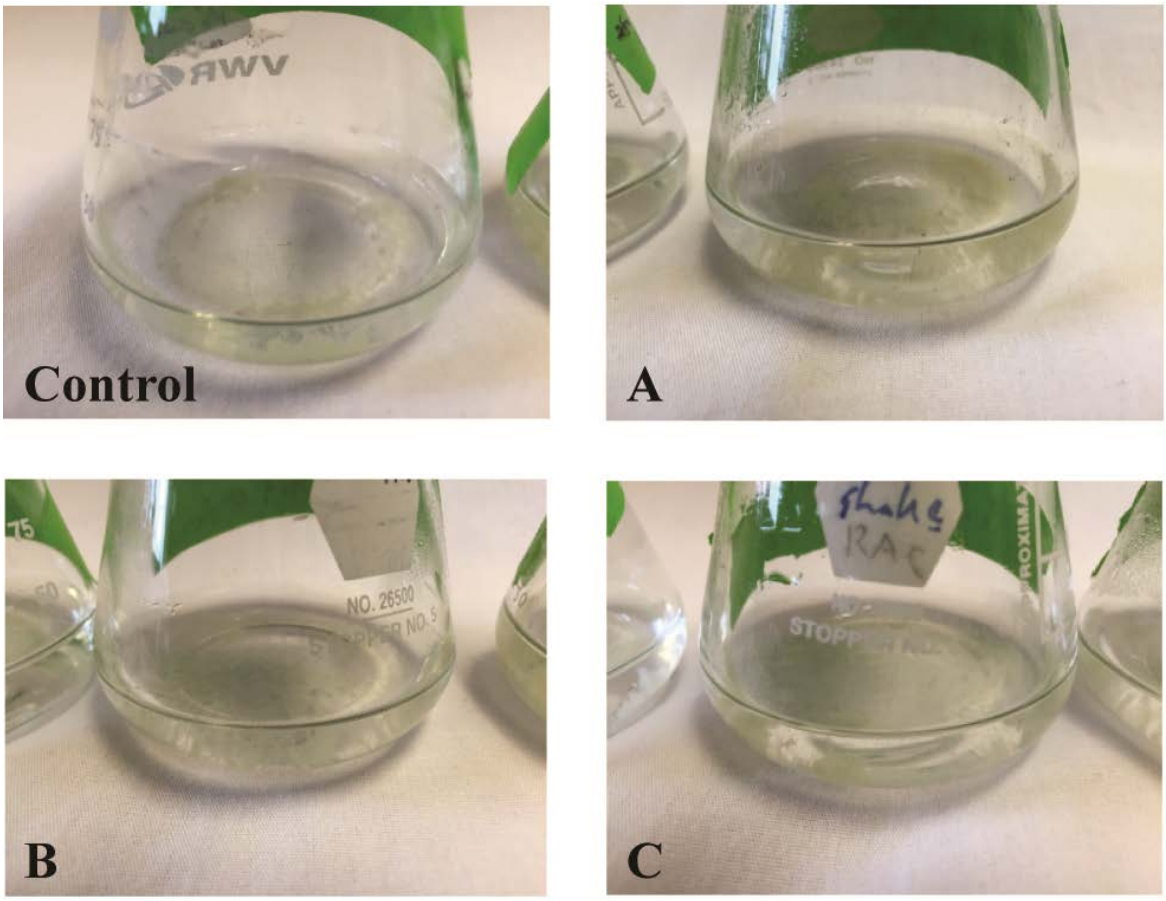

Figure 1.5. Failed biofilm disruption strategies. Previously reported strategies to disrupt bacterial communities had little effect on *Azotobacter2-Synechocystis* aggregates in SAV after 3 d. The control depicts the free-floating multispecies aggregates after 3 d of growth shown in (A) are the SAV aggregates grown in SAV media plus 500 μM iron (II) sulfate. Shown in (B) are the SAV aggregates grown in SAV media plus 50 nM D-Tyr, D-Met and D-Leu. Shown in (C) are the SAV aggregates grown in SAV media plus 50 nM alpha-methyl D-mannoside. Strategies A-C do not result in a visible decrease in bacterial aggregation.

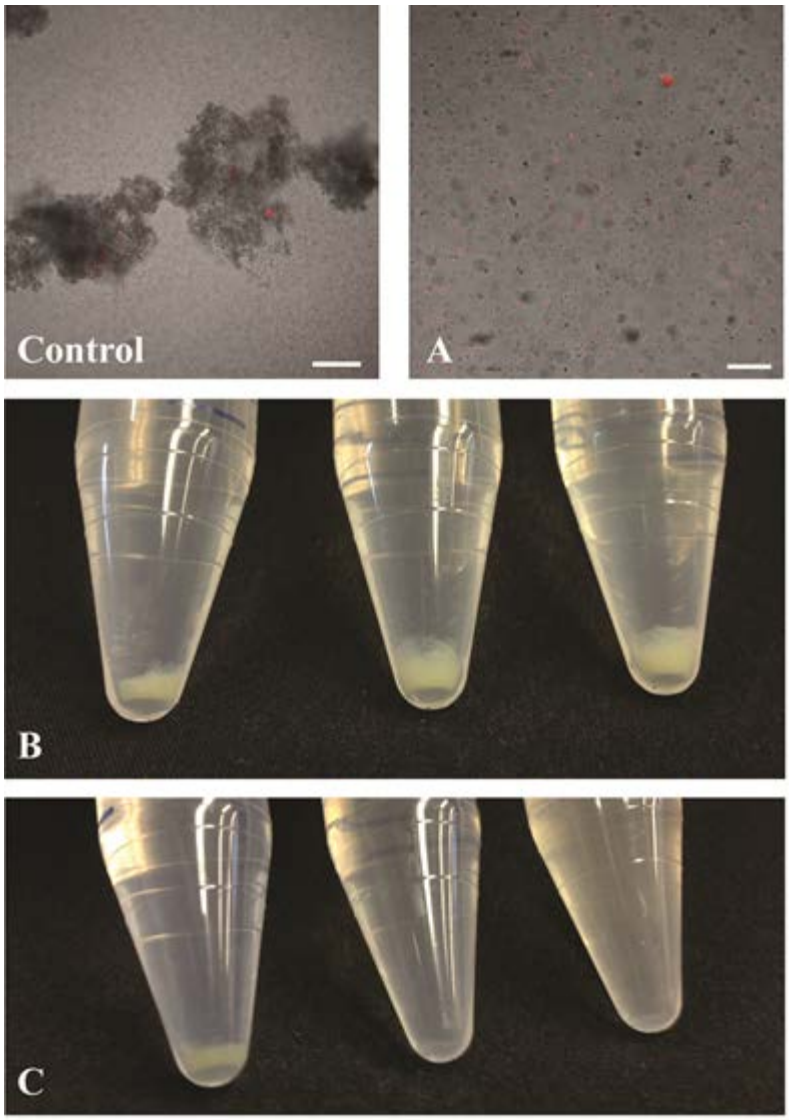

Figure 1.6. The biofilm is held together by alginate. Shown in (Control) and (A) is a 5 d SAV coculture grown without shaking with (A) and without (Control) 1 unit/mL of alginate lyase added every 2 d. The scale bars are 100 micrometers in length. (B and C) The presence/absence of cellular aggregates in Falcon tubes that have been incubated at 37 °C for 30 min at (B) pH=7.5 or (C) pH=6.4 after being grown for 7 d in SAV media that was then centrifuged at 100 x g for 10 s. The leftmost Falcon tube in (B) and (C) contains visible cellular aggregates and was incubated without added enzyme. The middle Falcon tube was incubated in (B) with 10 units/mL type VIII bacterial protease and in (C) with 8 units/mL alginate lyase. The rightmost Falcon tube was incubated in (B) with 5 units/mL of both ά-chymotrypsin and γ-chymotrypsin and in (C) with 4 units/mL alginate lyase. Only alginate lyase breaks apart the cellular aggregates. Scale bars are 100 μm.

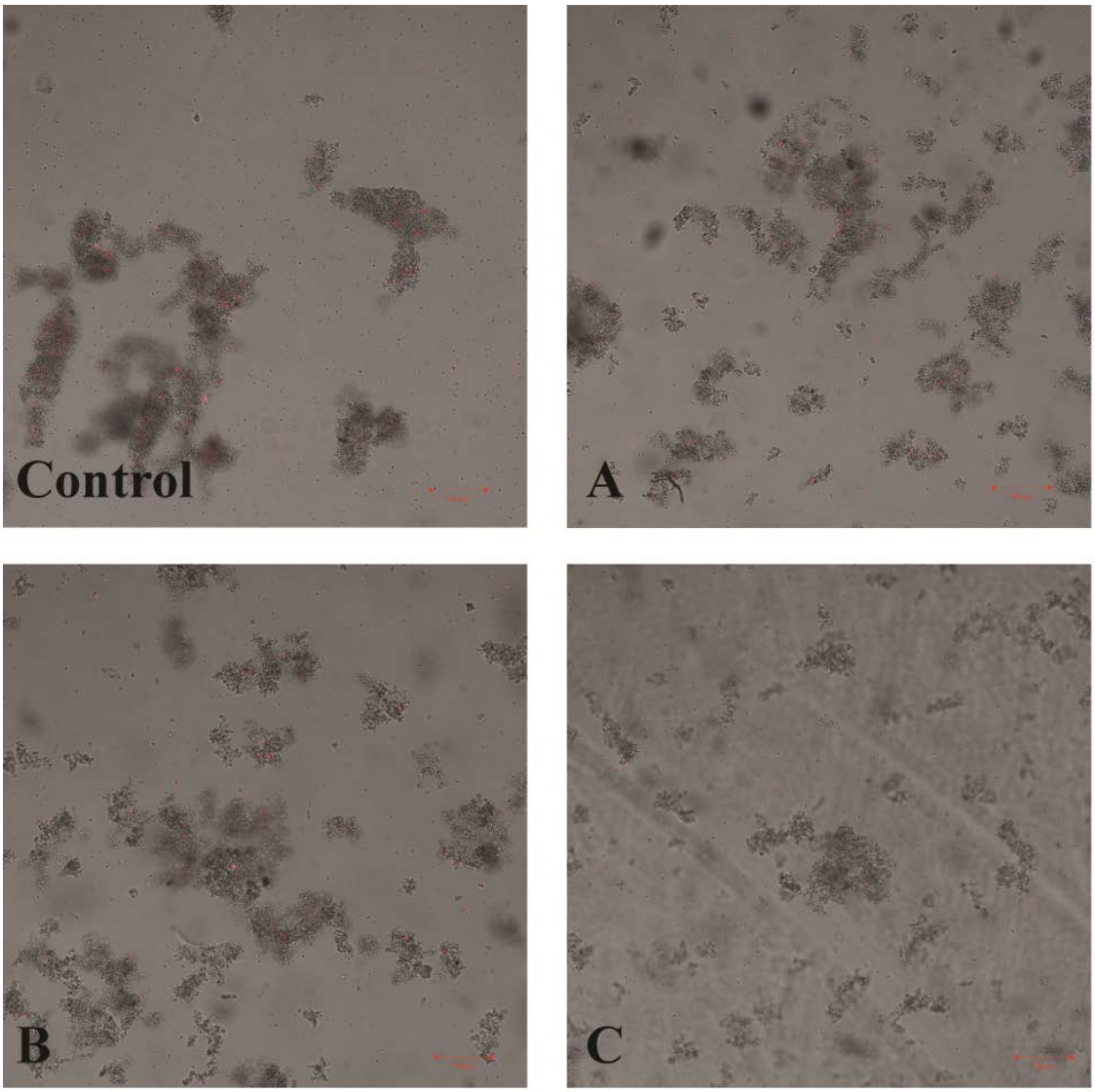

Figure 1.7. Proteases do not break up cellular aggregates. All samples were grown for 4 d in SAV media and were incubated at 37 °C for 30 min at pH=7.5. The control depicts the coculture incubated without any added enzyme. The coculture was incubated with (A) 10 units/mL alpha-chymotrypsin, (B) 10 units/mL gamma-chymotrypsin and (C) 10 units/mL type VIII bacterial protease. The above protease digestions result in cellular aggregates that approach/exceed 100 μm in diameter. The scale bars are all 100 μm in length.

In contrast, the addition of as little as 2 units/mL of alginate lyase degraded the cellular aggregates after 30 min at 37 °C (Figure 1.6C). The addition of alginate lyase (1 unit/mL) directly to the SAV media at time t=0 and t=48 h of coculture growth similarly prevented the formation of bacterial aggregates (Figure 1.6A). These results strongly suggest that alginate serves as the principal component of the observed biofilms, and also is responsible for the capture of the *Synechocystis* cells.

1.3.3. Evolution experiments alter microbial makeup of biofilm

Since alginate is produced as a part of the life cycle of *A. vinelandii*, but the adhesion of *Synechocystis* to *A. vinelandii* is not a part of the life cycle of *Synechocystis*, we devised an

evolution experiment to test our hypothesis for the formation of multicellular aggregates. We grew the SAV coculture for 8 d, centrifuged at 100 x g for 20 s to pellet the aggregates and collected and propagated the supernatant 8 times: centrifuging, collecting and propagating the coculture every 8 d. We then isolated the evolved *Synechocystis* and the evolved *A. vinelandii* by growing the organisms in BG-11 media and modified Burke's media respectively and then transferred the isolated cells back to SAV media and grew them with the wildtype coculture partner. The evolved *A. vinelandii* formed multispecies aggregates with wildtype *Synechocystis*, but, as we hypothesized, the evolved *Synechocystis* did not form aggregates with wildtype *A. vinelandii* (Figure 1.8). These findings suggest that in a population of *Synechocystis*, certain cells possess features that make association with the alginate matrix likely and other subpopulations of *Synechocystis* possess features that make this association less likely. The identification of these features/subpopulations would be an interesting area of investigation. In addition to supporting our hypothesis concerning the formation of the *Synechocystis*/*A. vinelandii* aggregates, this evolution experiment also suggests that the colocalization results in Figure 1.1 are not simply the result of statistical associations.

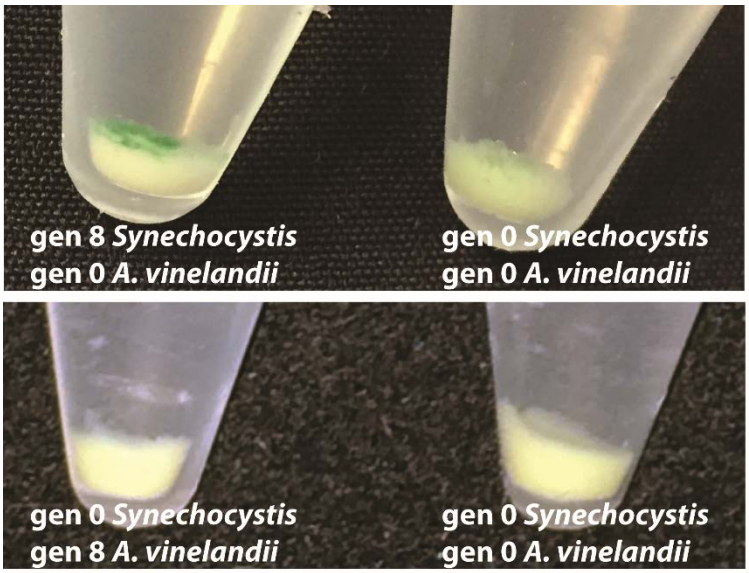

Figure 1.8. Evolution experiments. After 8 generations of selection, gen 8 *Synechocystis* was isolated into BG-11 media by diluting the coculture 1:100 and growing for 1 week. The evolved *Synechocystis* was then grown with gen 0 *A. vinelandii* in SAV media. Persistent multispecies aggregates did not form as compared to the wildtype coculture after 6 d based on the observation that the wildtype coculture pellet was uniformly green and the evolved coculture pellet had a distinct green layer and a distinct white layer (Upper figure). After 8 generations of selection, gen 8 *A. vinelandii* was isolated into Burke's media by diluting the coculture 1:100 and growing for 3 d and then grown with gen 0 *Synechocystis* in SAV media, multispecies aggregates did form as compared to the wildtype coculture in this experiment (lower figure). Aggregation was determined by centrifuging at 500 rpm for 30 seconds to pellet the aggregates, the dispersal of the green *Synechocystis* in the pellet was visualized above.

SEM images provided direct evidence for the presence of a polymer matrix that surrounded the *A. vinelandii* cells (Figure 1.9-red arrows). The SEM images also revealed persistent cellular contacts between multiple microbial phenotypes over a variety of timepoints from 4-16 d in unshaken SAV cocultures. Aggregates were not seen in shaken cocultures

analyzed by SEM (Figure 1.10). *A. vinelandii* is a rod-shaped bacterium that forms rounded or cocci-shaped cells after undergoing the transition to a cyst state.[44] *Synechocystis* also has a spherical cellular morphology[45] that makes distinguishing between *Synechocystis* and *A. vinelandii* cysts difficult unless the *Synechocystis* is caught in the act of dividing. For example, Figure 1.4A depicts both *Synechocystis*, seen in the process of dividing in the lower right-hand corner, and *A. vinelandii* cysts that are trapped in the extracellular mesh, closely resembling SEM images of *A. vinelandii* cysts taken by Efuet et al.[44]

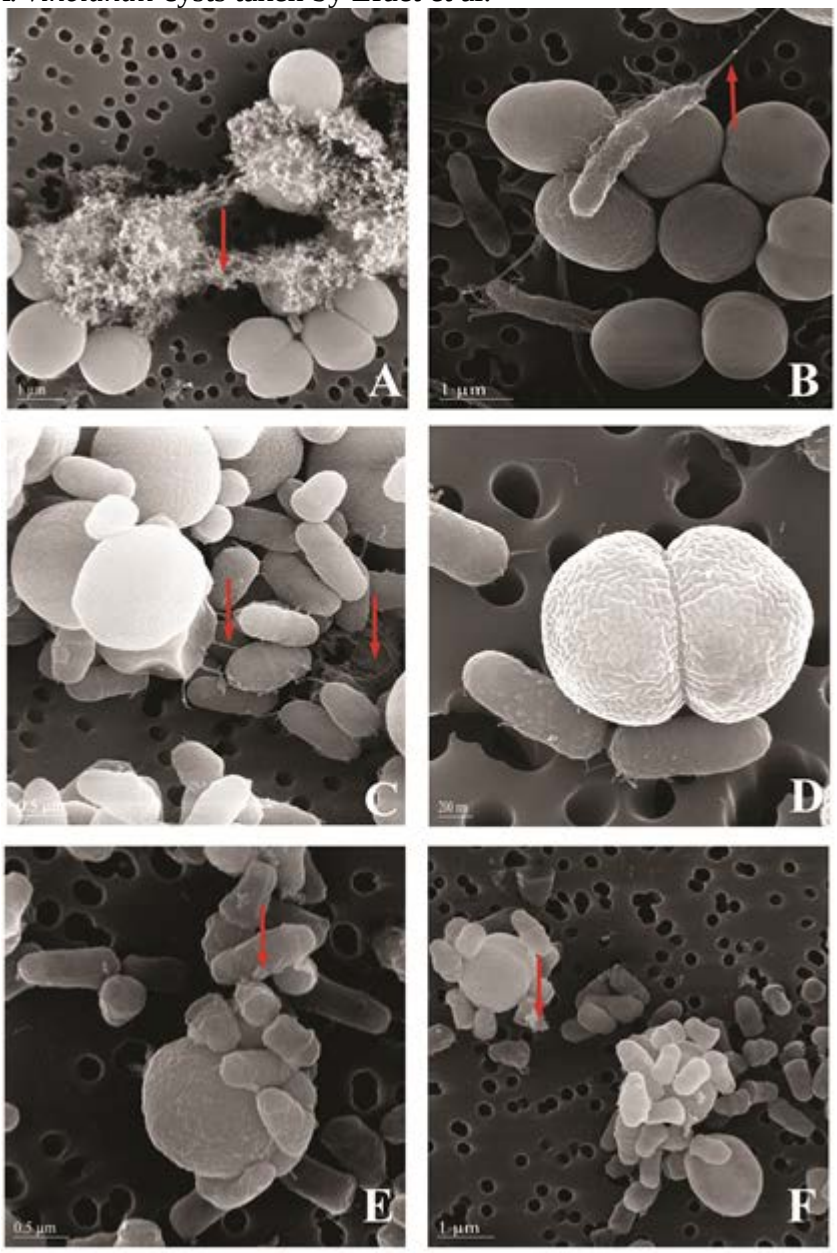

Figure 1.9. SEM images of SAV coculture. The SEM images were taken at different timepoints: (A) 4 d, (B) 6 d, (C) 8 d, (D) 11 d, (E) and (F) 15 d. Shown in (D) are both *A. vinelandii* and *Synechocystis* undergoing cellular division. The red arrows indicate an extracellular matrix that appears as either long filaments (B and C) or as fluffy clumps (A, E and F). The rod to oval shaped cells are *A. vinelandii* and the larger spherical cells are either *Synechocystis* or *A.*

vinelandii cysts. It is difficult to distinguish the two by SEM unless the *Synechocystis* is actively dividing as in (D), bottom right corner of (A), top left corner of (F).

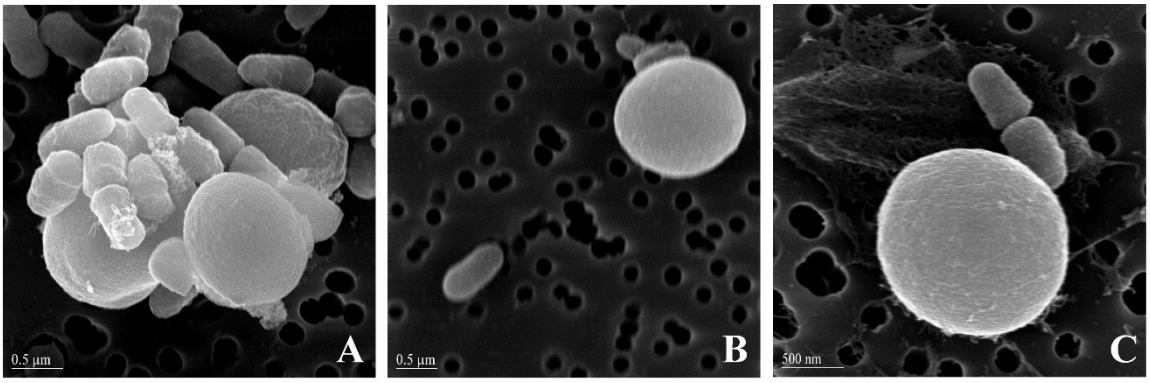

Figure 1.10. SEM images of shaken versus non-shaken SAV coculture. The SEM images were taken at 16 d. Shown in (A) is a non-shaken coculture and shown in (B) and (C) are shaken cocultures. Despite loading similar cell numbers onto the filter paper based on OD readings, only non-shaken cocultures showed cellular aggregates (A).

The dividing spherical cells in Figure 1.9A are likely not *A. vinelandii* emerging from the cyst state, as this emergence or germination is typically characterized by the presence of branch-like polymer strands and the discarding of the polymer shell.[46] An example of this is seen in Figure 9B as the elongated rod-shaped *A. vinelandii* cell covered in polymer. The interconnected web of *A. vinelandii* in Figure 1.9C appears to be cells that have emerged from the cyst state and undergone at least one round of division while still maintaining a few branch-like polymer contacts. Figure 1.9D shows both *Synechocystis* and *A. vinelandii* cells actively dividing at day 11. Figures 1-9E and 1-9F show the close associations between the two species in the unshaken coculture. In summary, these images suggest that *A. vinelandii* after 4 d has at least partly undergone the transition into the cyst state (Figure 1.9A) and then at around 6 d transitions out of the cyst state and back into the vegetative state (Figure 1.9B). From 6 - 16 d, *A. vinelandii* is present in the vegetative state (Figure 1.9C-F).

1.3.4. Coculture is a facultative mutualism from the perspective of *Synechocystis*

We next sought to determine the nature of the mutualism between *A. vinelandii* and *Synechocystis* in SAV media. The SEM images depict *A. vinelandii* emerging from the cyst state, which implied that some metabolic byproduct from *Synechocystis* was responsible for this emergence. However, this also could be explained by attributing the phenotypic changes to the life cycle of *A. vinelandii* and the switch from growth to minimal media. To distinguish between these possibilities, we first compared the growth of the monocultures and coculture in SAV media with and without shaking.[22] The *Synechocystis*/*A. vinelandii* coculture grew significantly faster than the monocultures when not shaken (Figure 1.11A). When grown *with* shaking at 150 rpm, the coculture grew at the same rate as the monocultures for 12 d, but eventually reached the same optical density as the unshaken culture. In addition, the shaken coculture did not exhibit aggregate formation, presumably due to increased shear forces (Figure 1.2). We therefore attribute the increased growth rates of the unshaken coculture to the intimate contact between the two species that can only occur in the aggregate. The ability of the shaken coculture to reach the same density at long time points likely occurs when the global concentration of nutrients matches that of the local concentrations in the cellular aggregates. This claim is supported by the

observation that in monoculture both organisms grow at the same rate with and without shaking (Figure 1.11A). This coculture does not grow in the absence of glutamate and the growth of the monocultures in SAV media indicates that both organisms can utilize glutamate.

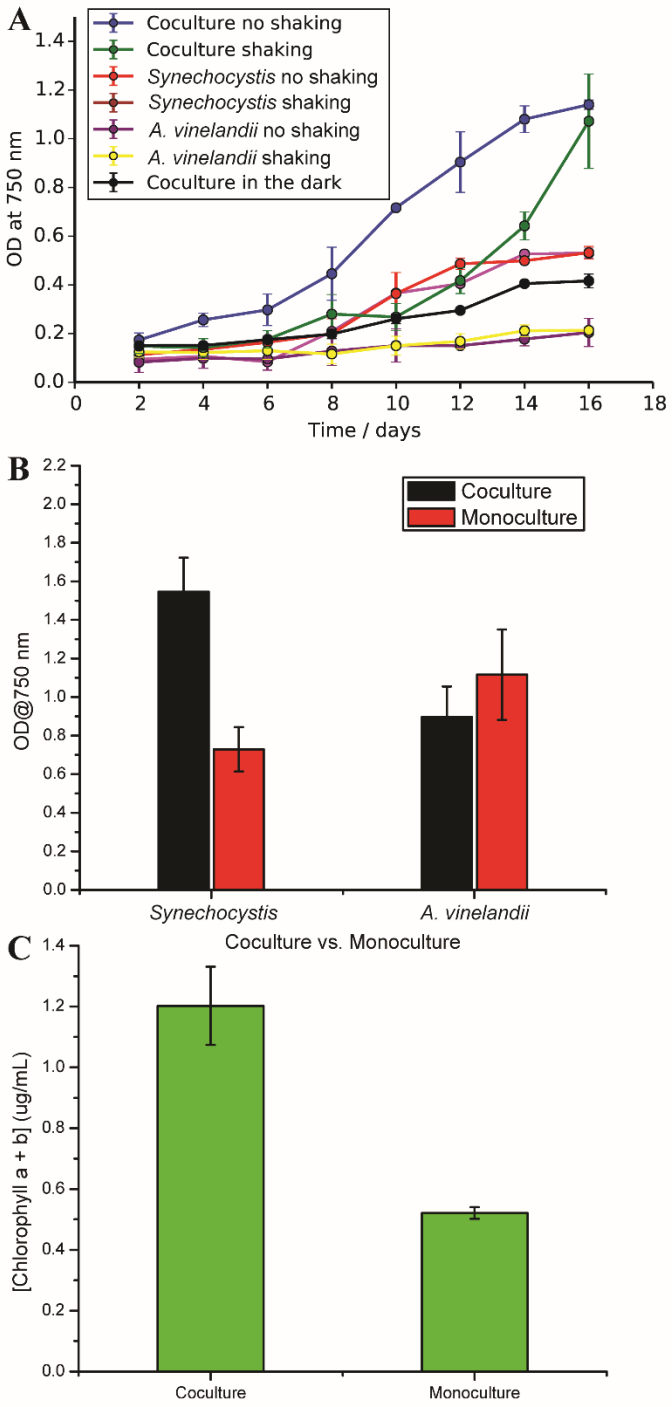

Figure 1.11. Coculture has enhanced growth over monocultures and coculture in the dark. (A) Growth assays of the coculture and monocultures grown with and without shaking in SAV media. Each unshaken coculture timepoint was its own experiment, performed after vortexing

the solution to break up the cellular aggregates so as not to bias the OD results. (B and C) The coculture was grown in dialysis bags. *Synechocystis* benefited from the presence of *A. vinelandii* in terms of both OD (B) and chlorophyll synthesis (C). *A. vinelandii* did not benefit from the presence of the cyanobacteria (+/- SD, N=3).

The differential growth with shaking of the coculture suggests at least some nutrients are being shared. *A. vinelandii* secretes ammonia in nutrient rich media[21,47] and we hypothesized and experimentally concluded that *A. vinelandii* secretes ammonia in SAV media as well (Figure 1.12). *A. vinelandii* secretes amino acids into solution under a variety of conditions[48] and this could also lead to enhanced *Synechocystis* growth (Figure 1.13). *Synechocystis* likely does not secrete a usable carbon source for *A. vinelandii* when grown photoautotrophically, as it has been shown to secrete only glycolate under these conditions.[49] Glycolate cannot be utilized by *Azotobacter vinelandii*.[50]

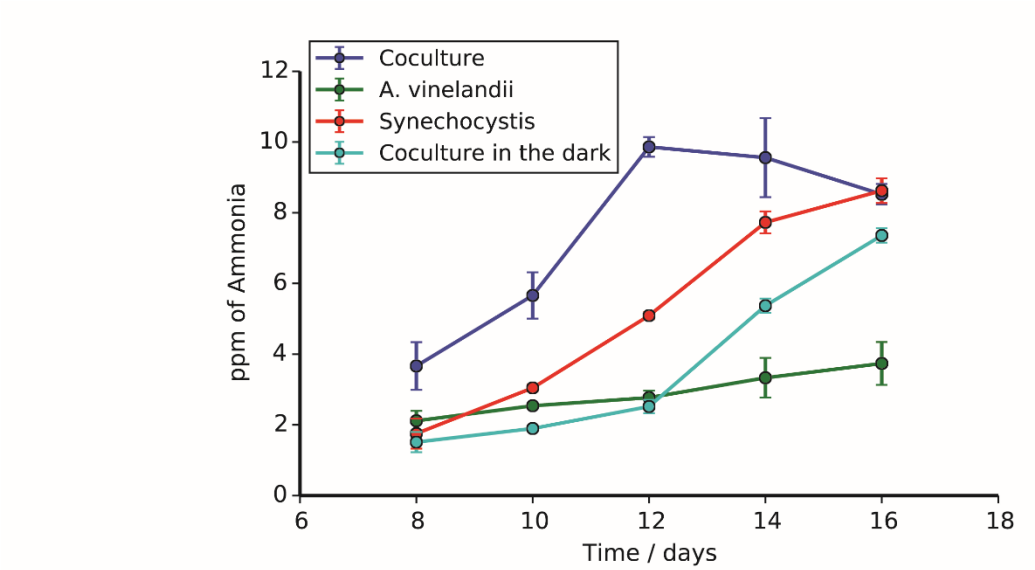

Figure 1.12. Coculture has enhanced ammonia production over monocultures and coculture in the dark. More ammonia is produced in the coculture than in the respective monocultures or coculture in the dark. Each timepoint was performed in biological triplicate. The metabolism of glutamate by *Synechocystis* results in ammonia release in addition to *A. vinelandii* secreting ammonia (+/-SD, N=3).

Our dialysis experiments thus support the conclusion that *A. vinelandii* supplies ammonia and possibly amino acids to *Synechocystis* (Figure 1.11B and 1-11C), but that *Synechocystis* likely does not supply carbon to *A. vinelandii* (Figure 1.11B). Ortiz-Marquez et al. reached a similar conclusion when they cultured a microalgae with *A. vinelandii*.[47] *A. vinelandii* does not benefit from the presence of *Synechocystis* in terms of biomass (Figure 1.11B), but *Synechocystis* does benefit from *A. vinelandii* both in terms of OD (Figure 1.11B) and chlorophyll production (Figure 1.11C). Chlorophyll production was measured after 10 days in solution. The unshaken coculture also produced more ammonia than the respective monocultures in SAV media (Figure 1.12). Flow cytometry indicated that the percentage of photoautotrophic *Synechocystis* in the coculture steadily increased to roughly 50% of the total number of cells after 16 d in solution (Figure 1.14).

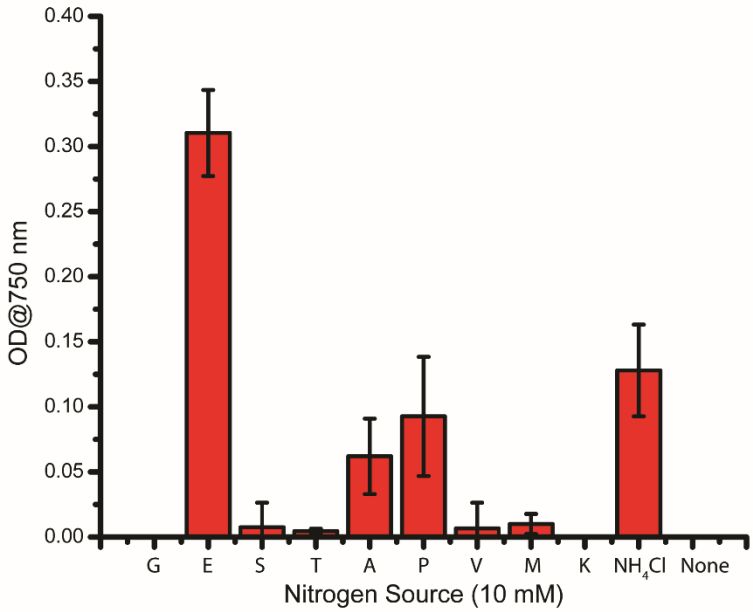

Figure 1.13. *Synechocystis* grown on a variety of nitrogen sources that *A. vinelandii* has been shown to secrete. Growth was determined by subtracting the OD at 5 d and the OD at 0 d (+/- SD, N=3).

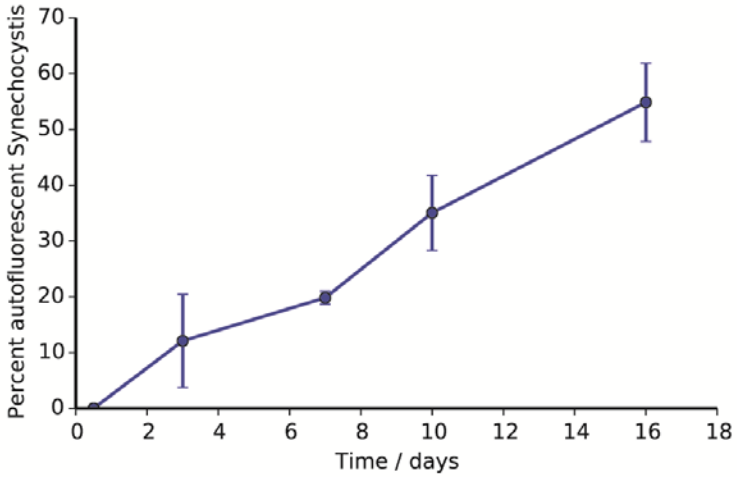

Figure 1.14. Percent of autotrophic cells in total cell count. Flow cytometry was used to determine how the percentage of autotrophic *Synechocystis* changes over time. These experiments were performed in biological duplicate and the percentages were determined after a 30,000-particle count.

1.4. Conclusions

Most microbes exist as members of surface-attached communities in an extracellular matrix for at least a portion of their life cycle.[6] This property is incredibly useful for survival in environments, such as in the gut or on the skin or teeth of animals or the surface of a plant root.[15] However, surface attached microbial communities are not ideal for many biotechnology applications as a consequence of surface area-to-volume ratio concerns during culture growth.

Due to the importance of cell-cell contacts in cocultures,[22,23] the design of a multispecies biofilm is an interesting strategy for the creation of a successful coculture. Interest in using cocultures to produce industrially relevant chemicals led us to focus on the creation of an unattached multispecies biofilm as opposed to a surface-anchored community.

Through these studies, we have demonstrated that the creation of a robust, unattached multispecies cooperative biofilm is possible. We have also provided evidence that *A. vinelandii* produces the polymer alginate due to low nutrient levels, and that this polymer then traps *Synechocystis* to generate viable cellular aggregates that last over two weeks in solution. Furthermore, this coculture leads to notably enhanced growth rates as compared to the monocultures and cocultures grown without light and can be extended to other species of cyanobacteria. While *A. vinelandii* does not benefit, in terms of biomass, from the presence of *Synechocystis*, *Synechocystis* does benefit from the presence of *A. vinelandii* in terms of both biomass generation and chlorophyll production. This is notable because it demonstrates that cocultures can lead to a more effective utilization of costly nutrients in bioproductions. Our lab is interested in expanding this coculture to include other microbes and to divert biomass towards the production of hydrogen and other metabolites of interest.

1.5. References

(1) Sachs, J. L.; Mueller, U. G.; Wilcox, T. P.; Bull, J. J. *Q. Rev. Biol.* **2004**, *79* (2).

(2) Douglas, A. E. *The symbiotic habit*; Princeton Univ. Press, 2010.

(3) Burmølle, M.; Ren, D.; Bjarnsholt, T.; Sørensen, S. J. *Trends Microbiol.* **2014**, *22* (2), 84.

(4) Kolenbrander, P. E.; Palmer, R. J.; Periasamy, S.; Jakubovics, N. S. *Nat. Rev. Microbiol.* **2010**, *8* (7), 471.

(5) Yang, L.; Liu, Y.; Wu, H.; Høiby, N.; Molin, S.; Song, Z. *Int. J. Oral Sci.* **2011**, *3* (2), 74.

(6) Elias, S.; Banin, E. *FEMS Microbiol. Rev.* **2012**, *36* (5), 990.

(7) Mitri, S.; Xavier, J. B.; Foster, K. R. *Proc. Natl. Acad. Sci. U. S. A.* **2011**, *108 Suppl 2* (Supplement 2), 10839.

(8) Bader, J.; Mast-Gerlach, E.; Popović, M. K.; Bajpai, R.; Stahl, U. *J. Appl. Microbiol.* **2010**, *109* (2), 371.

(9) Goers, L.; Freemont, P.; Polizzi, K. M. *J. R. Soc. Interface* **2014**, *11* (96), 20140065.

(10) Shapiro, J. A. *Sci. Am.* **1988**, 82.

(11) Claessen, D.; Rozen, D. E.; Kuipers, O. P.; Søgaard-Andersen, L.; van Wezel, G. P. *Nat. Rev. Microbiol.* **2014**, *12* (2), 115.

(12) Rainey, P. B.; Rainey, K. *Nature* **2003**, *425* (6953), 72.

(13) Merino-Puerto, V.; Schwarz, H.; Maldener, I.; Mariscal, V.; Mullineaux, C. W.; Herrero, A.; Flores, E. *Mol. Microbiol.* **2011**, *82* (1), 87.

(14) Harcombe, W. *Evolution (N. Y).* **2010**, *64* (7), 2166.

(15) Davey, M. E.; O'toole, G. A. *Microbiol. Mol. Biol. Rev.* **2000**, *64* (4), 847.

(16) Kolodkin-Gal, I.; Romero, D.; Cao, S.; Clardy, J.; Kolter, R.; Losick, R. *Science (80-.).* **2010**, *328* (5978).

(17) Pratt, L. A.; Kolter, R. *Mol. Microbiol.* **1998**, *30* (2), 285.

(18) Jin, F.; Conrad, J. C.; Gibiansky, M. L.; Wong, G. C. L. *Proc. Natl. Acad. Sci. U. S. A.* **2011**, *108* (31), 12617.

(19) Alkawash, M. A.; Soothill, J. S.; Schiller, N. L. *APMIS* **2006**, *114* (2), 131.

(20) Cotton, L. A.; Graham, R. J.; Lee, R. J. *J. Exp. Microbiol. Immunol.* **2009**, *13*, 58.

(21) Twite, A. A.; Hsiao, S. C.; Onoe, H.; Mathies, R. A.; Francis, M. B. *Adv. Mater.* **2012**, *24* (18), 2380.

(22) Hom, E. F. Y.; Murray, A. W. *Science* **2014**, *345* (6192), 94.

(23) Christensen, B. B.; Haagensen, J. A. J.; Heydorn, A.; Molin, S. *Appl. Environ. Microbiol.* **2002**, *68* (5), 2495.

(24) Kim, H. J.; Boedicker, J. Q.; Choi, J. W.; Ismagilov, R. F. *Proc. Natl. Acad. Sci. U. S. A.* **2008**, *105* (47), 18188.

(25) Orive, G.; Hernández, R. M.; Gascón, A. R.; Calafiore, R.; Chang, T. M. S.; Vos, P. De; Hortelano, G.; Hunkeler, D.; Lacík, I.; Shapiro, A. M. J.; Pedraz, J. L. *Nat. Med.* **2003**, *9* (1), 104.

(26) Smidsrod, O.; Skjak-Braek, G. *Trends Biotechnol.* **1990**, *8*, 71.

(27) Santos-Rosa, F.; Galvan, F.; Vega, J. M. *Appl Microbiol Biotechnol* **1989**, *32*, 285.

(28) Setubal, J. C.; dos Santos, P.; Goldman, B. S.; Ertesvag, H.; Espin, G.; Rubio, L. M.; Valla, S.; Almeida, N. F.; Balasubramanian, D.; Cromes, L.; Curatti, L.; Du, Z.; Godsy, E.; Goodner, B.; Hellner-Burris, K.; Hernandez, J. A.; Houmiel, K.; Imperial, J.; Kennedy, C.; Larson, T. J.; Latreille, P.; Ligon, L. S.; Lu, J.; Maerk, M.; Miller, N. M.; Norton, S.; O'Carroll, I. P.; Paulsen, I.; Raulfs, E. C.; Roemer, R.; Rosser, J.; Segura, D.; Slater, S.; Stricklin, S. L.; Studholme, D. J.; Sun, J.; Viana, C. J.; Wallin, E.; Wang, B.; Wheeler, C.; Zhu, H.; Dean, D. R.; Dixon, R.; Wood, D. *J. Bacteriol.* **2009**, *191* (14), 4534.

(29) Hamilton, T. L.; Ludwig, M.; Dixon, R.; Boyd, E. S.; Dos Santos, P. C.; Setubal, J. C.; Bryant, D. A.; Dean, D. R.; Peters, J. W. *J. Bacteriol.* **2011**, *193* (17), 4477.

(30) Clementi, F. *Crit. Rev. Biotechnol.* **1997**, *17* (4), 327.

(31) Page, W. *Appl. Microbiol. Biotechnol.* **1989**, *31* (4), 329.

(32) Mejía-Ruíz, H.; Moreno, S.; Guzmán, J.; Nájera, R.; León, R.; Soberón-Chávez, G.;

Espín, G. *FEMS Microbiol. Lett.* **1997**, *156* (1), 101.

(33) Moreno, S.; Nájera, R.; Guzmán, J.; Soberón-Chávez, G.; Espín, G. *J. Bacteriol.* **1998**, *180* (10), 2766.

(34) Núñez, C.; León, R.; Guzmán, J.; Espín, G.; Soberón-Chávez, G. *J. Bacteriol.* **2000**, *182* (23), 6550.

(35) Knoop, H.; Gründel, M.; Zilliges, Y.; Lehmann, R.; Hoffmann, S.; Lockau, W.; Steuer, R. *PLoS Comput. Biol.* **2013**, *9* (6), e1003081.

(36) Anderson, S. L.; McIntosh, L. *J. Bacteriol.* **1991**, *173* (9), 2761.

(37) Yu, Y.; You, L.; Liu, D.; Hollinshead, W.; Tang, Y.; Zhang, F. *Mar. Drugs* **2013**, *11* (8), 2894.

(38) D'mello, R.; Hill, S.; Poole, R. K. *Microbiology* **1994**, *140*, 1395.

(39) Stanier, R. Y.; Kunisawa, R.; Mandel, M.; Cohen-Bazire, G. *Bacteriol. Rev.* **1971**, *35* (2), 171.

(40) Musk, D. J.; Banko, D. A.; Hergenrother, P. J. *Chem. Biol.* **2005**, *12* (7), 789.

(41) Rediers, H.; Vanderleyden, J.; De Mot, R. *Microbiology* **2004**, *150* (5), 1117.

(42) Hahn Berg, I. C.; Kalfas, S.; Malmsten, M.; Arnebrant, T. *Eur. J. Oral Sci.* **2001**, *109* (5), 316.

(43) Hangler, M.; Burmølle, M.; Schneider, I.; Allermann, K.; Jensen, B. *Biofouling* **2009**, *25* (7), 667.

(44) Efuet, E. T.; Pulakat, L.; Gavini, N. *J. Basic Microbiol.* **1996**, *36* (4), 229.

(45) Osanai, T.; Kuwahara, A.; Iijima, H.; Toyooka, K.; Sato, M.; Tanaka, K.; Ikeuchi, M.; Saito, K.; Hirai, M. Y. *Plant J.* **2013**, *76* (3), 456.

(46) Sadoff, H. L. *Bacteriol. Rev.* **1975**, *39* (4), 516.

(47) Ortiz-Marquez, J. C. F.; Do Nascimento, M.; Dublan, M. de L. A.; Curatti, L. *Appl. Environ. Microbiol.* **2012**, *78* (7), 2345.

(48) Revillas, J. J.; Rodelas, B.; Pozo, C.; Martínez-Toledo, M. V.; López, J. G. *Amino Acids* **2005**, *28* (4), 421.

(49) Knoop, H.; Gründel, M.; Zilliges, Y.; Lehmann, R.; Hoffmann, S.; Lockau, W.; Steuer, R. *PLoS Comput. Biol.* **2013**, *9* (6), e1003081.

(50) Kurz, W. G. W.; LaRue, T. A. G. *Can. J. Microbiol.* **1973**, *19* (3), 321.

Chapter 2

Generating a microbial coculture that grows without fixed carbon or nitrogen

Abstract

This work was motivated by both (1) the desire to make interesting products without the reliance on fixed carbon or fixed nitrogen using microbial cocultures, and (2) the desire to develop new methods for growing microbial communities. The bioplastic polyhydroxybutyrate (PHB), for example, is considered prohibitively expensive to make from sugar (compared to polypropylene). Microbial mutualisms play critical roles in a diverse number of ecosystems and have the potential to improve the efficiency of bioproduction for desirable chemicals. Utilizing and building on engineered strains of *Synechococcus elongatus* and *Azotobacter vinelandii*, we have combined a nitrogen-fixing organism with a carbon-fixing organism to make PHB from air, water, sunlight, and trace minerals. Our observations of coculture growth in batch culture led us to develop an improved system based on manipulating the osmotic pressure within a hydrogel. The growth of this hydrogel-based coculture has several advantages over batch cultures, including better growth over a longer period of time and decreased salt stress on *A. vinelandii*.
Keywords: Engineered coculture, metabolic syntrophy, cyanobacteria, diazotroph, hydrogel, sucrose production, coculture, mutualism

Portions of the work described in this chapter have been reported in separate publications.[1,2]

2.1. Introduction

2.1.1 Motivation for designing novel cocultures

Microbial cocultures could enable bioproductions from cheaper, more renewable chemical feedstocks. Furthermore, the design of microbial cocultures is a relatively unexplored but promising area of synthetic biology.[3,4] In our lab, we sought to engineer a coculture to share metabolites in order to gain a function not present in either microbe individually. Specifically, we engineered *Azotobacter vinelandii* and *Synechococcus elongatus* PCC 7942 to share nutrients and grow in the absence of fixed carbon and nitrogen. The engineered *A. vinelandii* transfers ammonium to *S. elongatus* and the engineered *S. elongatus* transfers sucrose to *A. vinelandii*. This coculture produces the bioplastic polyhydroxybutyrate (PHB) from phosphate buffer, trace metals, and sunlight.[1]

Azotobacter vinelandii is an obligate aerobe that fixes diatomic nitrogen and exists as free-living bacteria in soil.[5] *A. vinelandii* can produce PHB and accumulate it under certain conditions at up to 90% of its dry cell weight.[6] The deletion of the *nifL* gene, a protein involved in regulation of the expression of nitrogenase, results in an increase in the level of ammonium secreted into the media.[7] We utilize a *nifL* knockdown of *A. vinelandii*, refered to as *A. vinelandii* AV3, to improve ammonium release and, thus, coculture growth. Ortiz-marquez et al. uses the ammonium secreted from a *nifL* knockdown of *A. vinelandii* to supply nitrogen to algae.[8] However, the *A. vinelandii* do not benefit from the presence of the algae in this coculture. We wanted to develop a system where both the nitrogen-fixing organism and the carbon-fixing organism benefited from being cultured together.

2.1.2. The engineered coculture system

We chose to work with the carbon-fixing organism *Synechococcus elongatus*, a naturally competent freshwater cyanobacterium. Ducat et al. engineered *S. elongatus* to secrete sucrose in the presence of salt and high pH by expressing a sucrose permease on the inner membrane of *S.*

elongatus.[9] Sucrose permease expressing *S. elongatus*, *cscB S. elongatus*, was used to supply the sugar as a carbon source to *A. vinelandii* in our work. *cscB S. elongatus* only secretes sucrose in the presence of osmotic stress, in our case, 150 mM NaCl.

The engineered coculture we designed between *A. vinelandii* AV3 and *cscB S. elongatus* grows in the absence of fixed carbon and nitrogen and produces PHB from carbon dioxide. This success both supports our model of syntrophy and provides a promising biosynthetic "chassis" that can be engineered further for the production of energy-rich products from air, water, trace minerals, and sunlight. In investigating how this coculture grows, we found that coculture growth in our media is not nutrient limited; it instead depends on cell ratio. The coculture generates biomass until a certain equilibrium cell ratio is reached, and then it no longer increases in biomass. We wanted to design this coculture to grow more like a monoculture of *E. coli*, where growth resumes once spent media is diluted with fresh media. Since our coculture is cell ratio dependent, when we dilute the spent media with fresh media, or start a subculture of the coculture after the coculture reaches maximum optical density, growth does not resume because the coculture has already reached its equilibrium ratio.

To solve this problem, we developed a system where the *S. elongatus* was contained in a spatially constrained crosslinked polyacrylate hydrogel and the *A. vinelandii* was in the media surrounding the hydrogel.[2] By spatially constraining a hydrogel inside dialysis tubing we can control the chemical potential of the water inside the hydrogel and exert osmotic stress on embedded *cscB S. elongates*. This causes the cells to secrete sucrose. The use of a spatially constrained hydrogel enables us to grow this coculture over multiple subcultures, unlike when we grow the organisms in batch culture. This system has the added benefit of growing *A. vinelandii* in the absence of osmotic stress, as these conditions lower the yield of PHB in *A. vinelandii*. Interestingly, the swelling state of the polymer hydrogel strongly influences the sucrose production of the cyanobacteria, demonstrating that the physical properties of the gel can be used to influence production directly. In addition to addressing the problems described above, this technique is synthetically accessible and cost effective, suggesting that it could be useful in industrial coculturing systems.

It is our hope that this work inspires others to design engineered microbial communities for the production of a more diverse array of products from more varied chemical feedstocks. Since publishing our work, others have already begun investigating other coculture partners in the production of PHB from the sugar produced by *cscB S. elongatus*.[10,11] The engineering of microbial communities promising to be an exciting area of future research.

2.2. Materials

2.2.1. BG-11 media[12]

Stock Solutions:
Micronutrients (A5), 100X, listed in g/L: 0.3 g H_3BO_3, 0.2 g $MnCl_2*4H_2O$, 0.023 g $ZnSO_4*7H_2O$, 0.010 g $CuSO_4*5H_2O$, 0.048 g $Na_2MoO_4*2H_2O$, 0.028 g $NaVO_3$, 0.005 $CoCl_2*7H_2O$
$NaNO_3$ Stock: 30 g/L K_2HPO_4 Stock: 7.6 g/L
$MgSO_4*7H_2O$ Stock: 15 g/L
$CaCl_2$ Stock: 9 g/L
Citric acid Stock: 1.5 g/L
Ferric ammonium citrate Stock: 1.5 g/L
EDTA Stock: 0.2 g/L

Na_2CO_3 Stock: 5 g/L

BG-11 liquid growth media:

A 909 mL portion of Milli-Q water was combined with 50 mL of $NaNO_3$ solution, 4 mL of K_2HPO_4 solution, 5 mL of $MgSO_4*7H_2O$ solution, 4 mL of $CaCl_2$ solution, 4 mL of citric acid solution, 4 mL of ferric ammonium citrate solution, 5 mL of EDTA solution, 4 mL of Na_2CO_3 solution, 10 mL of Micronutrient (A5) solution. The media was then autoclaved and, after cooling, the pH of the media should be about 7.1. A yellowish precipitate formed after autoclaving. The media was shaken before use.

BG-11 liquid media for *cscB S. elongatus* sucrose production:

A 909 mL portion of Milli-Q water was combined with 50 mL of $NaNO_3$ solution, 4 mL of K_2HPO_4 solution, 5 mL of $MgSO_4*7H_2O$ solution, 4 mL of $CaCl_2$ solution, 4 mL of citric acid solution, 4 mL of ferric ammonium citrate solution, 5 mL of EDTA solution, 4 mL of Na_2CO_3 solution, and 10 mL of Micronutrients (A5) solution. A 2 g/L potion of HEPES buffer was added to the media. A 8.766 g/L portion of NaCl was added to the media (final concentration of 150 mM). The pH was adjusted to pH = 8.8 with KOH. The media was then autoclaved.

BG-11 agar plates:

A 2X BG-11 solution (500 mL) and a 2X agar solution (15 g Noble agar in 500 mL of Milli-Q water) were autoclaved separately. The two solutions were mixed after autoclaving. A 1 mL portion of 1 M sodium thiosulfate was added to 1 L of BG-11 agar just prior to pouring plates. A 40 mL portion of BG-11 agar was poured into each plate.

2.2.2. Burke's media[13]

To make Burke's media, the following stock solutions were prepared.

1000X Burke's micronutrient solution:

2.8 g/L H_3BO_3, 1.592 g/L $MnSO_4·H_2O$, 0.752 g/L $Na_2MoO_4·2H_2O$, 0.24 g/L $ZnSO_4·7H_2O$, 0.04 g/L of $NiCl·6H_2O$ and $CuSO_4·5H_2O$, 0.056 g/L $CoSO_4·7H_2O$

Solution 1 (20X), pH=7:

4.0 g/L KH_2PO_4, 16 g/L K_2HPO_4

Solution 2 (5X):

0.45 g/L $CaCl_2*2H_2O$, 1 g/L $MgSO_4*7H_2O$, 0.025 g/L $FeSO_4*7H_2O$

Burke's liquid media:

A 738 mL portion of Milli-Q water was combined with 50 mL of 20X Solution 1, 200 mL of 5X Solution 2, 1 mL of 1000X Burke's micronutrients solution, 20 g of sucrose, and 12 mL of 0.5 mg/mL iron(II) citrate. The media was then filter sterilized, but not autoclaved.

2.2.3. SAV media

A 700 mL portion of Milli-Q water was combined with 50 mL of 20X Solution 1, 200 mL of 5X Solution 2, and 1 mL of 1000X Burke's micronutrients solution. These are all components of Burke's liquid media. To the above solution were added 5 mL of $MgSO_4*7H_2O$ solution, 4 mL of $CaCl_2$ solution, 4 mL of citric acid solution, 5 mL of EDTA solution, 4 mL of Na_2CO_3 solution and 10 mL of Micronutrients (A5) solution. These are all components of BG-11 liquid media. A 0.338 g/L portion of monosodium glutamate was added to the media (2 mM final concentration). The volume was adjusted to 1 L with Milli-Q water. The media was autoclaved and allowed to cool. A precipitate forms after autoclaving. The media was shaken before use. After cooling, a 12 mL portion of a filter sterilized 0.5 mg/mL iron(II) citrate solution (2 mM) was added to the media. This media will also support the growth of a coculture between *A. vinelandii* and *Synechocystis* 6803. We did not pursue engineering *Synechocystis* 6803 for this

work largely because it is harder to engineer than *S. elongatus* and it can grow heterotrophically and this would complicate analysis of the coculture.

2.2.4. CAV media

A 700 mL portion of Milli-Q water was combined with 50 mL of 20X Solution 1, 200 mL of 5X Solution 2, and 1 mL of 1000X Burke's micronutrients solution. These are all components of Burke's liquid media. To the above solution were added 5 mL of $MgSO_4*7H_2O$ solution, 4 mL of $CaCl_2$ solution, 4 mL of Na_2CO_3 solution and 10 mL of Micronutrients (A5) solution. These are all components of BG-11 liquid media. A 8.766 g/L portion of NaCl was added to the media (final concentration of 150 mM). Optional: A 2 g/L potion of HEPES buffer was added to the media. In Smith et al.[1] 2 g/L HEPES buffer was not added to the CAV media only because the goal was to grow the coculture without any fixed carbon or nitrogen (including fixed carbon or nitrogen that *A. vinelandii* and *S. elongatus* cannot metabolize). No growth difference was observed between CAV media and CAV media with HEPES buffer; however, the pH of CAV media was more stable with added HEPES buffer. The pH of the media was adjusted to 8.4 with KOH. For sucrose production from *cscB S. elongatus*, the pH needs to be between 7.8 and 8.9.[9] This is because sucrose permease is a proton and sucrose symporter. Furthermore, sucrose is produced by *S. elongatus* as an osmoprotectant, so NaCl (optimally 150 mM) is required for sucrose to be exported out of the cyanobacteria. The media was filled to 1 L. The media was autoclaved and allowed to cool. After cooling, a 12 mL portion of a filter sterilized 2 mM iron(II) sulfate solution was added to the media.

2.2.5. Engineered strains of *Azotobacter vinelandii and Synechococcus elongatus*

Professor Leonardo Curatti (Centro de Estudios de Biodiversidad y Biotecnología (CEBB-MdP), CONICET, Mar del Plata, Argentina) generously provided the *ΔnifL A. vinelandii* strain.[8]

Engineering cscB Synechococcus elongatus:[9]

Plasmids with regions homologous to neutral site II of *S. elongatus* were obtained from Professor David Savage (UC Berkeley). They contained a kanamycin resistance cassette. A similar plasmid can be purchased from Addgene (plasmid #40240). We used Golden Gate cloning[14] to insert sucrose permease (cscB) from *E. coli* (ATCC 700927) containing a psbA1 light-activated promoter into the plasmid. The plasmid was then transformed into *S. elongatus* via method 3.1.

DNA Sequence of psbA1+sucrose permease:

AGGTCTCTGTCCTAGCAAGAGTTTTTAACTAAGACTCTTGCCCTTTACAACCTCGAA
GGAGCGTCAGATCTCATATGGCACTGAATATTCCATTCAGAAATGCGTACTATCGTT
TTGCATCCAGTTACTCATTTCTCTTTTTTATTTCCTGGTCGCTGTGGTGGTCGTTATAC
GCTATTTGGCTGAAAGGACATCTAGGGTTGACAGGGACGGAATTAGGTACACTTTAT
TCGGTCAACCAGTTTACCAGCATTCTATTTATGATGTTCTACGGCATCGTTCAGGATA
AACTCGGTCTGAAGAAACCGCTCATCTGGTGTATGAGTTTCATCCTGGTCTTGACCG
GACCGTTTATGATTTACGTTTATGAACCGTTACTGCAAAGCAATTTTTCTGTAGGTCT
AATTCTGGGGGCGCTCTTTTTTGGCCTGGGGTATCTGGCGGGATGCGGTTTGCTTGA
CAGCTTCACCGAAAAAATGGCGCGAAATTTTCATTTCGAATATGGAACAGCGCGCG
CCTGGGGATCTTTTGGCTATGCTATTGGCGCGTTCTTTGCCGGCATATTTTTTAGTAT
CAGTCCCCATATCAACTTCTGGTTGGTGTCGCTATTTGGCGCTGTATTTATGATGATC
AACATGTGTTTTAAAGATAAGGATCACCAGTGCGTAGCGGCGGATGCGGGAGGGGT
AAAAAAAGAGGATTTTATCGCAGTTTTCAAGGATCGAAACTTCTGGGTTTTCGTCAT
ATTTATTGTTGGGACGTGGTCTTTCTATAACATTTTTGATCAACAACTTTTTCCTGTCT
TTTATGCAGGTTTATTCGAATCACACGATGTAGGAACGCGCCTGTATGGTTATCTCA

ACTCATTCCAGGTGGTACTCGAAGCGCTGTGCATGGCGATTATTCCGTTCTTTGTGA
ATCGGGTAGGGCCAAAAAATGCATTACTTATCGGTGTTGTGATTATGGCGTTGCGTA
TCCTTTCCTGCGCGCTGTTCGTTAACCCCTGGATTATTTCATTAGTGAAGCTGTTACA
TGCCATTGAGGTTCCACTTTGTGTCATATCCGTCTTCAAATACAGCGTGGCAAACTTT
GATAAGCGCCTGTCGTCGACGATCTTTCTGATTGGTTTTCAAATTGCCAGTTCGCTTG
GGATTGTGCTGCTTTCAACGCCGACTGGGATACTCTTTGACCACGCAGGCTACCAGA
CAGTTTTCTTCGCAATTTCGGGTATTGTCTGCCTGATGTTGCTATTTGGCATTTTCTTC
CTGAGTAAAAAACGCGAGCAAATAGTTATGGAAACGCCTGTACCTTCAGCAATATA
GAGCGAGAGACCA

2.2.6. Crosslinked hydrogel synthesis

A 1.5 g portion of sodium acrylate and 0.056 g of *N*,*N*-methylene bisacrylate were added to 5 mL of DI water (11.2 mg crosslinker/mL). A stir bar was added and the solution was mixed. To the stirring solution, 0.04 g of ammonium persulfate was added. The solution was then stirred and heated at 70 ℃ for 2 h. After 2 h the aqueous solution was a transparent gel. The gel was placed in 1 L of water and left overnight to remove excess reagent. The excess liquid was removed. The gel was additionally rinsed 2X for 1 h with 1 L of water. The hydrogel was then placed in a 100 ℃ oven overnight or until the hydrogel was a dry and porous powder. The dried hydrogel was stored in a desiccator until use.

2.3. Methods

2.3.1. *Synechococcus elongatus* transformation

S. elongatus cells were passaged so they would reach an OD_{750} = 0.6 on the day set aside for transformation. When the *S. elongatus* cells were ready for transformation, a 1.5 mL portion of cells per transformation was centrifuged at roughly 16,000 g at room temperature for 2 min. A 1.5 mL portion of cells was included for the negative control as well. The *S. elongatus* cell pellet was resuspended in 750 µL of 10 mM NaCl and centrifuged again. The cell pellet was resuspended in 150 uL of BG-11 media and ~100-200 ng of plasmid were added. For the negative control no plasmid was added. Eppendorf tubes containing *S. elongatus* cells were covered in aluminum foil to block light and shaken in a 30 ºC incubator at 150 rpm for 16-24 h. A few hours before the transformation was ready, antibiotics were top-plated onto BG-11 plates. For spectinomycin, we used 35-40 µL of a 50 mg/µL spectinomycin stock on a 40 mL agar plate. After 16-24 h,100-150 µL of cells from the transformation were spread on the top- plated BG-11 agar plate. This included the negative control sample. The plates were wrapped with Parafilm and incubated under light (we used a 9 W GE spiral bulb that gave off 25 µmoles photons m^{-2} s^{-1} irradiance of cool white fluorescent light) in a 30 ºC warm room with the agar side on bottom. When successful, colonies formed after 6-12 d.

2.3.2. Growing wildtype *A. vinelandii*/*S. elongatus* cocultures

A. vinelandii was grown to mid log phase in Burke's media. *S. elongatus* was grown to mid log phase in BG-11 media. Both cell types were washed 3X via centrifugation and resuspension with SAV media. Washed *A. vinelandii* and *S. elongatus* cells were added to a preferred amount of SAV media. The coculture was grown at 30 °C under 25 µmoles photons m^{-2} s^{-1} irradiance of cool white fluorescent light without shaking. Both SAV and CAV cocultures and CAV cocultures with an *S. elongatus* hydrogel were grown without shaking.[4,10] SAV cocultures (between wildtype *A. vinelandii* and *S. elongatus*) with shaking grow slower in the first few days of culturing as compared to growing without shaking. However, coculture growth with shaking quickly recovers and both cultures reach the same late-stage optical density.

Presumably, this is due to the fact that when grown without shaking multicellular aggregates enable higher local concentrations of ammonia then in the global solution. Over time the local concentrations of ammonia equals the global concentrations of ammonia and the difference between coculture growth with and without shaking becomes less apparent. In CAV cocultures, the cocultures were grown without shaking so as not to impact carbon dioxide concentrations in the solution. Shaking the *cscB S. elongatus* hydrogel/*A. vinelandii* coculture slightly improved *A. vinelandii* AV3 growth. Growth of the coculture via UV-Vis was monitored at 750 nm to avoid absorbance by chlorophyll. Also, to avoid cellular aggregates impacting absorbance, the coculture was mixed thoroughly or vortexed prior to taking the optical density measurements. Each optical density reading was its own experiment.

2.3.3. Cocultures in dialysis tubing

Dialysis tubing was purchased from Sigma-Aldrich with a MWCO of 12,000 Da (product no. D6066-25EA). The dialysis tubing was soaked in DI water for 30 min, and then they were soaked in 70% ethanol for 1 h to sterilize. The dialysis tubing was washed twice with either SAV or CAV media, depending on the coculture prior to use. For the SAV coculture, 10 mL of sterile phosphate buffer was added to a sterile 250 mL Erlenmeyer flask. Sterile phosphate buffer was used to prevent cell growth to too high of an optical density. For the CAV coculture, 10 mL of CAV media was added to a sterile 250 mL Erlenmeyer flask. The dialysis tubing was sealed with a clamp with 10 mL of SAV or CAV media containing *A. vinelandii* or *S. elongates*, or (as a control) no cells. The additional cell type was placed in 10 mL of media in another dialysis tube. The total volume of liquid was always 30 mL. At the end of the experiment the dialysis tubes were removed from the flask and analyzed for optical density and chlorophyll content.

2.3.4. Growing engineered *A. vinelandii*/*S. elongatus* cocultures

A. vinelandii was grown to mid log phase in Burke's media. *S. elongatus* was grown to mid log phase in BG-11 media. Both cell types were washed 3X via centrifugation and resuspension with SAV media. Washed *A. vinelandii* and *S. elongatus* cells were added to a preferred amount of CAV media. Optional: A 0.05 g portion of sodium bicarbonate was added to the media as a sterile 10% solution in water for every 25 mL of CAV media. The coculture was grown at 30 °C under 25 μmoles photons m^{-2} s^{-1} irradiance of cool white fluorescent light without shaking.

2.3.5. Chlorophyll concentration measurements[15]

The cells (from a coculture or monoculture) were centrifuged and the cell pellet was kept. A solution of aqueous 85% methanol containing 1.5 mM sodium dithionite was used to resuspend the cell pellet. The solution was vortexed and stored on ice for 10 min. The absorbance was taken using a UV-Vis spectrometer. The spectrometer was zeroed at 750 nm. The wavelengths taken were 665 minus 750 nm and 652 minus 750 nm. The constants given in Table 2 and 3 of Porra et al. were used to determine the concentration of chl a + b (μg/mL).[15]

2.3.6. Monitoring coculture cell ratio with flow cytometry

Cells were incubated with 5 μM of CFDA for 20 min. The cells were injected onto a BD Bioscience LSR Fortessa X20. 300,000 events were monitored for each experiment. Several plots were made including a side scatter vs. forward scatter plot, a count vs. Cy5 channel fluorescence and a count vs. FITC fluorescence plot. Monoculture samples were used to define the relevant gates. The ratio of *S. elongatus* to *A. vinelandii* was determined via the number of cells that were both green and red fluorescent (*S. elongatus*) vs. the number of cells that were only green fluorescent (*A. vinelandii*).

2.3.7. PHB production in coculture

Sodium bicarbonate (0.1 g), either with or without an isotopic label, was added to 40 mL of CAV media containing the coculture. After 2 d of growth without shaking under the standard light conditions, the CAV media and coculture were transferred to a sealed flask. The headspace was purged with nitrogen gas for 1 min and sodium bicarbonate (0.1 g) was added to the flask again. PHB was isolated after 3 d.

2.3.8. PHB isolation and analysis

The protocol of Law et al. was followed to isolate PHB.[16] Cell pellets were resuspended in commercial sodium hypochlorite solution (Clorox Regular Bleach). The cells were incubated for 1 h at 37 ℃. The resulting granules of PHB and lipids were centrifuged and the supernatant was discarded. The pellet was then washed with water, recentrifuged, and the supernatant was discarded. This step was repeated with acetone and then ethanol. The cell pellet was then dissolved in boiling chloroform and the chloroform solution was filtered. The filtrate contained PHB. The PHB content was analyzed via UV-Vis and GC-MS. For analysis via UV-Vis, the chloroform was evaporated and concentrated sulfuric acid was added to the PHB. The PHB and sulfuric acid was heated for 10 min at 100 ℃ to hydrolyze the PHB to crotonic acid. After cooling, the absorbance was monitored at 235 nm against a sulfuric acid blank. A standard curve from a commercial PHB source was used to quantify the amount of PHB. For analysis via GC-MS, PHB was hydrolyzed as described above in number 9. Then, the sulfuric acid was diluted with water (10% sulfuric acid in water). The crotonic acid in aqueous sulfuric acid was extracted into dichloromethane (DCM). For every mole of crotonic acid, 2 moles of *N,O-bis*(trimethylsilyl)acetamide (BSA) were added to the dichloromethane solution. BSA is a derivatization agent that helps carboxylic acids ionize via GC-MS (see Figure 2.12). After a 10 min incubation at room temperature, the BSA-derivatized crotonic acid was injected onto an Agilent 6890 GC with a 5973 MS. The fragment monitored via GC-MS is depicted in Figure 2.12. EI settings used: Energy, 70 eV; Emission, 35 μA; Repeller, 25 V; Ion Focus, 80 V, EMVolts, 1682.353; Filament, 1.0; Source temp, 230 ℃; Quad temp, 150 ℃; Autotune, Yes. GC-MS was used to monitor the degree to which ^{13}C was incorporated into the PHB polymer.

2.3.9. Sucrose production monitoring from *cscB S. elongatus* hydrogels

cscB S. elongatus at an $OD_{750\ nm}$ = 0.6 in 3 mL of BG-11 media with 2 g/L HEPES buffer at pH=8.8 was added to a known mass of dehydrated hydrogel material (in these experiments this was the variable we were changing). The *S. elongatus* and hydrogel combination was added to a dialysis tube clamped at one end. The second clamp was then placed to close the dialysis tube. The dialysis tubes used were the same as in section 3.3 and were prepared for use in the same way (steps 1 and 2, Section 3.3). The hydrogel inside the dialysis tubing was soaked in 10 mL of BG-11 media with 2 g/L HEPES buffer at pH=8.8 for 24 h in the presence of light (50 μmoles photons m^{-2} s^{-1} irradiance of cool white fluorescent light) in a 30 ºC warm room without shaking. The hydrogel was transferred to 10 mL of fresh BG-11 media with 2 g/L HEPES buffer at pH=8.8 for 2 d. After 2 d, the supernatant or media outside the hydrogel was tested for sucrose concentration. Then, the 10 mL of media was replaced with 10 fresh mL of media and after 2 d tested for sucrose concentration. This was repeated every 2 d.

2.3.10. Sucrose detection

A sucrose assay kit from Sigma-Aldrich was used to detect sucrose from *cscB S. elongatus* (Catalog # SCA20). A calibration curve from 0.025 mM to 5 mM was used to determine the concentration of sucrose in the media surrounding the hydrogel. Sample preparation: a 1 mL media sample was pushed through a 0.2 μm spin column to remove bacteria from the sample. The filtrate was tested for sucrose concentration.

2.3.11. Coculture growth in hydrogels

cscB S. elongatus at an $OD_{750\ nm}$ = 0.6 in 3 mL of BG-11 media with 2 g/L HEPES buffer at pH=8.8 was added to a known mass of dehydrated hydrogel material (0.5 g typically used). The *S. elongatus* and hydrogel combination was added to a dialysis tube clamped at one end. The second clamp was then placed to close the dialysis tube. The dialysis tubes used are the same as in section 3.3 and were prepared for use in the same way (steps 1 and 2 - section 3.3). The hydrogel inside the dialysis tubing was soaked in 10 mL of BG-11 media with 2 g/L HEPES buffer at pH=8.8 for 24 h (see Figure 2.14). The swelled hydrogel and dialysis tubing was, after 24 h, transferred to 10 mL of CAV media without NaCl containing either *A. vinelandii* AV3 or *A. vinelandii*. The cocultures were grown in the presence of light (50 µmoles photons m^{-2} s^{-1} irradiance of cool white fluorescent light) in a 30 ºC warm room without shaking. To perform the subculture experiments (see Figure 2.21):[2] after two days 9 mL of the total 10 mL of CAV media were replaced with 9 mL of fresh CAV media. This was repeated every 2 d. Sodium bicarbonate was not added to the hydrogel cocultures.

2.4. Results and Discussion

2.4.1. Wildtype coculture growth and behavior

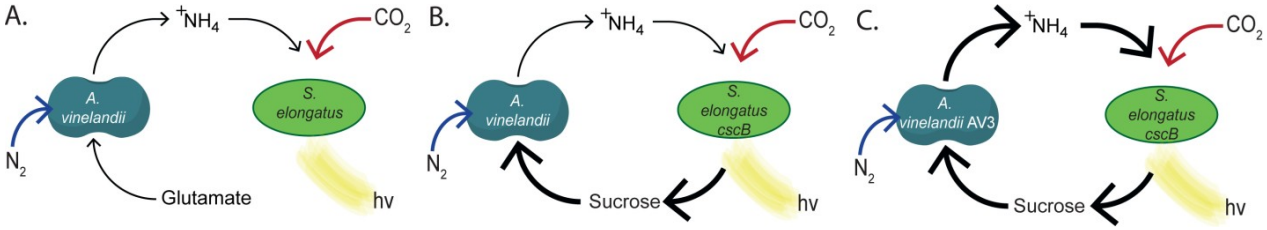

Figure 2.1. Proposed models of metabolic cross-feeding. (A) Only *A. vinelandii*, not *S. elongatus*, can metabolize glutamate. *S. elongatus* intakes nitrogen from *A. vinelandii* in the form of ammonia. (B) *cscB S. elongatus* supplies *A. vinelandii* with a reduced carbon source, sucrose, that enables the coculture to grow in the absence of glutamate. (C) *cscB S. elongatus* and AV3 *A. vinelandii* grow to higher optical densities and synthesize more chlorophyll suggesting ammonia transport was a bottleneck in the metabolic model of syntrophy between the two microbes.

We initially tested the validity of the basic cross-feeding model depicted in Figure 2.1A. In media containing glutamate and the trace metals necessary for both *Azotobacter vinelandii* and *Synechoccocus elongatus* growth (SAV media), it was noted that *S. elongatus* only grew in the presence of *A. vinelandii* (Figure 2.2, blue curve). *A. vinelandii* also grew to much lower optical 2densities when cultured alone (Figure 2.2, green curve). We further determined that *A. vinelandii* secretes ammonia into the media when grown in the SAV media under these conditions (Figure 2.3). We therefore hypothesized that the obligate photoautotroph *S. elongatus* was using secreted products from *A. vinelandii*, not glutamate, as its nitrogen source. In addition

to ammonia, *A. vinelandii* secretes amino acids into the media when grown on a wide variety of substrates,[17] which could provide additional nitrogen sources for *S. elongatus*. Accordingly, we tested the ability of *S. elongatus* to utilize several nitrogen feedstocks, including glutamate, ammonia, and several other amino acids found to be excreted by *A. vinelandii*.[17] As shown in Figure 2.4, *S. elongatus* can indeed be grown using either ammonia or lysine, but not glutamate or the other amino acids tested as a nitrogen source. These results suggest that the nitrogen-containing species secreted by *A. vinelandii* fulfulled the nitrogen source requirements of *S. elongatus* in this growth media, thus confirming a key aspect of the nutrient sharing model.

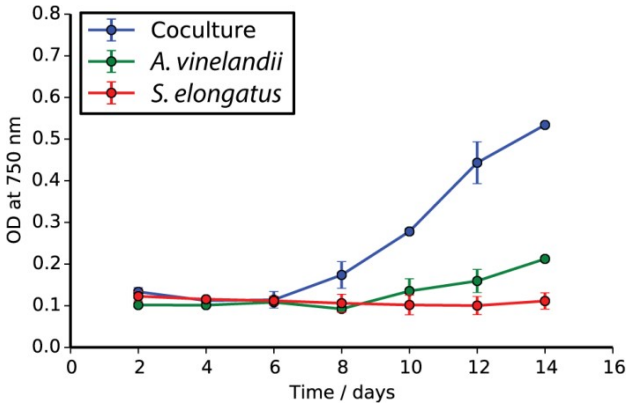

Figure 2.2. Growth assays of the coculture and the corresponding monocultures grown in SAV media. The *S. elongatus-A. vinelandii* coculture has enhanced growth over the monocultures. *S. elongatus* does not grow in the absence of *A. vinelandii* in SAV media. In B the growth of the coculture in dialysis bags is depicted. In the leftmost flask is one dialysis bag with *S. elongatus* (green) and one dialysis bag with *A. vinelandii*. In the rightmost flask is one dialysis bag with *S. elongatus* (now colorless) and one with SAV buffer.

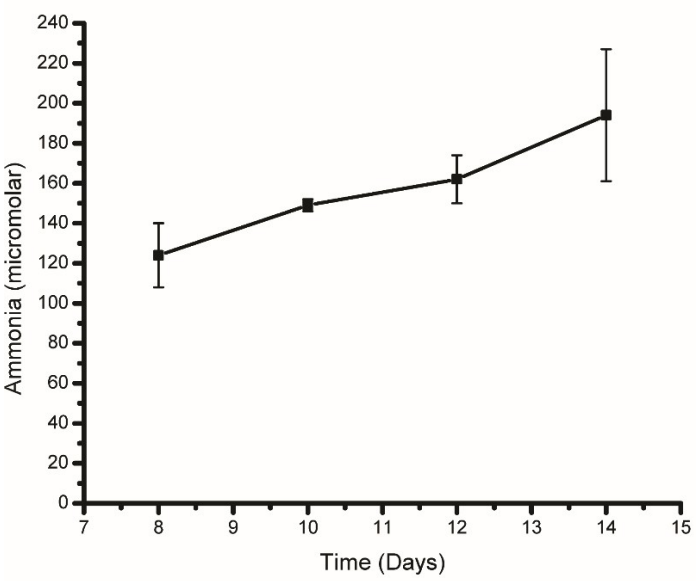

Figure 2.3. Ammonia production by *A. vinelandii* grown in monoculture in SAV media (=/-SD, N=3).

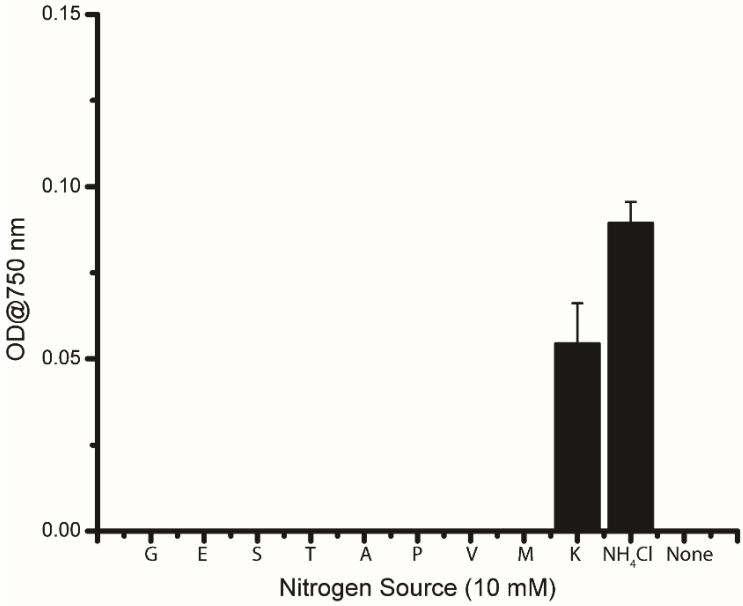

Figure 2.4. *S. elongatus* growth in SAV media grown on a variety of different nitrogen sources at 10 mM. Axis letters represent amino acid single letter codes. *S. elongatus* can only uptake ammonia and lysine as nitrogen sources. Data are the OD measurements at 5 d, with the OD at 0 d subtracted as a background level. The amino acids tested are those that have been found to be excreted by *A. vinelandii* (+/-SD, N=2).

We next asked whether *A. vinelandii* also benefits from the coculture depicted in Figure 2.2.

While carbon fixation by communities of cyanobacteria in the ocean likely play a key role in supplying carbon to heterotrophic organisms,[18] wildtype freshwater cyanobacteria cultured in a laboratory setting have not been shown to secrete significant amounts of carbon.[9,19]

Freshwater cyanobacteria have been shown to secrete small amounts of glycolate, a byproduct of photorespiration, into the supernatant.[20] However, glycolate cannot be utilized by *A. vinelandii*.[21] Interestingly, the closely related organism *A. chroococcum* can grow on glycolate, but the substrate is too oxidized to support nitrogen fixation.[21] Based on this, we hypothesized that *A. vinelandii* did not benefit from *S. elongatus* in terms of the generation of biomass. To test this, we grew the cells in dialysis bags in which the neighboring bag contained either the coculture partner or SAV media (Figure 2.5A). Cells in adjacent dialysis bags could share metabolities and other biomolecules, but the transfer of whole cells was prevented to allow accurate quantification of both species at the end of the experiment. The dialysis experiments demonstrated that, while *S. elongatus* benefited from the presence of *A. vinelandii* in SAV media both in terms of OD (Figure 2.5B) and chlorophyll synthesis (Figure 2.5C), *A. vinelandii* did not benefit from the presence of *S. elongatus*. Ortiz-Marquez et al. observed similar results when they cocultured microalgae with *A. vinelandii*.[8] Taken together, these results suggested that if we engineered *S. elongatus* to secrete a reduced carbon source, we could obtain a mutually beneficial coculture.

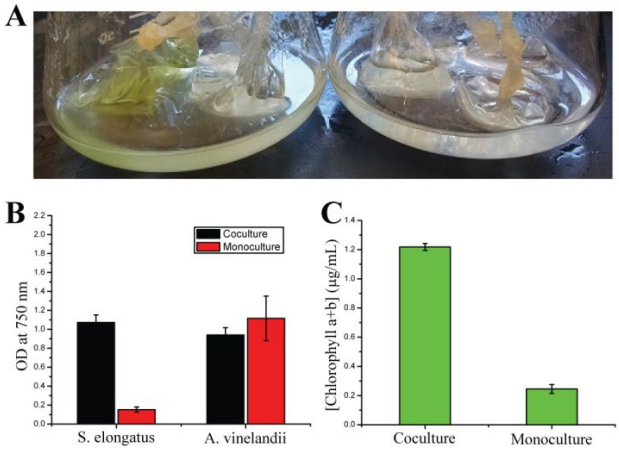

Figure 2.5. Dialysis tests to determine nature of coculture. (A) *S. elongatus* benefits from the presence of *A. vinelandii* in terms of (B) OD and (C) chlorophyll production. *A. vinelandii* does not benefit from the presence of *S. elongatus*. Each timepoint was performed in biological triplicate. (+/- SD, N=3)

2.4.2. Engineering the coculture to grow without fixed carbon and nitrogen

Ducat et al. have reported the development of an engineered *cscB S. elongatus*, which fixes CO_2 from the atmosphere and exports sucrose in salt water.[9] We engineered *cscB S. elongatus* in an analogous fashion, but used either an IPTG-inducible promoter or a light-activated psbA1 promoter (Figure 2.6).[22] The results shown in Figures 2.7-2.28 were obtained with the psbA1 promoter, as the IPTG-inducible promoter resulted in similar coculture growth. We also redesigned the SAV media to contain neither fixed carbon nor nitrogen, including no citrate and no EDTA. Sodium bicarbonate was added to the media prior to use to increase the concentration of dissolved carbon dioxide and, thus, the growth rate. This modified minimal media is referred to as "CAV" herein. In Figure 2.7 we depict the growth of the coculture with and without sodium bicarbonate present.

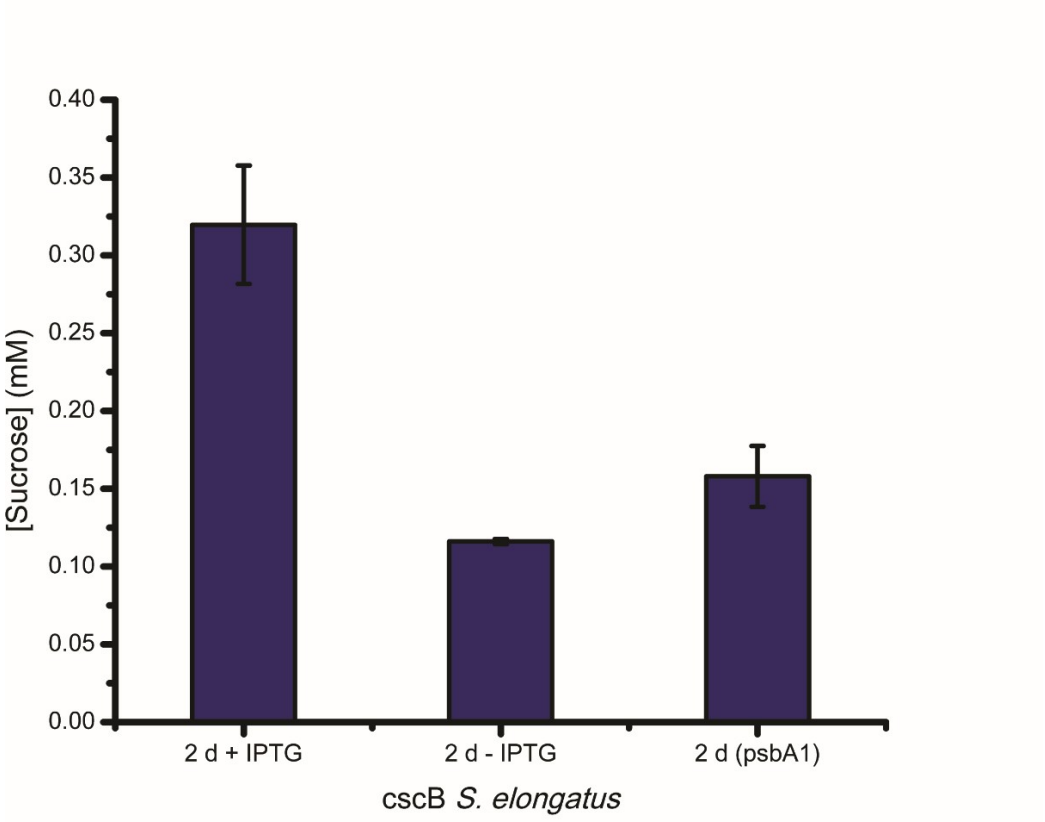

Figure 2.6. Sucrose production by various *cscB S. elongatus* mutants measured after 2 d using a sucrose assay kit. Each timepoint was performed in biological triplicate (+/-SD, N=3).

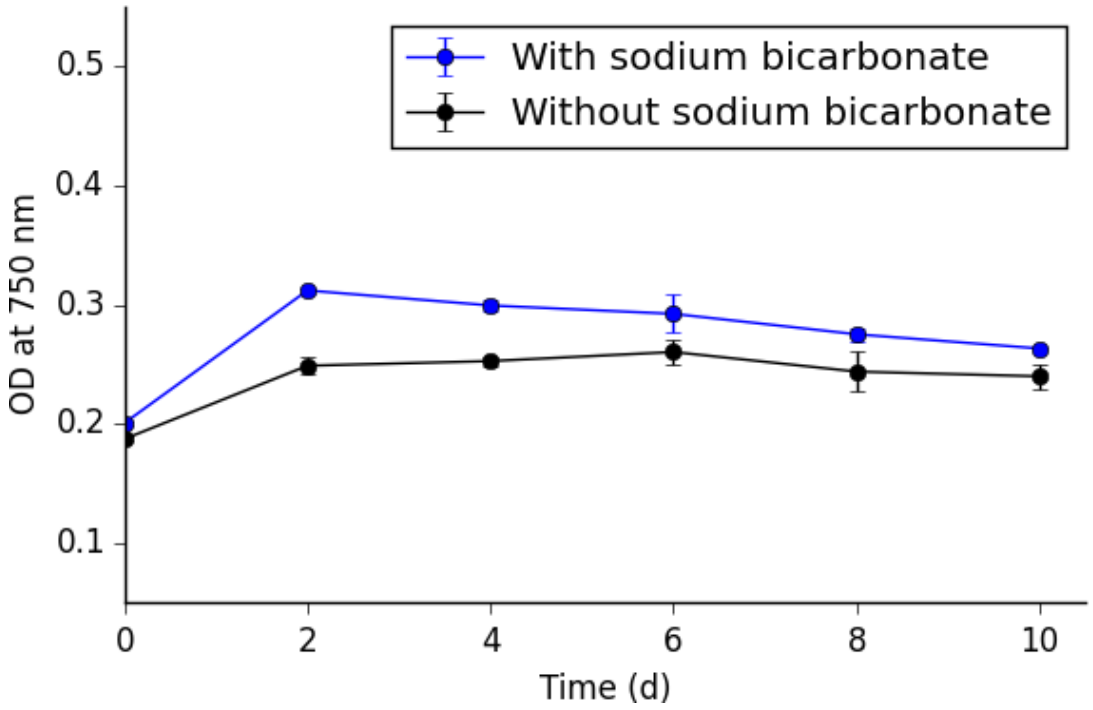

Figure 2.7. Coculture grown with and without sodium bicarbonate. A *cscB*-AV3 coculture (3:1 initial ratio) was grown in 30 mL of media with or without 0.05 g of sodium bicarbonate.

As shown in Figure 2.8, wildtype *A. vinelandii* grown with *cscB S. elongatus* grows without fixed carbon or nitrogen (albeit slowly), whereas wildtype *A. vinelandii* with wildtype *S. elongatus* does not grow at all. At this point, we hypothesized that a reduced carbon source was now available to *A. vinelandii*, and ammonia secretion had become limiting (Figure 2.1B).

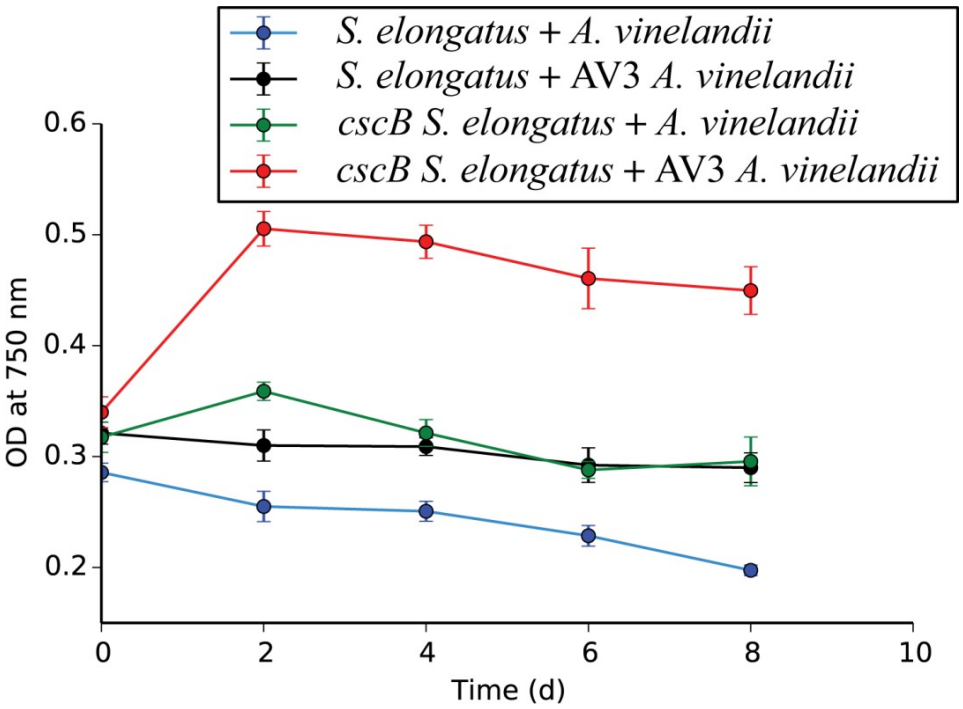

Figure 2.8. Engineered and wildtype cocultures grown without any fixed organic carbon or nitrogen. (A) The wildtype coculture does not grow over a period of 12 d and (B) exhibits less chlorophyll production than the engineered cocultures. The *cscB S. elongatus* + wt *A. vinelandii* coculture grows slower and synthesizes less chlorophyll than the *cscB S. elongatus* + AV3 *A. vinelandii* combination over 10 d. The starting cell ratios of the wt+wt coculture=96:4 *S. elongatus*:*A. vinelandii*, wt+AV3=96:4, *cscB*+wt=95:5, *cscB*+AV3=96:4. (C) Dialysis experiments were performed in CAV media. OD was measured after 10 d in solution (+/- SD, N=3).

It has been known for over a decade that deleting the *nifL* gene of *A. vinelandii* results in constituitive nitrogenase expression, and therefore the enhanced secretion of ammonia.[23] This is particularly effective due to the aerobic tolerance of the nitrogen fixing system used by this

organism. Thus, to improve the efficiency of our system, we added a Δ*nifL A. vinelandii* (AV3)[8] to the coculture and observed a significant increase in the overall growth (Figure 2.9) and the chlorophyll content after 10 d in solution (Figure 2.10A). This further validates our model of cross-feeding, and shows the direct improvement obtained by engineering both components (Figure 2.1C).

To quantify the increase in biomass that was derived from air, we lyophilized and weighed 10 mL portions of the AV3+*cscB* culture grown without sodium bicarbonate at 0 d and 6 d and saw roughly a 60% increase in mass (0 d: 91 ± 6 mg; 6 d: 145 ± 5 mg; +/- SD, N=3). A control coculture comprising AV3 *A. vinelandii* and wildtype *S. elongatus* did not grow in in CAV media (Figure 2.9).

Dialysis experiments were again performed to demonstrate that *A. vinelandii* grew to higher optical densities in CAV media going from (1) the wildtype coculture to (2) the *cscB* + wildtype coculture to (3) the *cscB* + AV3 coculture (Figure 2.10B). *S. elongatus* received only a small growth benefit in the engineered cocultures, suggesting that it grew slowly in the CAV coculture overall.

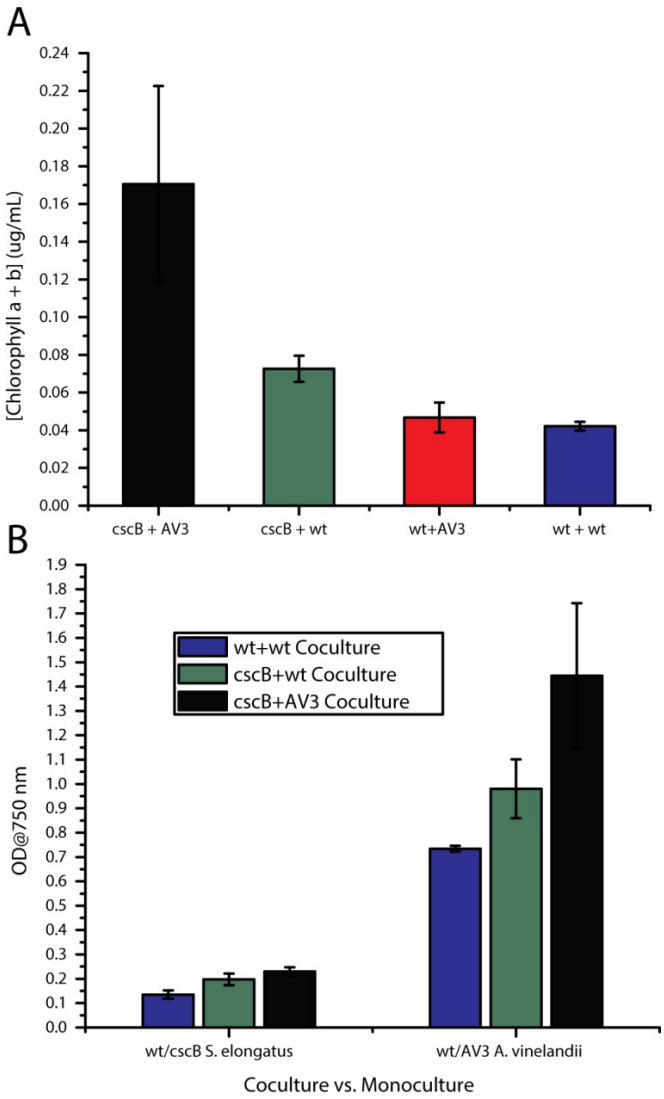

Figure 2.9. Engineered and wildtype cocultures grown without any fixed organic carbon or nitrogen. (A) The wildtype coculture does not grow over a period of 12 d and (B) exhibits less chlorophyll production than the engineered cocultures. The *cscB S. elongatus* + wt *A. vinelandii* coculture grows slower and synthesizes less chlorophyll than the *cscB S. elongatus* + AV3 *A. vinelandii* combination over 10 d. The starting cell ratios of the wt+wt coculture=96:4 *S. elongatus*:*A. vinelandii*, wt+AV3=96:4, *cscB*+wt=95:5, *cscB*+AV3=96:4. (C) Dialysis experiments were performed in CAV media. OD was measured after 10 d in solution (+/- SD, N=3).

We would expect that the enhanced ammonia-excreting strain of *A. vinelandii* would lead to a higher relative ratio of *S. elongatus* to *A. vinelandii* cells, and flow cytometry data after 24 d in CAV media, diluting 1 to 10 every 8 d, supported this conclusion (Figure 2.10A). After 24 d,

the viable cell population for the *cscB S. elongatus* and AV3 *A. vinelandii* coculture contained roughly 10% *cscB S. elongatus*, which was higher than that for the *cscB S. elongatus* and wildtype *A. vinelandii* coculture (Figure 2.10A).

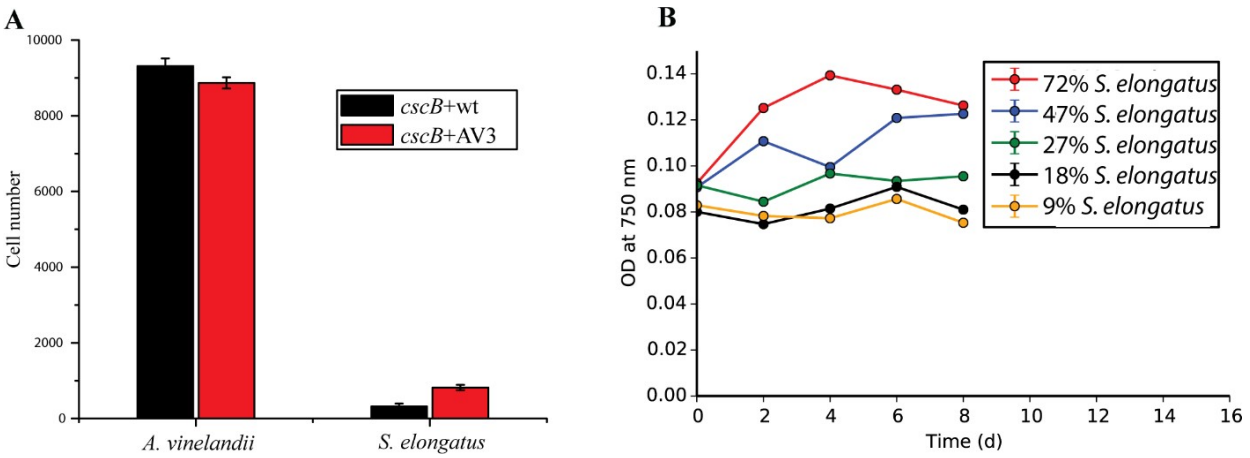

Figure 2.10. Coculture growth as a function of cell ratio and density. (A) The cell ratios after 24 d in CAV media, diluting 1:10 every 10 d, were determined by flow cytometry. *A. vinelandii* cells were the viable non-autofluorescent cells. *S. elongatus* were the viable autofluorescent cells. There were more *S. elongatus* cells in the *cscB*+AV3 coculture. Viability was determined via CFDA dye (+/- SD, N=3). (B and C) The starting cell ratio affected the cell growth of the *cscB*+AV3 coculture at various starting cell densities. Ratio 1= 9:91 *S. elongatus*:*A. vinelandii*, Ratio 2= 18:82, Ratio 3= 27:73, Ratio 4= 47:53, Ratio 5= 72:28 *S. elongatus*:*A. vienlandii*. (D) The starting cell density affected the cell growth of *cscB*+AV3 coculture. Green line=95:5 *S. elongatus*:*A. vinelandii*, Black line=95:5, Blue line=72:28 (+/- SD, N=3).

Growth of the *cscB S. elongatus* and AV3 *A. vinelandii* coculture in CAV media was found to be highly dependent on both the starting cell ratio (Figure 2.10B and 2.11A) and the starting cell density (Figure 2.11B). In contrast, the growth of the wildtype coculture in SAV media was ultimately dependent on the amount of glutamate added to the media. Figure 2.8 represents the growth of the coculture with a starting cell ratio for all 4 cocultures of roughly 95:5 *S. elongatus* to *A. vinelandii*, which is far from the equilibrium value reported above (Figure 2.10A). Coculture growth was observed when the starting cell ratio was enriched in *cscB S. elongatus* (Figure 2.10B and 2.11A). The importance of the starting cell ratio to coculture growth supports our observations that the *cscB* + AV3 coculture resulted in a higher concentration of chlorophyll, but only a slight increase in *S. elongatus* biomass after 10 d in solution. Figure 2.11A demonstrates that coculture growth is affected by the number of *S. elongatus* cells used to initiate the coculture. This result can be explained by the dependence of the coculture on the sucrose exported by *S. elongatus* and the minimal growth of *S. elongatus* in coculture. Volumetric flow cytometry analysis supports this conclusion and enables the correlation of optical density data to increases in the number of *A. vinelandii* cells (Figures 2.12 and 2.13). Furthermore, using flow cytometry data, the generation time of *A. vinelandii* over 0 d to 2 d was plotted versus the starting percentage of *S. elongatus*. This analysis demonstrated that AV3 *A.*

vinelandii grows faster in the presence of increasing amounts of *cscB S. elongatus* (Figure 2.13).

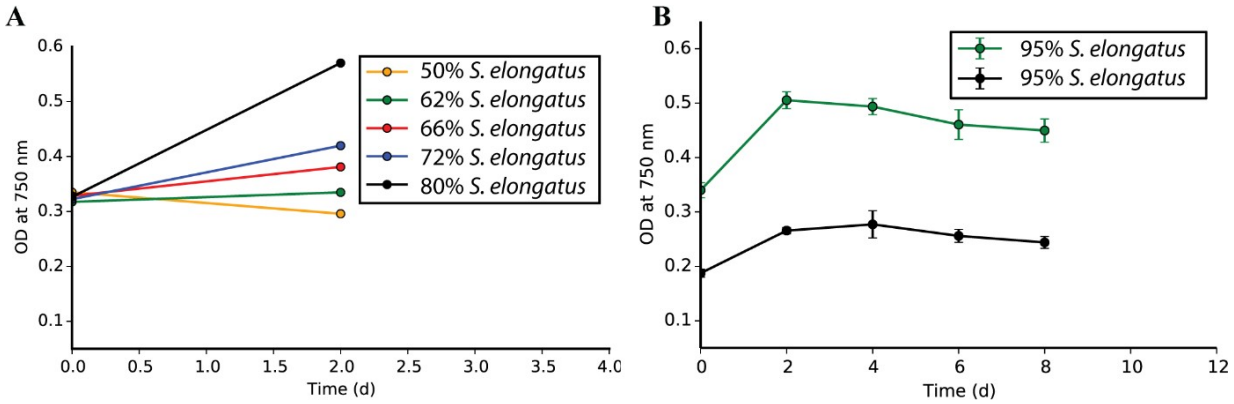

Figure 2.11. Coculture growth as a function of cell ratio and density. (A) The cell ratios after 24 d in CAV media, diluting 1:10 every 10 d, were determined by flow cytometry. *A. vinelandii* cells were the viable non-autofluorescent cells. *S. elongatus* were the viable autofluorescent cells. There were more *S. elongatus* cells in the *cscB*+AV3 coculture. Viability was determined via CFDA dye (+/- SD, N=3). (B and C) The starting cell ratio affected the cell growth of the *cscB*+AV3 coculture at various starting cell densities. Ratio 1= 9:91 *S. elongatus*:*A. vinelandii*, Ratio 2= 18:82, Ratio 3= 27:73, Ratio 4= 47:53, Ratio 5= 72:28 *S. elongatus*:*A. vienlandii*. (D) The starting cell density affected the cell growth of *cscB*+AV3 coculture. Green line=95:5 *S. elongatus*:*A. vinelandii*, Black line=95:5, Blue line=72:28 (+/- SD, N=3).

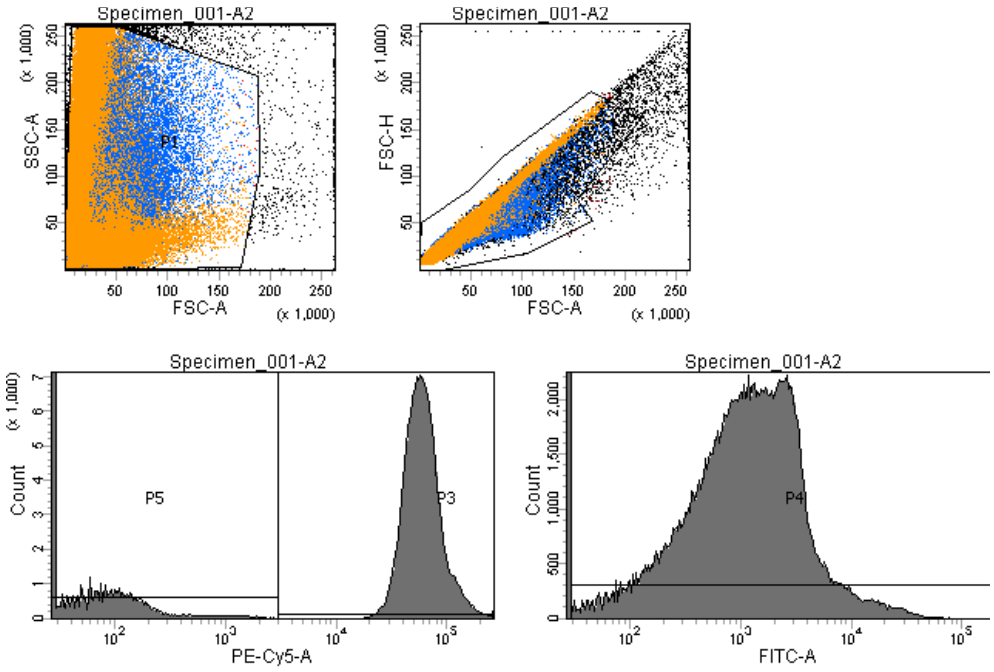

Well: A2

Population	#Events	%Parent	%Total
All Events	299,387	####	100.0
P1	271,597	90.7	90.7
P2	271,577	100.0	90.7
P3	165,131	60.8	55.2
P5	106,446	39.2	35.6
P4	56,865	53.4	19.0

Figure 2.12. Flow cytometry setup. The obligate photoautotrophic *S. elongatus* cells were identified via their red autofluorescence and the gates were established using a monoculture sample. *A. vinelandii* were identified as any cell that was not autofluorescent in the red channel but that fluoresced green in the presence of carboxyfluorescein diacetate (CFDA). Gates were established using monoculture samples.

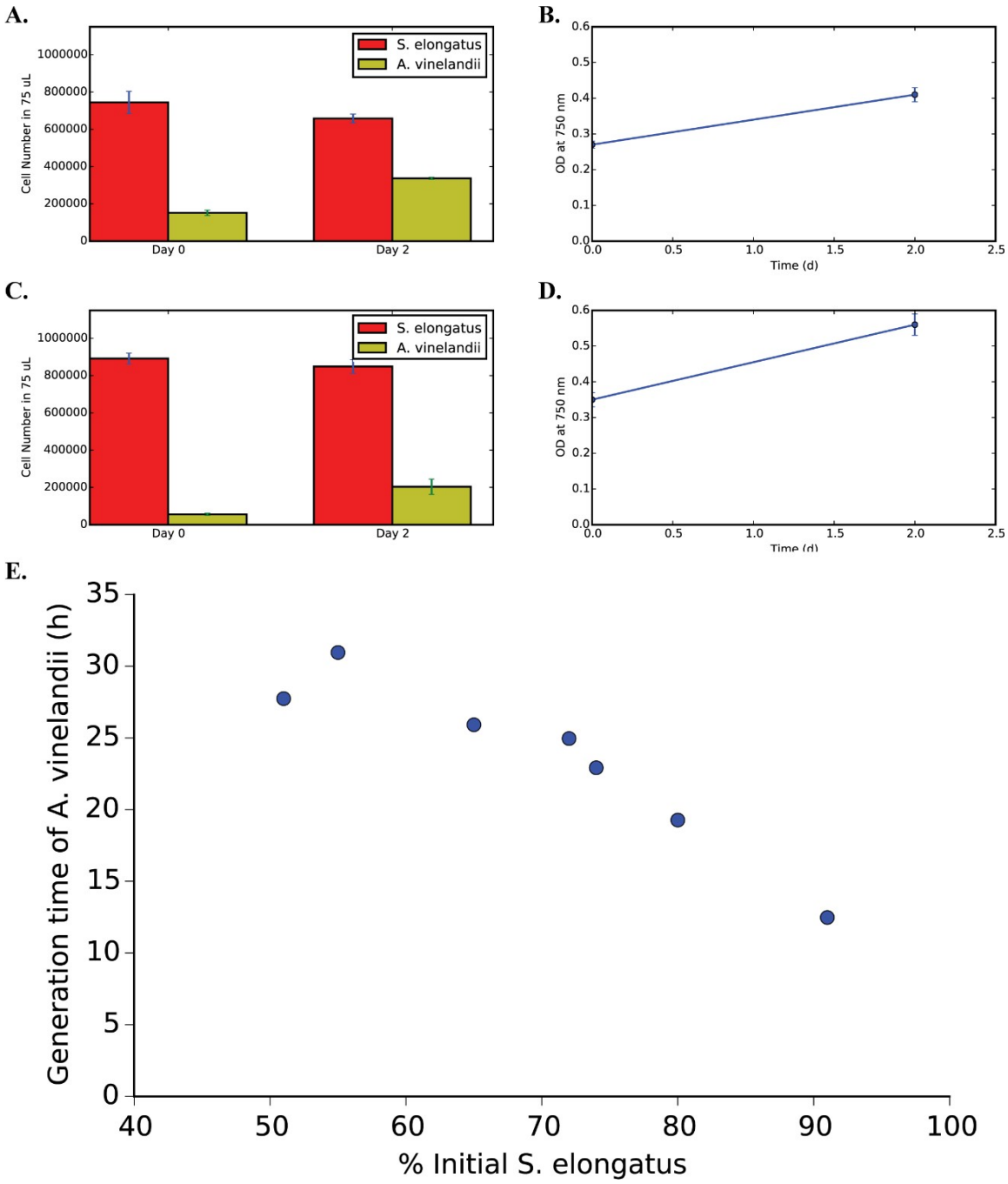

Figure 2.13. Flow cytometry analysis of AV3 *A. vinelandii* and *cscB S. elongatus* coculture growth. (A-D) Optical density growth at 750 nm (B and D) correlated to volumetric flow cytometry data (A and C) indicates that from 0 d to 2 d *S. elongatus* grows very little and *A. vinelandii* is responsible for most of the coculture growth. (E) The generation time of *A. vinelandii* from 0 d to 2 d versus the percent *S. elongatus* in the initial coculture was plotted.

We next investigated the ability of this coculture to make PHB. After 5 d of growth, PHB production as a percent of the dried coculture cell weight was 19 ± 2%. The starting optical density at 750 nm of these cocultures was 0.3 and the starting cell ratio was 90:10 *S. elongatus*:*A.vinelandii*. *Azotobacter vinelandii* can accumulate under some conditions between 80-90% of their dry weight as PHB.[24] However, we are measuring the percentage of PHB in the coculture, so much of the dry weight is due to non-PHB accumulating *S. elongatus* cells. Furthermore, optimal PHB accumulation occurs when carbon is present in excess and a nutrient such as oxygen is limiting and the only supplied carbon source we provided for growth was bicarbonate/carbon dioxide. For these reasons, we feel that our PHB yield is promising, though there is room for improvement.

^{13}C labeled bicarbonate was used to demonstrate that *A. vinelandii* synthesized PHB from the sucrose secreted by *S. elongatus* (Figure 2.14). The incorporation of ^{13}C into PHB was quantified via analyzing the four-carbon containing monomer of PHB, crotonic acid, via GC-MS (Figure 2.15). Figure 2.14 demonstrates that the majority of the PHB found in the coculture is ^{13}C labeled, indicating that PHB was synthesized from carbon fixed and then secreted by *S. elongatus* and not from stored carbon present in the initial amount of *A. vinelandii* added, for example. Only 6% of the PHB monomer contained no ^{13}C label and roughly 57% of the analyzed monomer contained total ^{13}C incorporation. Furthermore, in Figure 2.14 the expected isotope pattern for crotonic acid with four ^{13}C labels incorporated was observed, with the 5 outcomes of the ^{13}C labeling of crotonic acid being color-coded. Growing AV3 *A. vinelandii* in the presence of non-isotopically enriched sucrose and ^{13}C bicarbonate resulted in unlabeled PHB, as expected (Figure 2.16).

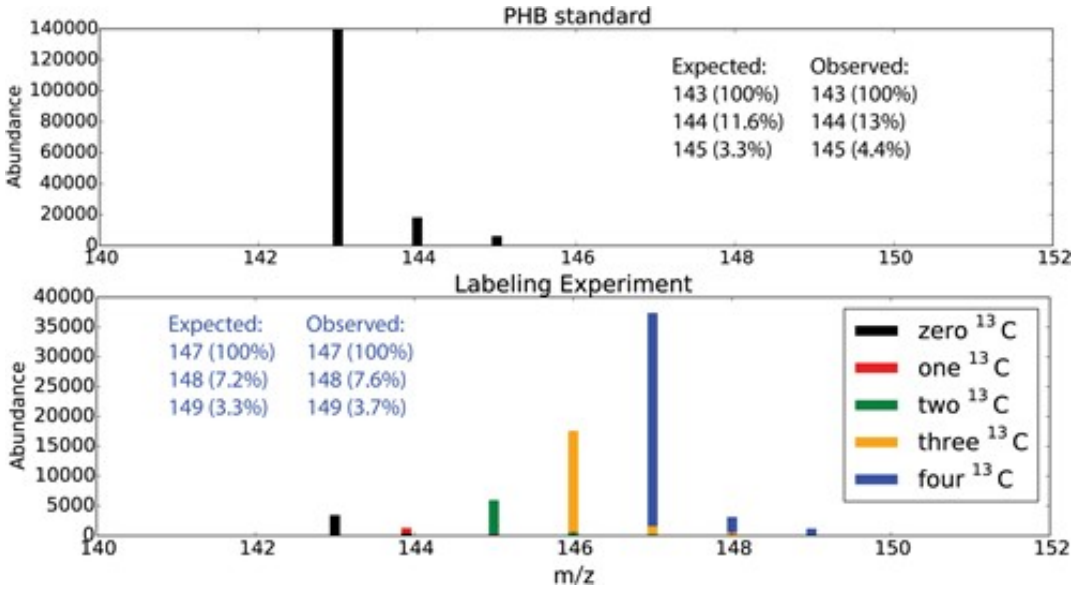

Figure 2.14. GC-MS traces demonstrating ^{13}C bicarbonate labeling. PHB either from a standard or that was extracted from the *cscB*-AV3 coculture that was grown in the presence of ^{13}C bicarbonate was hydrolyzed to crotonic acid, derivatized with BSA, and analyzed by GC-MS. The resulting isotopic patterns were compared. The labeling experiment demonstrates that the majority of the PHB monomer contains four ^{13}C incorporations (peak at 147 m/z).

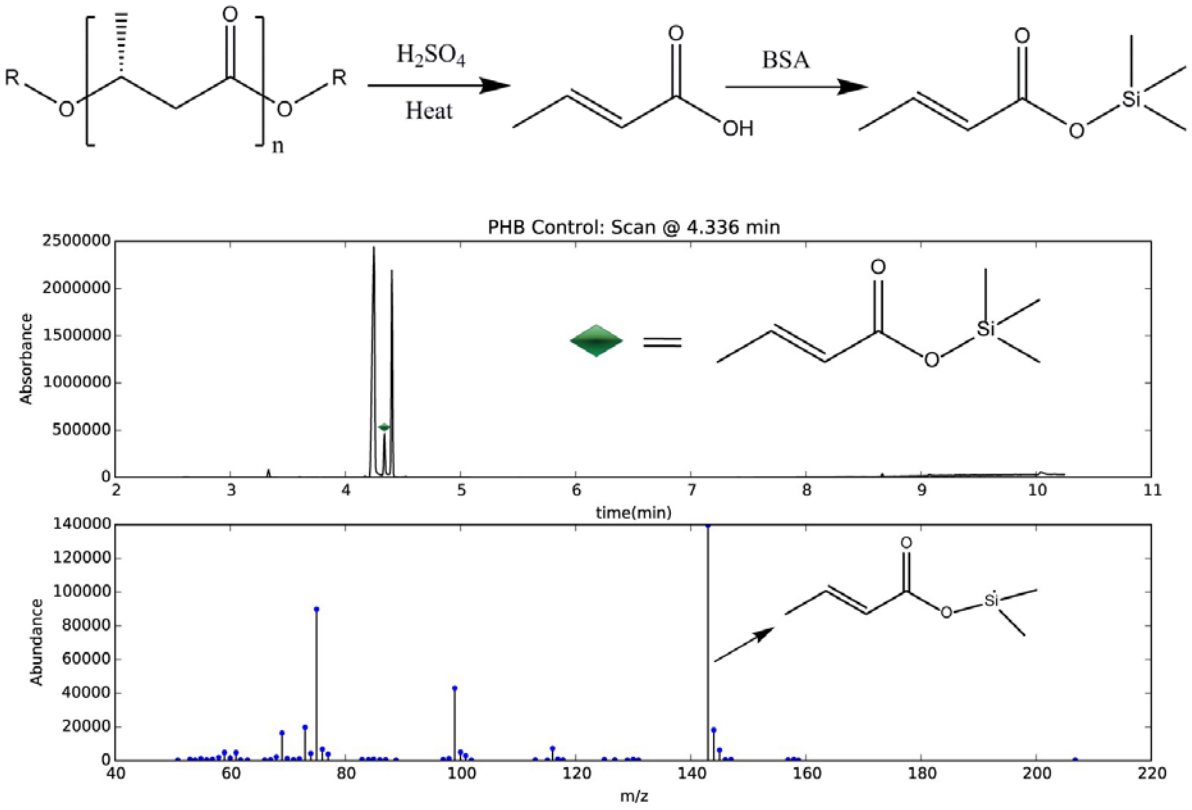

Figure 2.15. Analysis of ^{13}C incorporation into PHB. PHB was hydrolyzed in sulfuric acid to crotonic acid and then derivatized with BSA before injecting on the GC-MS. The derivatized crotonic acid eluted at 4.336 minutes. The peaks before and after 4.336 minutes are byproducts of the derivatization.

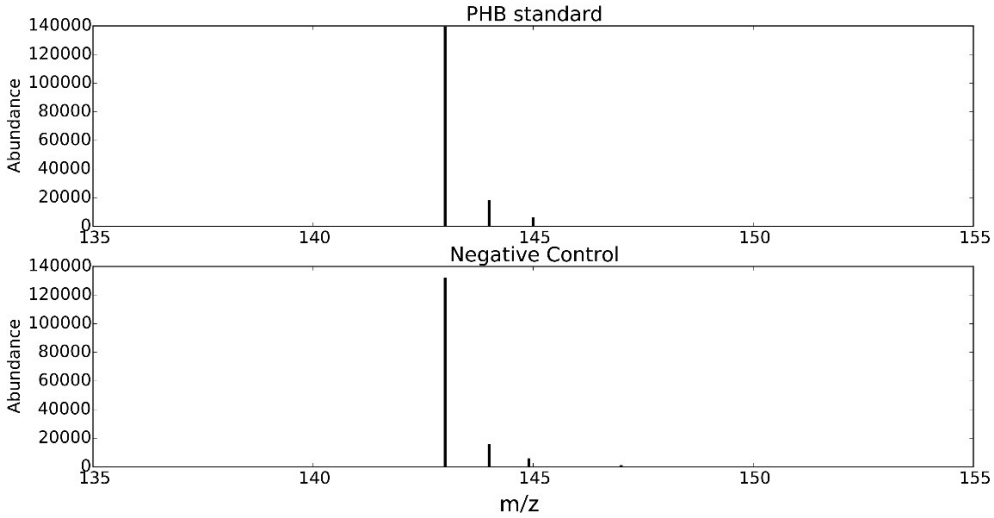

Figure 2.16. ^{13}C PHB negative control. *A. vinelandii* was grown in the presence of 0.5 g of sucrose and 0.2 g of ^{13}C labeled bicarbonate in 50 mL of liquid. The PHB was extracted from

these cells and analyzed via GC-MS.

This work started with an investigation of the growth of a wildype cyanobacteria and diazotroph. However, our investigation into the syntrophy of this coculture ultimately led us to develop a system where both carbon and nitrogen are shared and growth occurs in the absence of either fixed carbon or nitrogen. The engineered cocultures serve both to support our model of cross-feeding and represent an interesting synthetic biology platform (Figure 2.1).

However, this coculture does not grow over multiple subcultures as a consequence of the growth of the coculture being cell ratio controlled (Figure 2.10 and 2.11). Furthermore, salt stress triggers the production of osmoprotectants in *A. vinelandii* as well as *S. elongatus*. We hypothesized that this may limit the yield of PHB in our coculture. Both the issue of growth over multiple subcultures and the downsides of osmotic stress in our coculture led us to develop a novel way to grow cocultures where the autotrophic and heterotrophic components of the coculture were separated and the relative concentrations of the two microbes were controlled.

2.4.3. A biomaterial solution to coculture growth

Our efforts to develop a new method for growing the *A. vinelandii*/*S. elongatus* coculture began with the hypothesis that the swelling pressure[25,26] of a hydrogel would put osmotic stress on embedded cyanobacteria, thereby leading to sucrose production in *cscB S. elongatus* (Figure 2.17). Normally, given enough water, an unconstrained ionic hydrogel would expand to an equilibrium volume and experience no swelling pressure as the elastic forces of the polymeric material balance the osmotic forces within it.[27] Furthermore, at this equilibrium volume the chemical potential of the water outside the hydrogel is equal to the chemical potential inside the hydrogel. When we use a dialysis tube to constrain the hydrogel we apply a force on the hydrogel that raises the chemical potential of the water. However, if the hydrogel is confined within a volume that is smaller than this equilibrium amount, we hypothesized that it can exert an osmotic pressure on objects within that could be similar to that produced by high salt culturing conditions.

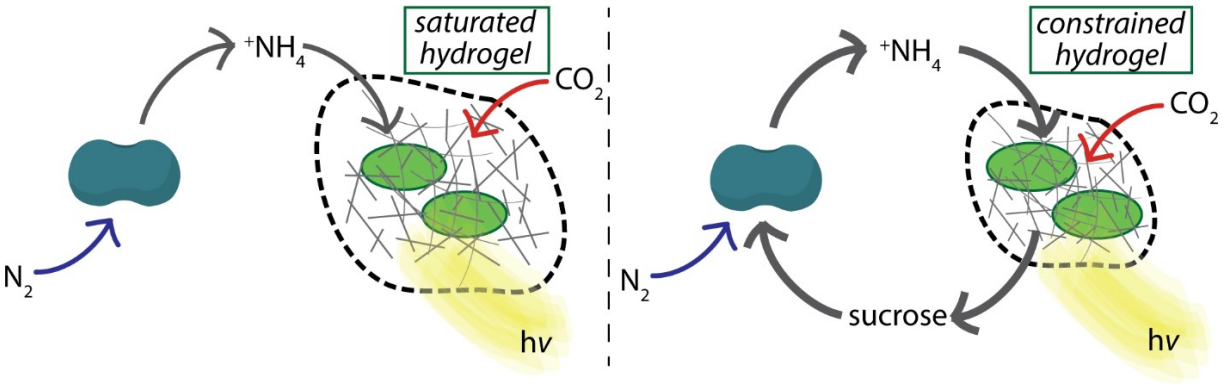

Figure 2.17. Sucrose production in spatially constrained hydrogels. (A) and (B) show a non-spatially constrained hydrogel containing *cscB Synechococcus elongatus* on the left and a spatially constrained hydrogel constaining *cscB S. elongatus* on the right. The hydrogels were spatially constrained in dialysis tubing by securing the ends with clamps. The hydrogel on the right secreted sucrose in media (0.2 mM sucrose after 2 d), while the hydrogel on the left did not (See Table 1 for data).

In this work, the hydrogel matrix is confined with limited media volumes or within dialysis tubes that constrain the volume of the hydrogel (Figure 2.18). There is literature

precedent for cells embedded in alginate hydrogels maintaining their viability, and even possessing greater enzymatic activity.[28] Alginate hydrogels containing embedded cells have also been reported in the context of a bioreactor.[29] However, the use of constrained ionic hydrogels to exert osmotic pressure on a species inside has not been reported.

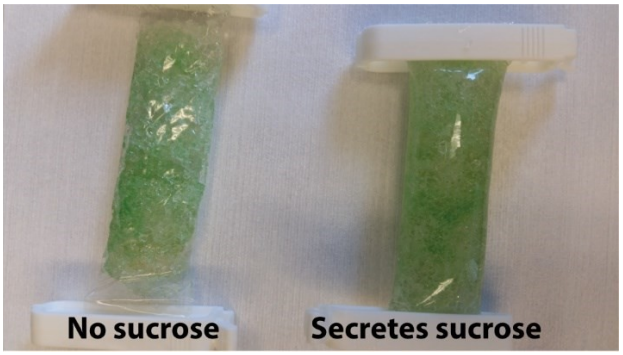

Figure 2.18. Sucrose production in spatially constrained hydrogels. (A) and (B) show a non-spatially constrained hydrogel containing *cscB Synechococcus elongatus* on the left and a spatially constrained hydrogel constaining *cscB S. elongatus* on the right. The hydrogels were spatially constrained in dialysis tubing by securing the ends with clamps. The hydrogel on the right secreted sucrose in media (0.2 mM sucrose after 2 d), while the hydrogel on the left did not (See Table 1 for data).

Crosslinked poly(sodium acrylate) hydrogels were chosen for this purpose because of their synthetic accessibility and low cost. We have found that they can be reused simply by washing with water and heating to 90 °C for 15 h. We first prepared polymers with varying *N*,*N*-methylene bisacrylate crosslinker ratios to determine the optimal structure of the resulting material for sucrose production (Figure 2.19). Varying the crosslinker ratio does not significantly impact the transparency of the hydrogel, at least not until a density of 16.8 mg/mL of the crosslinker (Figure 2.20). The swelling volume of each sample was determined by adding a fixed mass of polymer to a large volume of BG-11 media. After equilibration and full swelling, the excess media was removed and the remaining samples were weighed to determine the amount of liquid that was absorbed. As expected, increases in the amounts of crosslinker led to reductions in the swelling volumes of the polymers (Figure 2.19, black line). Other work has established quantitatively that changes in crosslinker density influence swelling pressure.[26]

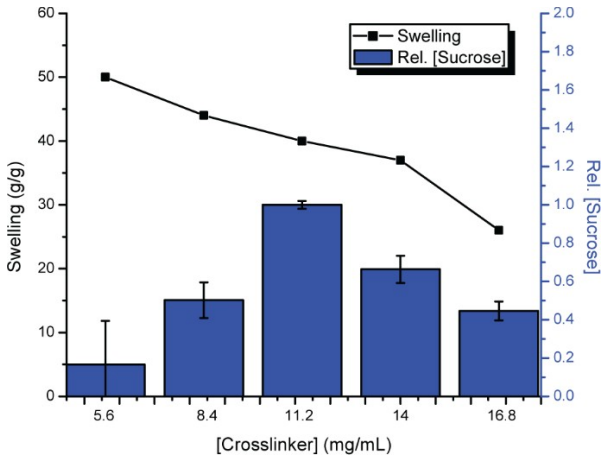

Figure 2.19. Sucrose production in hydrogels. (A) Sucrose production from *cscB S. elongatus* in sodium polyacrylate hydrogels varies with degree of crosslinker. Swelling is reported in grams of swelled hydrogel over grams of dry hydrogel. (B) The sucrose production by *cscB S. elongatus* in an optimized hydrogel (bar 2) is comparable to the sucrose production in media with 150 mM NaCl (bar 1). Wild-type *S. elongatus* in a hydrogel does not secrete sucrose, as seen in bar 3. *cscB S. elongatus* does not secrete sucrose without the hydrogel or the NaCl, bar 4 (N=3, +/- SD).

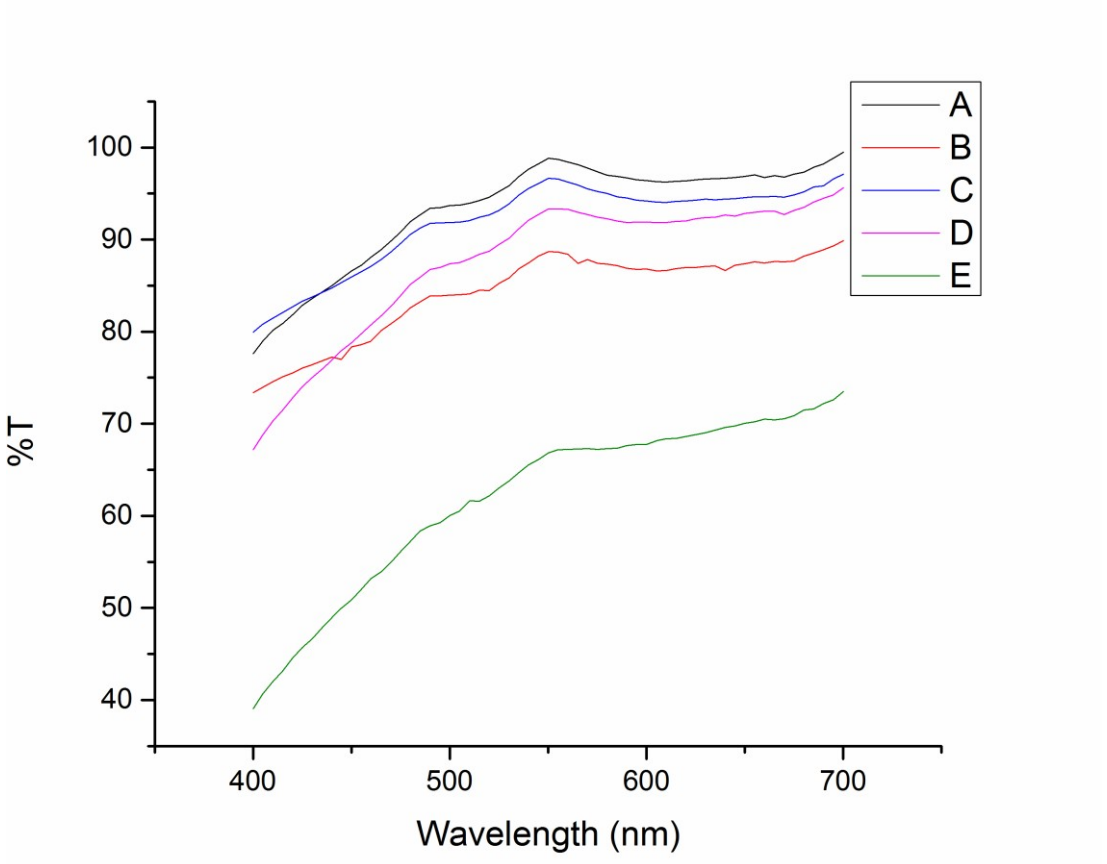

Figure 2.20. Percent transmittance with varying degrees of crosslinking. These values were obtained by adding roughly 0.05 g of hydrogel with different degrees of crosslinking

to 1 mL of H_2O in a cuvette. (A= 5.6 mg/mL crosslinker, B = 8.4 mg/mL, C = 11.2 mg/mL, D = 14 mg/mL, E = 16.8)

2.4.4. Sucrose production in the *cscB S. elongatus* hydrogel

Next, a uniform amount of *cscB S. elongatus* was added to equal weights of each polymer sample, along with an insufficient amount of water to saturate the hydrogels. By holding the volume of water constant, samples with similar ionic strengths, but differing swelling pressures were produced. After 2 d of culture under a constant light source, the sucrose concentration was determined using an enzymatic assay. The amount of sucrose produced was strongly affected by the degree of crosslinking, with an optimum amount of 56 mg/1.5 g sodium acrylate or 11.2 mg/mL of a 5 mL solution (Figure 2.19, blue bars). This generally reflects the literature observation that *cscB S. elongatus* sucrose production peaks at 150 mM NaCl and drops at both 100 and 200 mM NaCl.[19]

Based on visual inspection, the pore sizes of each hydrogel sample were sufficiently large to enable cell entrapment throughout the material. Confocal microscopy analyses of the strained *cscB S. elongatus* hydrogels indicated that the *S. elongatus* are found suspended throughout the hydrogel and tend to aggregate at bubbles and defects in the material (Figure 2.21). Furthermore, *cscB S. elongatus* only secretes sucrose in salt water or a hydrogel, but not in BG-11 media lacking either. In addition, no sucrose production was observed for *cscB S. elongatus* in calcium and barium cross-linked alginate hydrogels, though the precise reason for this lack of production was not determined. Wildtype *S. elongatus* does not secrete sucrose under any conditions explored, including in the presence of 150 mM NaCl (Figure 2.22).

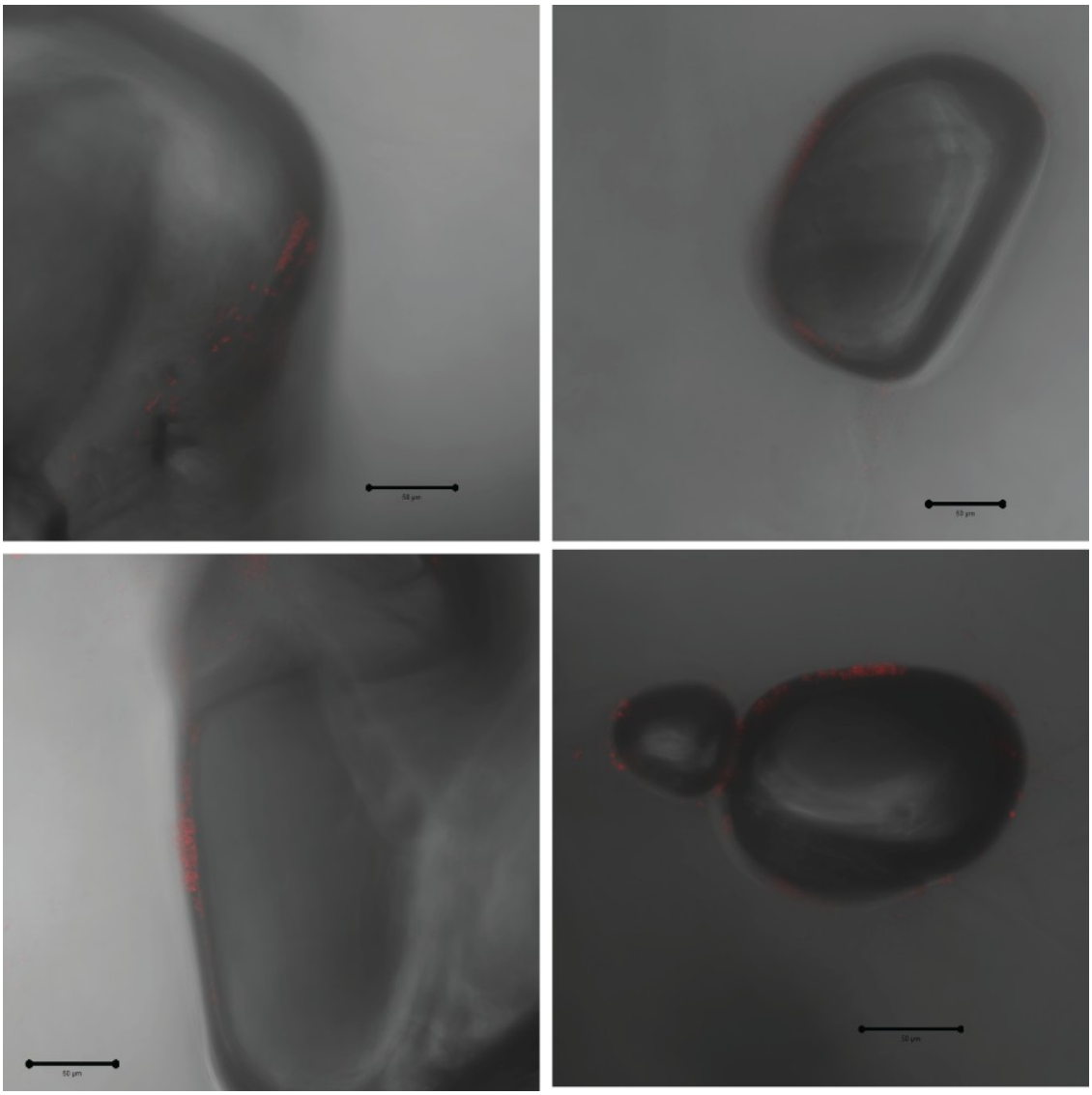

Figure 2.21. *cscB S. elongatus* in strained hydrogels. While *S. elongatus* can be found suspended throughout the hydrogel, it tends to aggregate around bubbles and defects in the material. Images taken on a Zeiss LSM 710 AxioObserver confocal microscope with a z-slice of 3.3 µm. Scale bars represent 50 µm.

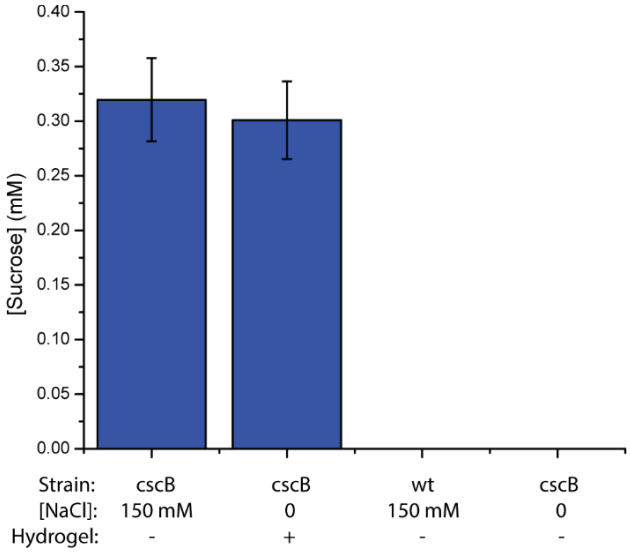

Figure 2.22. Sucrose production in hydrogels. (A) Sucrose production from *cscB S. elongatus* in sodium polyacrylate hydrogels varies with degree of crosslinker. Swelling is reported in grams of swelled hydrogel over grams of dry hydrogel. (B) The sucrose production by *cscB S. elongatus* in an optimized hydrogel (bar 2) is comparable to the sucrose production in media with 150 mM NaCl (bar 1). Wild-type *S. elongatus* in a hydrogel does not secrete sucrose, as seen in bar 3. *cscB S. elongatus* does not secrete sucrose without the hydrogel or the NaCl, bar 4 (N=3, +/- SD).

The goal of this work was to create a hybrid material that produces sucrose in low salt media, and to use this as a carbon source for additional organisms. To do this, we placed the hydrogels in dialysis tubing to constrain them spatially at sub-equilibrium volumes, while allowing small molecules to pass into the surrounding medium and preventing cells from leaving or entering the hydrogel. Known weights of hydrogel crosslinked at 11.2 mg/mL were combined with *cscB S. elongatus* and swelled initially in 3 mL of BG-11 medium. These samples were then added to dialysis tubes clamped at differing lengths to introduce volume constraints. Each sample was added to excess BG-11 media for 24 h, and then transferred to 10 mL of fresh media. Sucrose production was measured after 48 h of illumination. Following the experiment, the hydrogel materials were weighed to estimate their swelling volumes while in the dialysis tubes. Finally, each hydrogel was expanded to equilibrium with BG-11 media. A second determination of the weight allowed the fully saturated volume to be estimated. These data are summarized in Table 1. Notably, only hydrogels that were prevented from swelling to their maximum volume secreted sucrose into the media (Table 1; below the dashed line). Based on these data, the optimal culturing matrix of 0.5 g of polymer constrained in roughly 9 mL of BG-11 media was selected (represented by entry 7, Table 1).

Table 1. Sucrose production as a degree of hydrogel saturation. When the saturated mass of the hydrogel was equal to the mass of the hydrogel in the dialysis bag (entries above the dashed line), no detectable amounts of sucrose were produced (n.d = not detected). The sucrose concentration is measured in the 10 mL of media surrounding the hydrogel and the dialysis bag after 2 d, not including equilibration time. The hydrogel-dialysis bags were allowed to equilibrate in buffer for 24 h, at which point the buffer was replaced with the 10 mL of media

used to detect sucrose.

Sample	Dry hydrogel mass (g)	Init. vol. (mL)	Mass in dialysis bag (g)	Saturated mass (g)	[Sucrose] at 2 d (mM)
1	0.13	3	5.08	5.10	n.d
2	0.15	3	5.03	4.96	n.d
3	0.22	3	8.40	8.32	n.d
4	0.21	3	7.67	8.59	0.086
5	0.18	3	4.41	7.13	0.19
6	0.26	3	5.59	10.84	0.18
7	0.49	3	8.81	18.78	0.24
8	0.53	3	7.80	23.80	0.11

A new *cscB S. elongatus* culture was prepared using the optimized matrix and added to fresh media under illumination. The sucrose produced was determined at 2 d intervals. After each measurement, the media was replaced. As shown in Figure 2.23A, the strained hydrogel system secreted sucrose over multiple days, though the amount of sucrose decreased with time. This trend has also been demonstrated in other work for *cscB S. elongatus* UTEX 2973 in batch cultures in the presence of NaCl, though overall biomass accumulation continued to increase.[30] To determine whether the hydrogel-embedded *cscB S. elongatus* cells continued to grow, we monitored the concentration of chlorophyll over time in nine identically prepared strained *cscB S. elongatus* samples. The concentration of chlorophyll was found to increase over the 6 d monitoring period (Figure 2.23B) despite the fact that sucrose production decreased with time. It is anticipated that further optimizations of the *cscB* secretion system will yield more robust levels of sucrose secretion over multiple generations.

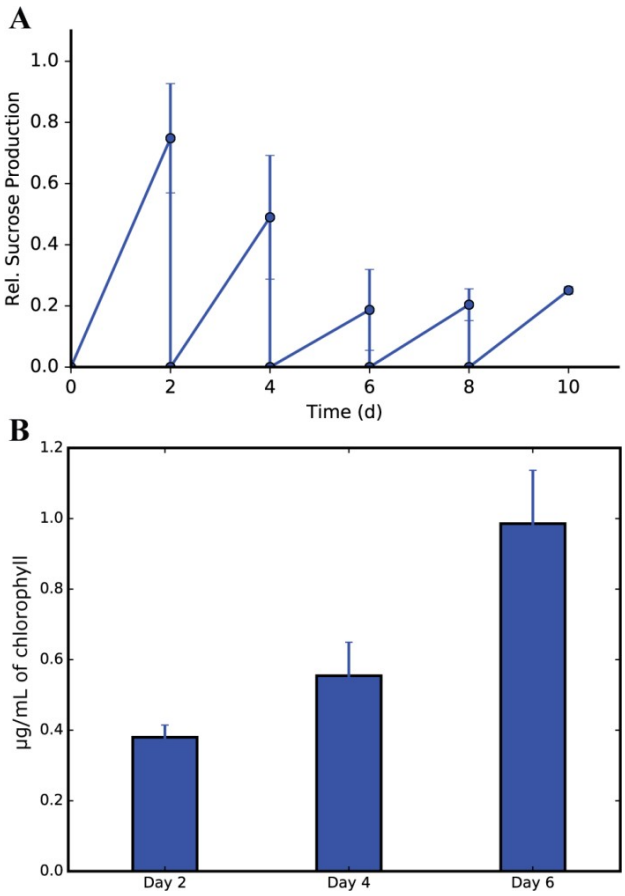

Figure 2.23. Sucrose production over time. (A) Sucrose production from a volume constrained *cscB S. elongatus* hydrogel over time in 10 mL of BG-11 media (pH = 8.8). The sample was diluted every 2 d (N=3, +/- SD). (B) Relative concentration of chlorophyll over time in dialysis bags prepared identically to sample 7 in Table 1 (N=3, +/- SD).

2.4.5. Use of the *cscB S. elongatus* hydrogel system in coculture

We next applied the use of the hydrogel system in a microbial coculture with *A. vinelandii* (Figure 2.24) as previously described by our lab.[1] In these experiments, the AV3 strain was used because it secretes more ammonia into the media than wildtype *A. vinelandii*.[8,23] We have found that PHB production by *A. vinelandii* decreases by roughly 50% upon the addition of 150 mM NaCl (Figure 2.25), making the strained hydrogel format potentially advantageous.

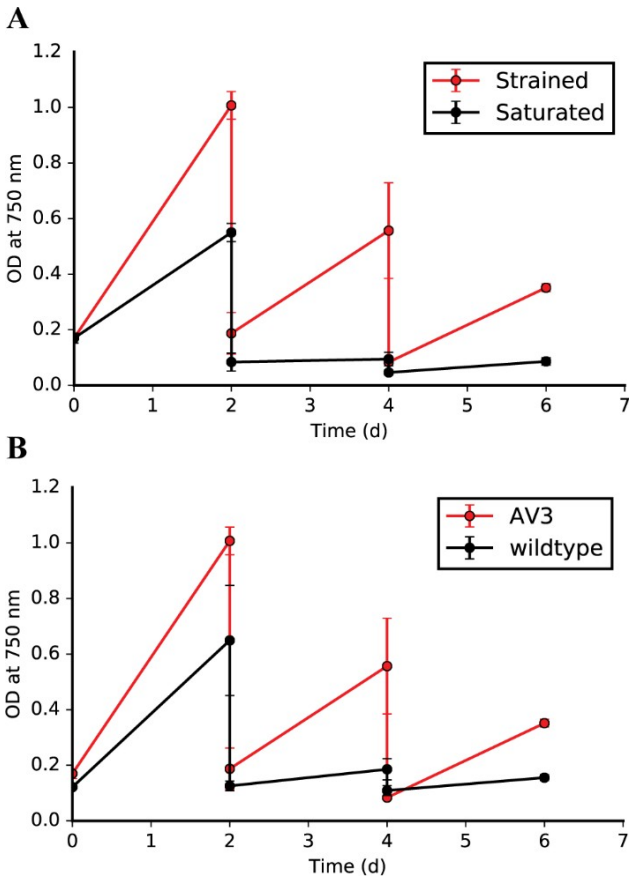

Figure 2.24. *A. vinelandii* growth supported by *cscB S. elongatus* hydrogels. The model shown in Figure 2.18 indicates that ammonia and sucrose are shared in the coculture system. (A) The growth of AV3 *A. vinelandii* was compared in saturated and strained hydrogels. (B) The growth of AV3 vs. wildtype *A. vinelandii* was compared with the constrained *cscB S. elongatus* hydrogel (N=3, +/- SD).

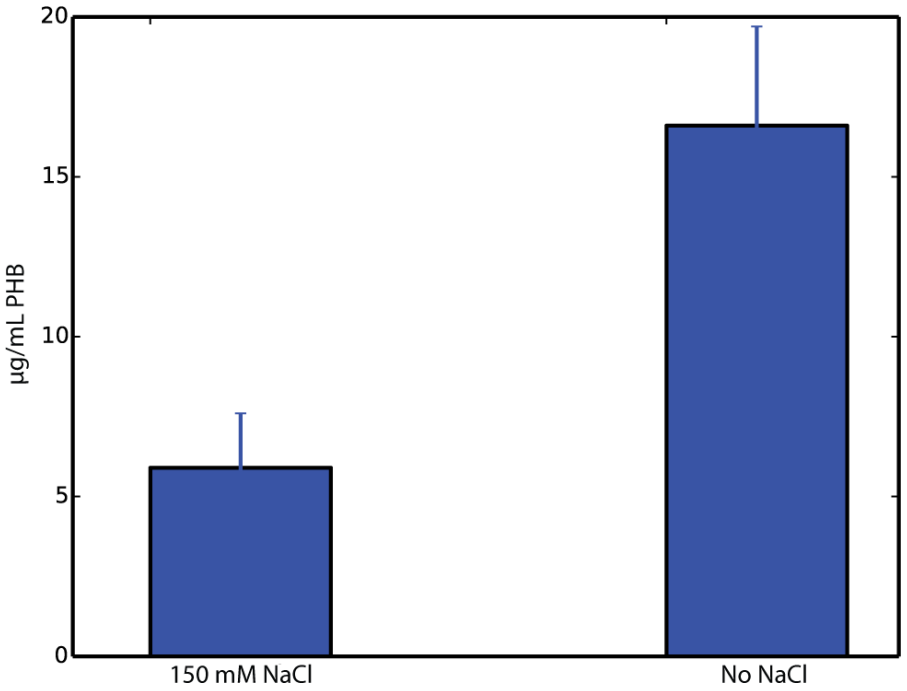

Figure 2.25. PHB production with or without NaCl. PHB was isolated from AV3 *A. vinelandii* after 3 d of growth in modified Burke's media at 250 rpm, 30 ºC, with or without 150 mM NaCl. The PHB was isolated from 5 mL cultures (N=3, ± SD).

As the growth of the analogous bulk coculture has been shown to be limited by the starting number of *cscB S. elongatus*,[1] a large, concentrated amount was first prepared in the hydrogel. A dialysis tubing constrained sample was placed in BG-11 media (pH = 8.8) for 1 d to ensure complete hydrogel swelling. The *cscB S. elongatus* hydrogel was then added to CAV media containing AV3 *A. vinelandii*. The AV3 *A. vinelandii* grew rapidly in the presence of the strained *cscB S. elongatus* hydrogel, compared to a control sample prepared with *cscB S. elongatus* in a fully saturated hydrogel (Figure 2.24B). Moreover, unlike the analogous batch coculture, we were able to dilute the AV3 *A. vinelandii* containing medium and see continued growth. The batch coculture sample exhibited minimal continuous growth over that time period (Figure 2.26).

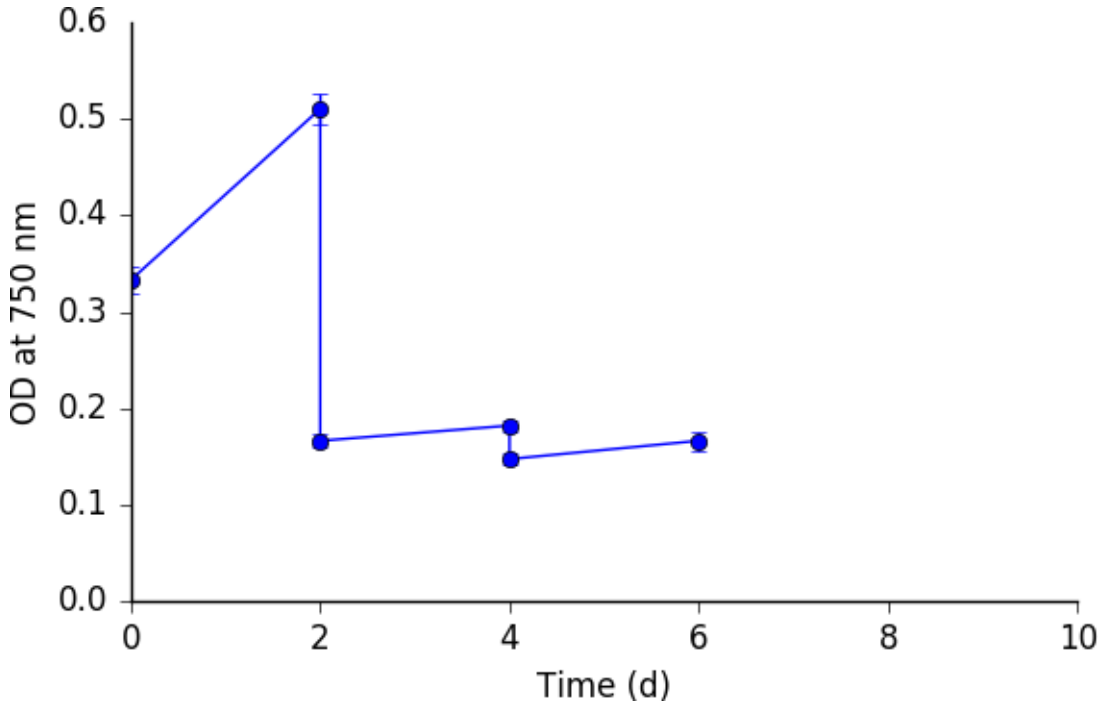

Figure 2.26. Continuous *S.elongatus*/*A. vinelandii* coculture growth. The *cscB S. elongatus*/AV3 *A. vinelandii* coculture does not grow continuously when grown in batch in CAV media. The sample was diluted 10-fold on days 2 and 4, resulting in the vertical line drops (N=3, ± SD).

The crossfeeding model in Figure 2.17 suggests that fixed nitrogen produced by *A. vinelandii* can support increased sucrose production by the *cscB S. elangatus*. One indication of this would be an increase in AV3 *A. vinelandii* growth relative to the wild-type strain, which produced less ammonia. Both strains grow at identical rates as monocultures (Figure 2.27). When grown in the presence of a constrained *cscB S. elongatus* hydrogel, AV3 *A. vinelandii* did exhibited markedly increased growth rates (Figure 2.24B).

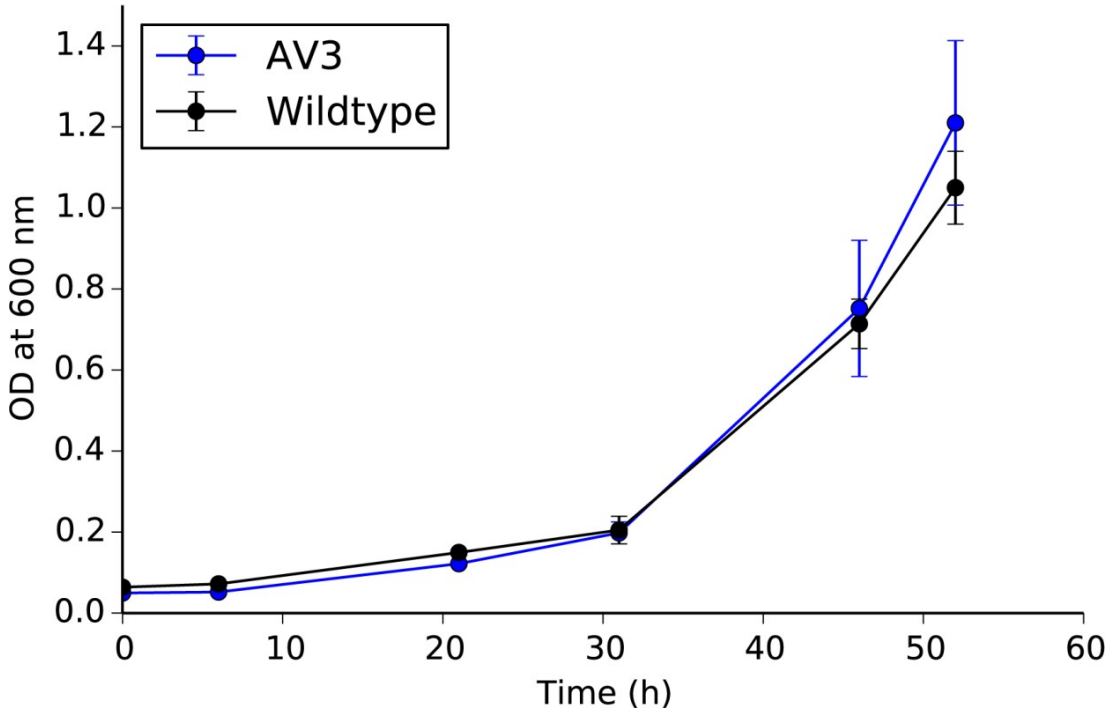

Figure 2.27. Growth of AV3 versus wildtype *A. vinelandii*. AV3 and wildtype *A. vinelandii* grow at similar rates in Burke's modified medium over 2 d at 250 rpm and 30 ºC. (N=3, ± SD)

At the same time points, PHB was isolated from each *A. vinelandii* sample. At 2, 4 and 6 d, significantly more PHB was isolated from AV3 *A. vinelandii* grown in contact with strained *cscB S. elongatus* hydrogels than in the presence of fully swelled hydrogels (Figure 2.28). This result confirms that the physical properties of the gel matrix can have a direct consequence on the production ability of metabolites by external organisms

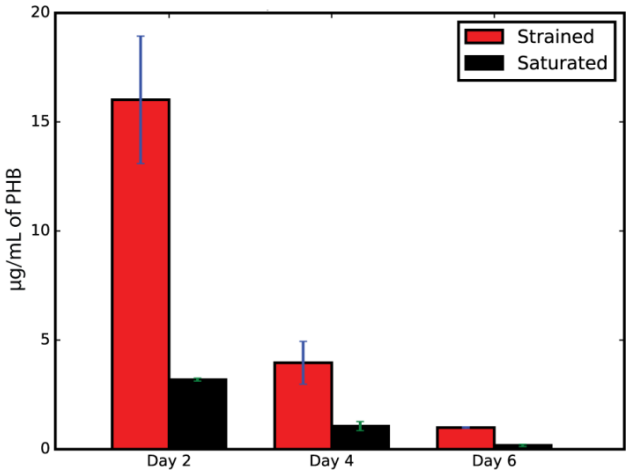

Figure 2.28. PHB production from AV3 *A. vinelandii*/*cscB S. elongatus* hydrogel cocultures. PHB was isolated from AV3 *A. vinelandii* every 2 d from media in contact with either strained or saturated *cscB S. elongatus* hydrogels. The media was replaced every 2 d (N=3, +/- SD).

2.5. Conclusions

A new swelling pressure mechanism has been demonstrated for controlling the osmotic stress endured by a coculture partner. The degree of crosslinking and the overall swelling volume of the anionic polymer matrix were both found to be important for this effect to occur. *cscB S. elongatus* embedded within the material secretes sucrose over multiple days in the presence of light. This system could be used to support the growth of a number of different producing organisms without requiring the use of high salt culturing conditions. Furthermore, this hydrogel has led to the improved growth of AV3 *Azotobacter vinelandii* in coculture. This coculture system produces a bioplastic, PHB, from minimal fixed carbon and nitrogen inputs.
In the broader context, this work indicates that material science strategies can help improve bacterial coculture growth. Industrially, cyanobacteria and algae have been grown using a variety of methods ranging from salt water pools[31] to suspended polyethylene bags.[32] Constrained poly(sodium acrylate) hydrogels could be ideal components in these systems due to their ease of synthesis, low cost, and potential reusability.

This system could be used to make a wide variety of interesting compounds/polymers in addition to PHB either with the system we describe or with additionally engineered *A. vinelandii* and/or *S. elongatus* strains. Engineered strains of *Azotobacter vinelandii* that overproduce either polyhydroxybutyrate or alginate have already been described,[24] and it seems likely that similar approaches would be amenable to Δ*nifL A. vinelandii*. Work towards this goal is currently underway in our lab. The growth dependency of the coculture on the starting cell ratio and starting cell number of *cscB S. elongatus* cells suggests the need for investigating coculture growth strategies that move beyond batch systems and possibly the development of a faster growing *cscB* cyanobacteria coculture partner, such as *S. elongatus* UTEX 2973.[33]

This coculture could serve as an interesting system for more basic science applications as well. Specifically, we envision that this system could be a useful model system for studying obligate mutualisms since both organisms are well-studied and their genomes have been sequenced.[5,34]

In this work, a system where both fixed carbon and fixed nitrogen are shared was designed allowing the coculture to grow from air, water, phosphate and trace metals. Designed microbial communities are underutilized in biotechnology applications and we hope that this research will join a growing body of work that suggests the designed coculture of microorganisms can lead to more sustainable materials for the chemical industry.

2.6. References

(1) Smith, M. J.; Francis, M. B. *ACS Synth. Biol.* **2016**, *5* (9), 955.

(2) Smith, M. J.; Francis, M. B. *Biotechnol. Bioeng.* **2017**, *114* (6), 1195.

(3) Bader, J.; Mast-Gerlach, E.; Popović, M. K.; Bajpai, R.; Stahl, U. *J. Appl. Microbiol.* **2010**, *109* (2), 371.

(4) Goers, L.; Freemont, P.; Polizzi, K. M. *J. R. Soc. Interface* **2014**, *11* (96), 20140065.

(5) Setubal, J. C.; dos Santos, P.; Goldman, B. S.; Ertesvag, H.; Espin, G.; Rubio, L. M.; Valla, S.; Almeida, N. F.; Balasubramanian, D.; Cromes, L.; Curatti, L.; Du, Z.; Godsy, E.; Goodner, B.; Hellner-Burris, K.; Hernandez, J. A.; Houmiel, K.; Imperial, J.; Kennedy, C.; Larson, T. J.; Latreille, P.; Ligon, L. S.; Lu, J.; Maerk, M.; Miller, N. M.; Norton, S.; O'Carroll, I. P.; Paulsen, I.; Raulfs, E. C.; Roemer, R.; Rosser, J.; Segura, D.; Slater, S.; Stricklin, S. L.; Studholme, D. J.; Sun, J.; Viana, C. J.; Wallin, E.; Wang, B.; Wheeler, C.; Zhu, H.; Dean, D. R.; Dixon, R.; Wood, D. *J. Bacteriol.* **2009**, *191* (14), 4534.

(6) Galindo, E.; Peña, C.; Núñez, C.; Segura, D.; Espín, G. *Microb. Cell Fact.* **2007**, *6* (7).

(7) Brewin, B.; Woodley, P.; Drummond, M. *J. Bacteriol.* **1999**, *181* (23), 7356.

(8) Ortiz-Marquez, J. C. F.; Do Nascimento, M.; Dublan, M. de L. A.; Curatti, L. *Appl. Environ. Microbiol.* **2012**, *78* (7), 2345.

(9) Ducat, D. C.; Avelar-Rivas, J. A.; Way, J. C.; Silver, P. A. *Appl. Environ. Microbiol.* **2012**, *78* (8), 2660.

(10) Hays, S. G.; Yan, L. L. W.; Silver, P. A.; Ducat, D. C. *J. Biol. Eng.* **2017**, *11* (1), 4.

(11) Löwe, H.; Hobmeier, K.; Moos, M.; Kremling, A.; Pflüger‐grau, K. *Biotechnol. Biofuels* **2017**, *10*.

(12) Stanier, R. Y.; Kunisawa, R.; Mandel, M.; Cohen-Bazire, G. *Bacteriol. Rev.* **1971**, *35* (2), 171.

(13) D'mello, R.; Hill, S.; Poole, R. K. *Microbiology* **1994**, *140*, 1395.

(14) Engler, C.; Kandzia, R.; Marillonnet, S.; Eldik, G. Van; Botterman, J. *PLoS One* **2008**, *3* (11), e3647.

(15) Porra, R. J. *Photosynth. Res.* **2002**, *73* (1/3), 149.

(16) Law, J. H.; Slepecky, R. A. *J. Bacteriol.* **1961**, *82* (1), 33.

(17) Revillas, J. J.; Rodelas, B.; Pozo, C.; Martínez-Toledo, M. V.; López, J. G. *Amino Acids* **2005**, *28* (4), 421.

(18) Lea-Smith, D. J.; Biller, S. J.; Davey, M. P.; Cotton, C. A. R.; Perez Sepulveda, B. M.; Turchyn, A. V.; Scanlan, D. J.; Smith, A. G.; Chisholm, S. W.; Howe, C. J. *Proc. Natl. Acad. Sci.* **2015**, *112* (44), 13591.

(19) Niederholtmeyer, H.; Wolfstadter, B. T.; Savage, D. F.; Silver, P. A.; Way, J. C. *Appl. Environ. Microbiol.* **2010**, *76* (11), 3462.

(20) Knoop, H.; Gründel, M.; Zilliges, Y.; Lehmann, R.; Hoffmann, S.; Lockau, W.; Steuer, R. *PLoS Comput. Biol.* **2013**, *9* (6), e1003081.

(21) Kurz, W. G. W.; LaRue, T. A. G. *Can. J. Microbiol.* **1973**, *19* (3), 321.

(22) Mulo, P.; Sicora, C.; Aro, E.-M. *Cell. Mol. Life Sci.* **2009**, *66* (23), 3697.

(23) Bali, A.; Blanco, G.; Hill, S.; Kennedy, C. *Appl. Environ. Microbiol.* **1992**, *58* (5), 1711.

(24) Segura, D.; Guzman, J.; Espin, G. *Appl. Microbiol. Biotechnol.* **2003**, *63* (2), 159.

(25) Zhao, S. *Environ. Sci. Technol.* **2014**, *48* (7), 4212.

(26) Ganji, F.; Vasheghani-Farahani, S.; Vasheghani-Farahani, E. *Iran. Polym. J.* **2010**, *19* (5), 375.

(27) De, S. K.; Aluru, N. R.; Johnson, B.; Crone, W. C.; Beebe, D. J.; Moore, J. *J. Microelectromechanical Syst.* **2002**, *11* (5), 544.

(28) Vilchez, C.; Vega, J. M. *Appl. Microbiol. Biotechnol.* **1994**, *41* (1), 137.

(29) Santos-Rosa, F.; Galvan, F.; Vega, J. M. *Appl Microbiol Biotechnol* **1989**, *32*, 285.

(30) Song, K.; Tan, X.; Liang, Y.; Lu, X. *Appl. Microbiol. Biotechnol.* **2016**, *100* (18), 7865.

(31) Suh, I. S.; Lee, C.-G. *Biotechnol. Bioprocess Eng.* **2003**, *8* (6), 313.

(32) Belicka, L.; Blanks, J.; Flores, H.; Holowell, I.; Jochem, F.; Meichel, G.; Miller, Harlan, I.; Phillips-Kress, J.; Scott, B.; Vasseur, C. Process for inoculating closed photobioreactors with cyanobacteria. WO2014145185 A1, September 19, 2014.

(33) Yu, J.; Liberton, M.; Cliften, P. F.; Head, R. D.; Jacobs, J. M.; Smith, R. D.; Koppenaal, D. W.; Brand, J. J.; Pakrasi, H. B. *Sci. Rep.* **2015**, *5*.

(34) Chen, Y.; Kay Holtman, C.; Magnuson, R. D.; Youderian, P. A.; Golden, S. S. *Plasmid*

2008, *59* (3), 176.

Chapter 3

Cellular photopatterning and electrochemical patterning

Abstract

DNA-hybridization based microbial patterning can enable the elucidation of the role of cell ratio, cell spacing, and cell-cell contact in microbial communities. Robust, easy-to-use DNA patterning chemistries are necessary for DNA-hybridization based cell patterning to become a more useful and more widely used technique. In this chapter, I discuss my efforts towards developing new microbial patterning techniques and their applications.
Portions of this work are described in the following publication.[1]

3.1. Introduction

3.1.1. Oxidative coupling reactions and their application towards DNA patterning

An oxidative coupling reaction is a reaction that in the presence of an oxidant forms a covalent bond between two reagents. The Francis lab has developed several oxidative coupling reactions to functionalize biomolecules.[2–5] The advantage of our oxidative coupling reactions is that they proceed on short time scales at an equimolar ratio of reagents. For this reason, oxidative coupling reactions have been used as a model by our lab to develop reactions to enable the patterning of DNA on surfaces[6] (Figure 3.1). The first DNA patterning technique developed in the Francis lab was a photopatterning reaction[6] (Figure 3.1B) based on a previously disclosed aminophenol-aniline oxidative coupling (Figure 3.1A). It should be noted that the reaction depicted in Figure 1B is not an oxidative coupling; however, the reaction goes through the same proposed intermediate[3] as the reaction depicted in Figure 3.1A. I utilize the photopatterning reaction to pattern microbes, namely *Synechocystis* PCC6803 and *Azotobacter vinelandii*, next to one another in various ratios (see section 3.3.1). For reasons discussed in section 3.1.3, a postdoc in the lab, Ariel Furst, and I developed an additional oxidative coupling strategy where we place a catechol on the surface of an electrode and through the application of an applied electrochemical potential generate a reactive intermediate that reacts selectively with aniline[1] (Figure 3.1C).

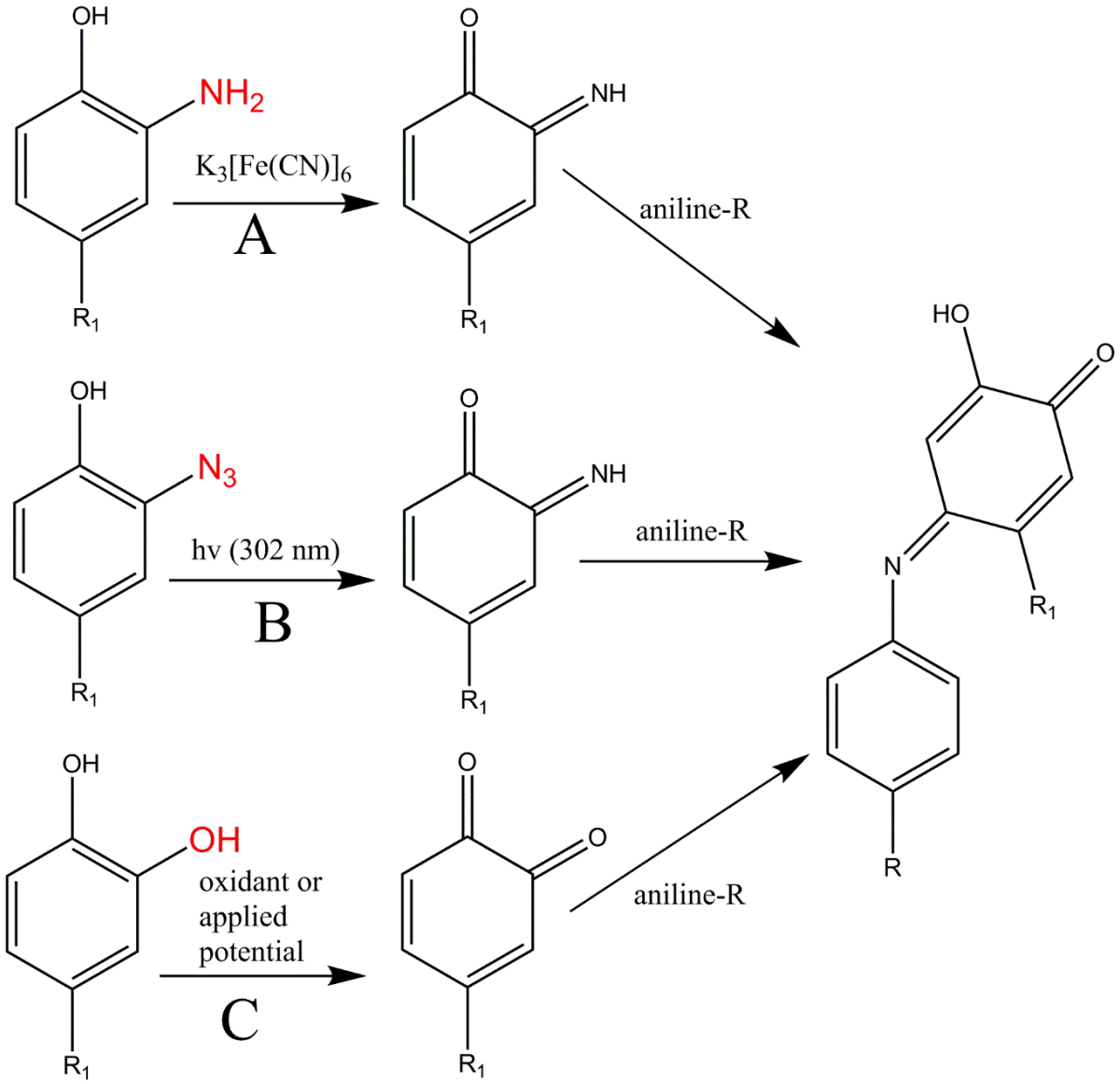

Figure 3.1. Three reactions developed by the Francis lab that go through a similar reaction intermediate and result in the same reaction product. These three reactions have different applications, from the photo (B)[6] or electropatterning (C)[1] of DNA to the modification of proteins (A).[2]

3.1.2. Using DNA patterning to pattern cells

DNA hybridization is unrivaled in its ability to anneal at low concentrations in complicated matrices. Several labs use DNA to assemble nanoparticles and chemicals to build novel shapes[7] or enable chemical reactivity.[8] Our lab and a few others use DNA to pattern cells, both microbial[9] and mammalian,[10,11] on surfaces or in the case of the Gartner lab as micro-tissues[12,13] to evaluate cellular phenotype and behavior. In my thesis work I have been chiefly interested in the patterning of microbial cells on surfaces. To pattern microbes on surfaces using DNA, we need to modify a surface, either glass or gold, with DNA and modify the surface of the microbial cells with DNA. To modify the surfaces we use silane[6] or thiol

chemistry.[1] The surfaces of microbial cells are modified via cleaving cell surface sugars with periodate to expose aldehydes that are subsequently modified with hydrazine DNA.

3.1.3. Other methods to pattern microbes

Most efforts towards patterning multiple cell types on surfaces have focused on mammalian cells; however, there are several interesting examples of cellular patterning techniques that have been developed specifically with microbes in mind. Mitchell and coworkers developed an aqueous two-phase system to pattern bacteria onto sheets of epithelial cells to simulate microbial communities that form on the surface of organs such as the skin or those of the digestive system.[14] This method enables one cell type to be patterned on top of another quickly and in a way that is applicable to a wide array of cell types including two different types of bacteria, but it does not enable defined spatial patterns to be created within a layer of cells on the same plane. Shear and coworkers have developed a technique that enables the 3-D printing of bacteria in a variety of well-defined protein-based structures and have used this methodology to pattern two different types of bacteria in different spatial orientations with respect to one another.[15] Shear and coworkers have used this methodology to make observations concerning antibiotic resistance in microbial communities[15] and to study quorum sensing.[16] Others have used similar 3-D printing strategies to make functional microbe-based materials that perform tasks such as degrading environmental pollutants.[17] The study of how microbial communities secrete and degrade chemicals of interest such as antibiotics is of great relevance to a number of fields of study particularly those studying antibiotic resistance or the fate of environmental pollutants. A number of microfluidic approaches have been developed to monitor the fate of secreted metabolites in microbial communities. One particularly interesting example of this was developed by Ismagilov and coworkers where microbes were placed in separated microfluidic channels but were allowed to interact via their secreted metabolites.[18] The above methods for patterning microbial communities do not allow for direct control over cell ratio or in most cases, cell-cell contacts.

3.1.4. Importance of the cellular patterning of bacteria

Microbes exist in diverse, interconnected, multi-species communities in a wide range of habitats, from soil to the human digestive system. However, researchers generally study and view microbes in isolation. Growing microbes even with just a single additional microbial species can change behavior. For example, Traxler and coworkers found that *S. coelicolor* when grown in the presence of an additional *actinomycetes* produces the red antibiotic prodiginine and, in general, secretes a more diverse set of metabolites.[19] DNA hybridization-based techniques can enable new questions to be addressed in the role of cell-cell contact, cell ratio and spatial arrangement in microbial communities. The idea that cell-cell contact is important in microbial cocultures and communities has been proposed in several interesting synthetic and natural multi-species microbial communities.[20,21] Furthermore, it has been demonstrated that cell ratio is critically important to the phenotype of designed cellular communities.[22] The spatial arrangement of bacteria in a multi-species community has also been demonstrated to influence the outcome of bacteria cocultures (i.e. competitive or cooperative).[23,24] DNA-based hybridization is one of the more promising methods to test hypotheses concerning the importance of cell-cell contacts, cell ratio and spatial arrangements in microbial multi-cultures.

Other methods to study bacterial multi-cultures are unable to test all these factors, despite their importance. For example, the technique Shear and coworkers developed that enables the 3-D printing of bacteria[15] is excellent for studying quorum sensing, but is not ideal for studying

communities with precisely controlled cell ratios or the effect of cell-cell contacts. Similarly, the microfluidic approach to studying microbial interactions, such as the experiment described by Ismagilov et. al. is similarly not suitable to studying microbial cell-cell contacts or well-defined cellular ratios.[18] In mammalian systems, DNA hybridization-based techniques have already demonstrated their utility in understanding the effects of difficult to control variables in multi-cell communities such as direct cell contact.[13]

Cellular patterning seeks to understand how specific cellular interactions, defined cell ratios and spatial arrangements impact cell behavior. In this chapter, we are specifically interested in the cellular patterning of bacterial communities. The ability to pattern bacteria in defined ratios and patterns allows for the testing of hypothesis not possible in batch culture or on agar. For this reason, there is a fair amount of interest in the literature on spatially patterning bacteria.[15,25–27] Our lab has developed techniques for patterning bacteria as described in section 3.1.1.[6,28] and it is this work that I built upon in patterning multiple bacteria next to one another and in developing an electrochemical patterning method.

3.1.5. Overview of the work presented

In this chapter, I describe my work photopatterning[6] *A. vinelandii* and *Synechocystis* together in different ratios using DNA. This work resulted in two observations: 1) The method is difficult to use to pattern multiple DNA sequences next to one another, especially going from two DNA sequences to three DNA sequences, and 2) Attempts to verify or measure interspecies interactions were unsuccessful. Based on these observations, a postdoc in the lab, Dr. Ariel Furst, and I developed an electrochemical method to pattern bacteria on electrodes. It is our hope that this method will enable easier multi-bacterial patterning and a means to monitor metabolite transfer between bacteria. An example of the utility of this technique for the study of *Shewanella oneidensis* is also described.

3.2. Materials and Methods

3.2.1. Photopatterning of *A. vinelandii* and *Synechocystis*

The photopatterning method is described in detail in El Muslemany et al.[6] To pattern multiple DNA sequences via photopatterning alignment marks were deposited via metal evaporation. Complementary photomasks were purchased from Fineline Imaging containing alignment marks to align the different DNA sequences. *A. vinelandii* and *Synechocystis* were covalently labeled with ssDNA following the procedure outlined in Twite et al.[9] Briefly, a 30 µL cell pellet was incubated in 1 mL of 0.5 mM sodium periodate in DPBS buffer for 20 min at ambient temperature. The cells were washed with DPBS via three rounds of centrifugation and cell pellet resuspension, and then incubated for 3 h (*A. vinelandii*) or 16 h (*Synechocystis*) with 1 mL of 30 µM ilinker DNA (Integrated DNA Technologies, San Diego, CA, USA) in MOPS buffer (pH=6) in the presence of 10 mM aniline. The excess DNA was removed via washing with DPBS. The i-linker is a proprietary hydrazide linker commonly used to tether DNA to a solid support. The cells (200 µL) from a 1 mL total volume in DPBS were incubated on the DNA-modified glass surface for 1 h. *Shewanella oneidensis* MR-1 was patterned following the same procedure as *Synechocystis* 6803.

3.2.2. Electrochemical patterning methodology

Unless otherwise noted, all chemicals were purchased from Sigma Aldrich (St. Louis, MO, USA). Additionally, unless otherwise noted, all experiments and reactions were conducted in air. For all electrochemical measurements, measurements were taken with a saturated AgCl/Ag reference electrode unless otherwise stated. Experiments conducted with

disposable electrodes from Dropsens (Asturis, Spain) were performed against an Ag pseudorefence electrode. Reported potentials are relative to the respective reference electrode. Nanopure water was collected with a resistivity of 18.2 MΩ-cm, and N_2 gas was 99.98% pure.

3.2.3. Synthesis of S1

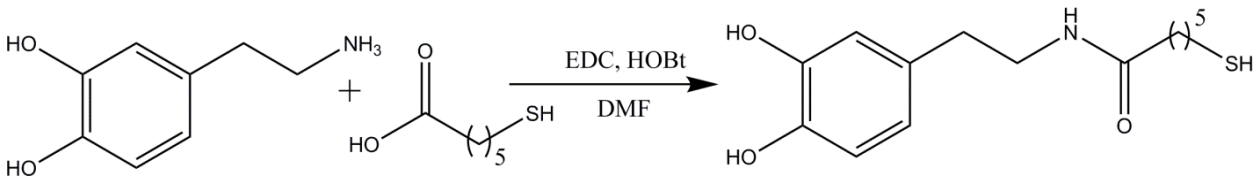

A solution of 6-mercaptohexanoic acid (2 mmol, 300 mg), 1-ethyl-3-(3-dimethylaminopropyl)carbodiimide (2.4 mmol, 480 mg) and hydroxybenzotriazole (2 mmol, 270 mg) in 10 mL dry DMF was stirred for 15 min, followed by the addition of 4-(2-aminoethyl)-1,2- benzenediol (2.5 mmol, 379 mg) and *N*,*N*-diisopropylethylamine (3 mmol, 0.52 mL). The reaction was stirred 3 h, followed by solvent removal *in vacuo*. The product S1 was purified by silica chromatography (5% MeOH:DCM), affording 510 mg of a clear oil (89% yield). 1 H NMR
(400 MHz, CDCl3): δ 6.82 (d, J = 8.0 Hz, 1H), 6.75 (d, J = 2.1 Hz, 1H), 6.59 (dd, J = 8.0, 2.1 Hz, 1H), 5.61 (s, 1H), 3.50 (q, J = 6.7 Hz, 2H), 2.72 (t, J = 7.0 Hz, 2H), 2.51 (q, J = 7.4 Hz, 2H), 2.17 (t, J = 7.4 Hz, 2H), 1.56 (m, 5H), 1.36 (dt, J = 15.5, 8.0 Hz, 3H). 13C NMR (100 MHz, DMSO-d6): δ, 172.2, 145.5, 143.85, 130.6, 119.5, 116.3, 115.7, 36.7, 33.6, 27.8, 25.1, 24.0. ESI-MS: calc'd 283.1, observed 283.1 m/z.

3.2.4. Synthesis of S2

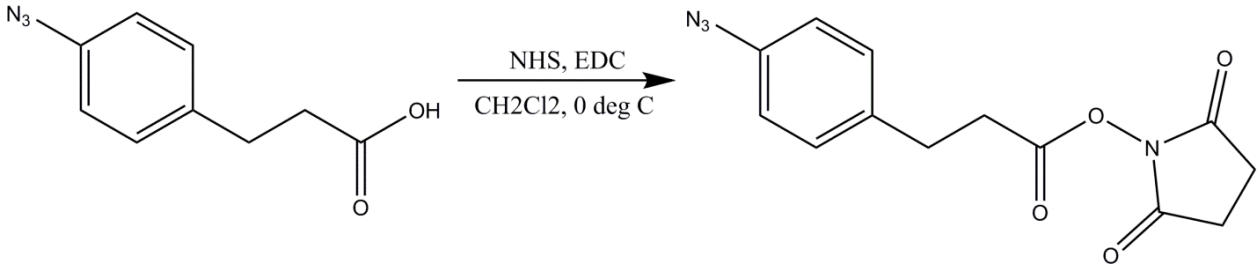

To a solution of 3-(4-azidophenyl)propionic acid (856 mg, 4.7 mmol) and *N*-hydroxysuccinimide (0.65 g, 5.7 mmol) in CH_2Cl_2 at 0 °C was added *N*-(3-dimethylaminopropyl)-*N'*-ethylcarbodiimide hydrochloride (1.09 g, 5.7 mmol). The reaction was stirred for 2 h and then diluted with DCM and washed with water. The combined organic layers were dried over sodium sulfate and the solvent was removed under reduced pressure. The reaction afforded 1.08 g of a white (86% yield). 1 H NMR (400 MHz, CDCl3): δ 7.25 – 7.20 (m, 2H), 7.02 – 6.95 (m, 2H), 3.05 (t, J = 7.6 Hz, 2H), 2.91 (t, J = 8.2 Hz, 2H), 2.85 (m, 4H). 13C NMR (100 MHz, CDCl3): δ, 168.02, 167.72, 138.48, 135.74, 129.68, 119.26, 32.60, 29, 81, 25, 55. ESI-MS (M+H): calc'd: 288.1, observed: 288.1 m/z.

3.2.5. Synthesis of aniline-DNA conjugates

Amine-modified DNA (obtained from Sigma Aldrich, St. Louis, MO, USA) was dissolved to 2.5 mM. The reaction conditions describe the generalized procedure for the

modification of amine functionalized DNA. [Representative DNA strand M2: 5'-/5AmMC6/ CCCTAGAGTGAGTCGTATGA-3' (5AmMC6 = 6-aminohexyl phosphate)]. To a solution of 60 µL of 100 mM pH 8.0 phosphate buffer was added 60 µL of a 2.5 mM amine DNA solution (0.15 µmol). To the DNA solution were added 70 µL of DMF and 50 µL of a 500 mM solution of **S2** (50 µmol) in DMSO. The solution was shaken overnight. The DNA was purified with a NAP-5 column (GE Healthcare, San Ramon, CA, USA) equilibrated with Nanopure water. To the resulting solution was added 10 mg (57 µmol) of TCEP to reduce the aryl azide to the desired aniline. The solution was shaken for 1 h before being directly loaded onto a NAP-10 column, and the elution process was repeated. The eluent was lyophilized, yielding ~0.5 mg of a white solid (50%). The DNA was prepared via C-18 Ziptip for MALDI-TOF analysis to confirm modification. Aniline-DNA stock solutions were prepared at 1 mM in water and stored at -20 °C for future use.

3.2.6. Synthesis of NHS−DNA conjugates

For mammalian cell adhesion studies, DNA was modified with an NHS ester to ensure coupling to the cell surfaces. Oligonucleotides were obtained from Sigma-Aldrich with thiol groups installed at the 5′-end. Thiol-modified DNA was dissolved to 500 µM in Nanopure water for storage at −20 °C until use. Prior to modification, 15 µL of the DNA stock was combined with 5 µL of 50 mM tris(2-carboxyethyl)phosphine (TCEP) in 70 µL pH 8.0 Na_2CO_3 buffer for 1 h. Succinimidyl-[(*N*-maleimidopropionamido)-hexaethyleneglycol] ester (NHS-PEO6-maleimide) (Pierce) was prepared as a stock solution by dissolving 5 mg of NHS-PEO6-maleimide into 1 mL of dry dimethyl sulfoxide (DMSO, Sigma). Aliquots of this solution (30 µL each) were then stored at −20 °C. Following TCEP treatment, DNA modification was achieved after the passage of the reduced thiol DNA through a NAP-5 size-exclusion column (GE Healthcare). The eluent was then addeds to 30 µL of the NHS-PEO6-maleimide solution at room temperature for 10 min. The reaction was again passed through a second NAP-5 column pre- equilibrated with PBS (pH 7.2). The concentration of DNA in the column eluent was verified by Nanodrop.

3.2.7. Functionalizing gold electrodes with catechols

Reusable gold rod electrodes (2 mm diameter, CH Instruments, Bee Cave, TX, USA) were polished with 0.05 µm alumina on microfiber cloth (Buehler, Lake Bluff, IL, USA). Electrodes were then cycled in 0.5 M H_2SO_4 from 1.6 V to -0.1 V v. AgCl/Ag until a consistent signal was observed (~20 scans). Electrodes were then rinsed with copious amounts of Nanopure water and dried under a stream of N_2.

Following H_2SO_4 electrode cleaning, electrodes were submerged in 50 µL of a 250 µM ethanoic solution of the desired thiols (a combination of **S1** and mercaptohexanol). Electrodes were allowed to incubate in the thiol solution for 12-18 h. Prior to use, electrodes were rinsed with ethanol and Nanopure water, followed by drying under a stream of N2. To evaluate monolayer formation, electrodes were scanned in 10 mL of DPBS.

3.2.8. General procedure for DNA modification of electrodes

Catechol functionalized gold surfaces were modified with ssDNA. A 20 µL drop of 50 µM aniline-modified DNA in PBS (pH 7.2) was placed on the center of the electrode. For the rod electrodes, the gel-tip reference electrode and a platinum counter electrode were inserted into the DNA-containing liquid drop. Constant potential amperometry at a potential of 0.3 V for 240 s was generally used to attach aniline-modified DNA to the surface. For the AUTR disposable electrodes, the reference and auxiliary electrodes incorporated on the surface were used. These electrodes were activated at 0.35 V for 240 s to induce DNA coupling. Following

the application of a potential, electrode surfaces were rinsed with PBS and Nanopure water.

3.2.9. Quantification of DNA on electrode surfaces

DNA-modified electrodes were subjected to electrochemical measurement with 20 μM ruthenium hexammine in 0.1 M Tris buffer (pH 7.6).[29] At this concentration of ruthenium hexammine, no signal is observed on monolayers containing no DNA and is at a concentration conventionally used for low-density DNA monolayers.[29] Cyclic voltammetry scans were obtained at a scan rate of 100 mV/s.

3.2.10. DNA sequences

M2: 5′-CCC TAG AGT GAG TCG TAT GA-3′
C2: 5′-TCA TAC GAC TCA CTC TAG GG-3′
M2 short: 5′-CCC TAG AGT GAG TCG TA-3′

3.2.11. DNA labeling of *Saccharomyces cerevisiae* and patterning on DNA-modified electrodes

S. cerevisiae was covalently labeled with ssDNA following the procedure outlined in Twite et al.[9] Briefly, a 30 μL cell pellet of S. cerevisiae was incubated in 1 mL of 0.5 mM sodium periodate in DPBS buffer for 20 min at ambient temperature. The cells were washed with DPBS via three rounds of centrifugation and cell pellet resuspension, and then incubated for 3 h with 1 mL of 30 μM ilinker DNA (Integrated DNA Technologies, San Diego, CA, USA) in MOPS buffer (pH=6) in the presence of 10 mM aniline. The excess DNA was removed via washing with DPBS. The cells (200 μL) from a 1 mL total volume in DPBS were incubated on the DNA-modified AUTR electrode for 20 min. The electrode was surrounded by a PDMS well to keep the solution in place. After 20 min, the electrode was placed in 10 mL of DPBS and the PDMS well was removed. The electrodes were then washed for 16 h with shaking at 60 rpm prior to imaging.

3.2.12. DNA labeling of Jurkat and Ramos cells and patterning on DNA-modified electrodes

Jurkat and Ramos cells were covalently labeled with ssDNA following the procedure outlined by Hsiao et al.[10] Immediately prior to modification, a sample of 5×10^6 Jurkat or Ramos cells was washed with PBS buffer three times to ensure the removal of any proteins from the cell culture medium. The cell suspension was then reacted with 1 mL of NHS−DNA (15 μM) solution synthesized and purified as described above (C2 sequence). The mixture containing cells was allowed to react at room temperature for 30 min. The cells were subsequently washed three times with PBS containing 1% FBS. The cells were resuspended in 250 μL of PBS containing 1% FBS. The cell mixture (30 μL) was then added to DNA-modified AUTR electrodes and allowed to incubate for 1 h. Following incubation, the electrodes were washed for 16 h in PBS containing 1% FBS.

3.2.13. Fluorescent cell imaging

For both *S. cerevisiae* and mammalian cells, cell-modified AUTR electrodes were incubated with 10 μM fluorescein diacetate in PBS for 15 min. Electrodes were rinsed with PBS prior to imaging. Electrodes were imaged on a Typhoon TRIO imager, and images were 2quantified using ImageJ software.

3.2.14. Scanning electron microscopy imaging

Mammalian cells, both Jurkat and Ramos, were imaged on AUTR electrodes using scanning electron microscopy (SEM). Cells wer attached to the surface as previously described. Following cell immobilization, cells were fixed on the electrode surface. Cells were initially treated with 2% glutaraldehyde in 0.1 M sodium cacodylate buffer (pH 7.2) for 1 h. Cells were subsequently washed three times with 0.1 M sodium cacodylate each for 15 min. Osmium tetroxide (1% in 0.1 M sodium cacodylate) was then added to the electrodes for 1 h in the dark. The surfaces were washed again three times for 5 min each with 0.1 M sodium cacodylate. Cells were then dehydrated with 10 min treatments of 30%, 50%, 70%, 85%, 95%, and 100% ethanol. Surfaces were then dried by critical point drying in ethanol. Surfaces were then sputter coated in gold to a surface thickness of 20 nm. Surfaces were imaged using an Hitachi S-5000 instrument.

3.3. Results and Discussion

3.3.1. Patterning *A. vinelandii* and *Synechocystis* PCC 6803 via DNA hybridization

The ability to pattern microbes with control over relative cell ratios and spacing would enable new hypotheses to be tested about the organization of microbial communities. Using the azidophenol DNA photopatterning method, two different DNA sequences were patterned onto a glass surface. A complementary DNA sequence was covalently attached to the cell surface of either *Azotobacter vinelandii* or *Synechocystis* via periodate chemistry. This technique was used to pattern *Azotobacter* and *Synechocystis* together in a well-defined pattern (Figure 3.2).

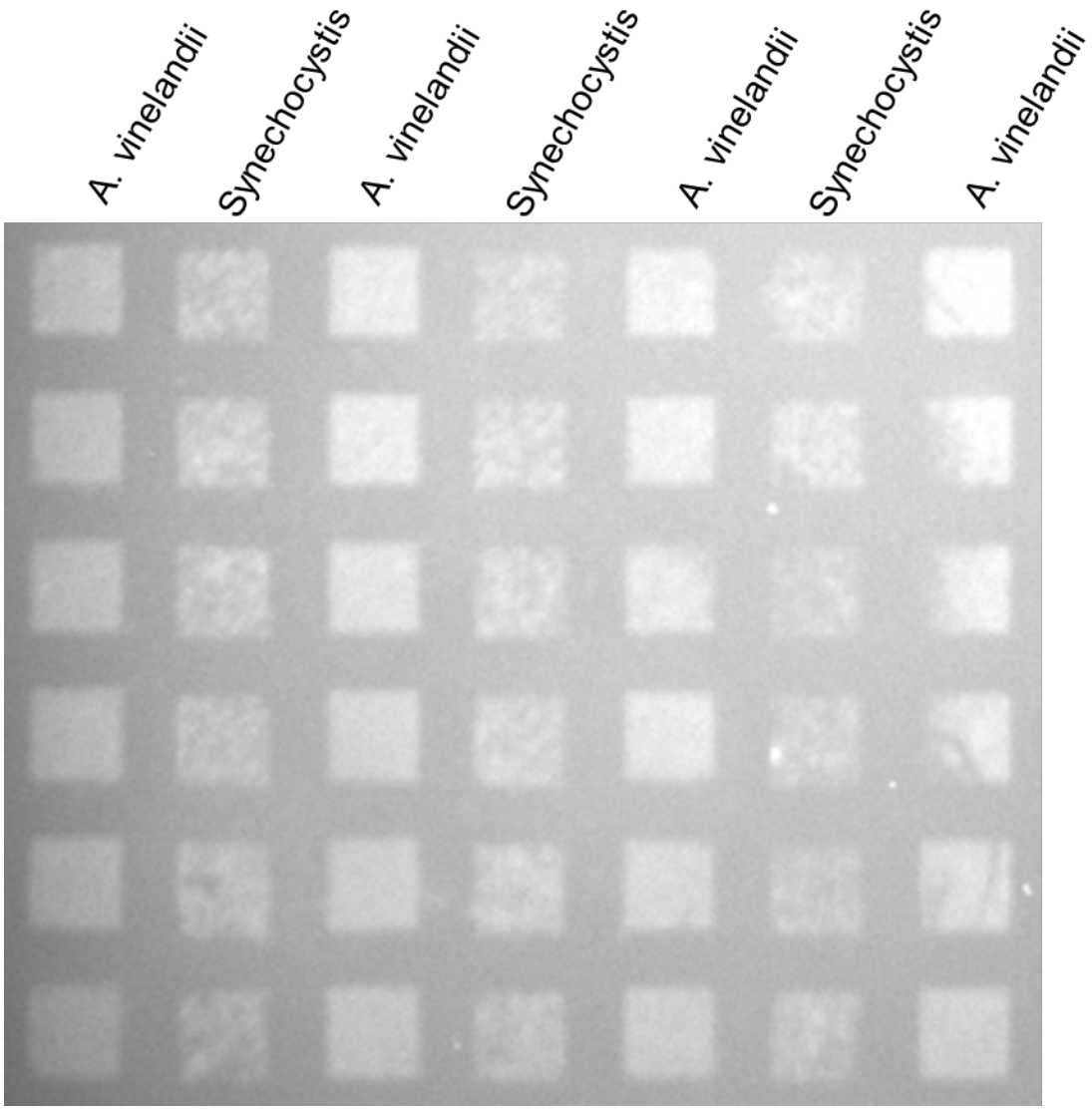

Figure 3.2. The cells were patterned in 300 μm^2 squares with 200 μm spacing between squares.

Cells could be patterned in a variety of ratios and spacings with respect to another cell type, in this case *A. vinelandii* and *Synechocystis* (Figure 3.3).

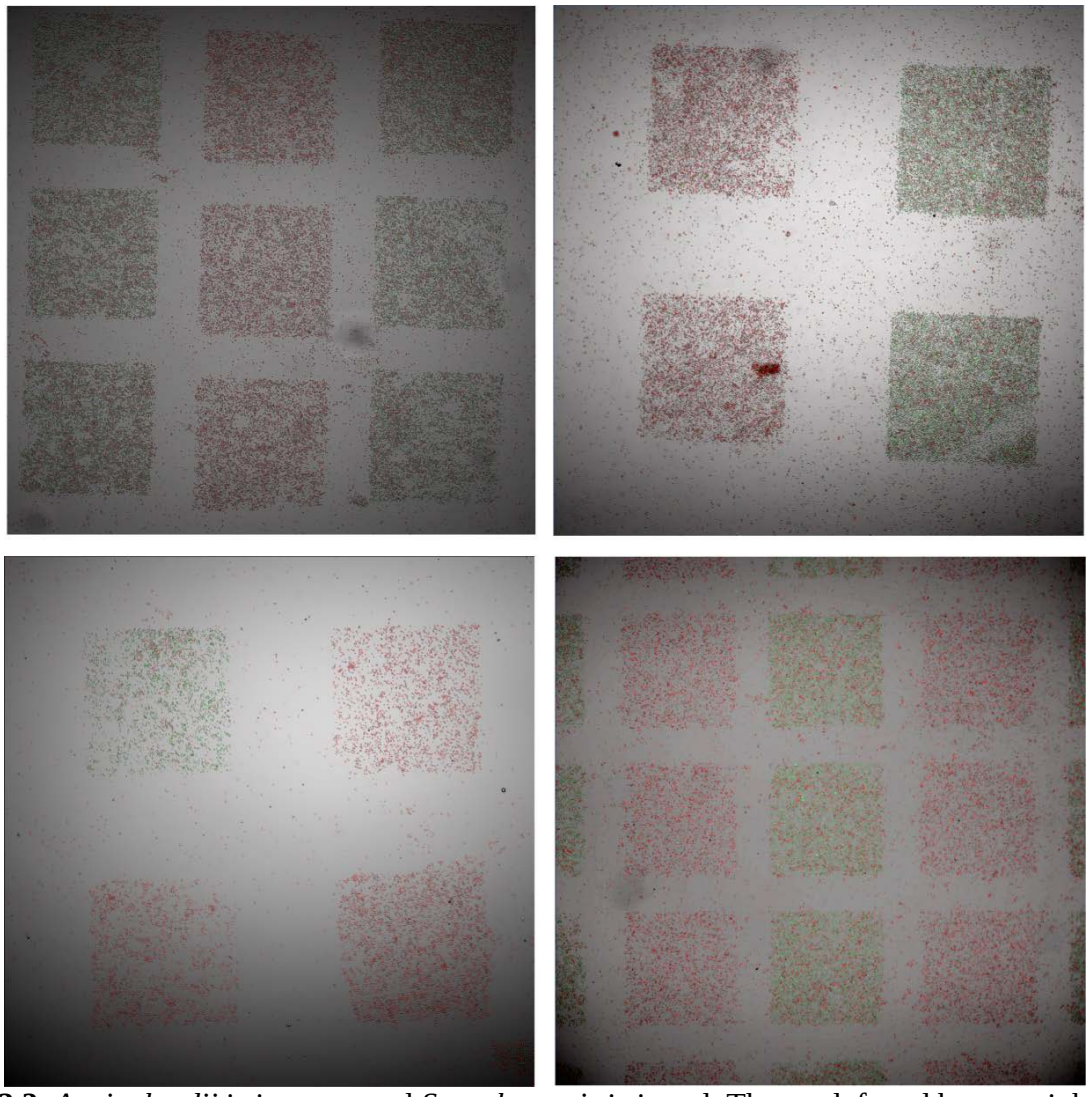

Figure 3.3. *A. vinelandii* is in green and *Synechocystis* is in red. The top left and bottom right squares are 300 μm^2 with a 100 µm spacing and a 1:1 ratio of cells. The top right squares have a 200 µm spacing and a 1:1 ratio of *A. vinelandii* to *Synechocystis*. The bottom left has a 200 µm spacing and a 1:3 ratio of cells.

The specific DNA sequence played a large role in the degree of background patterning observed. Sequences containing all four DNA bases showed no background hybridization to other sequences (Figure 3.4). However, polyA or polyT 50 mer sequences exhibited cross hybridization with sequence C2, C2=TCATACGACTCACTCTAGGG (Figure 3.4). The C2 sequence was designed to contain no hairpins.

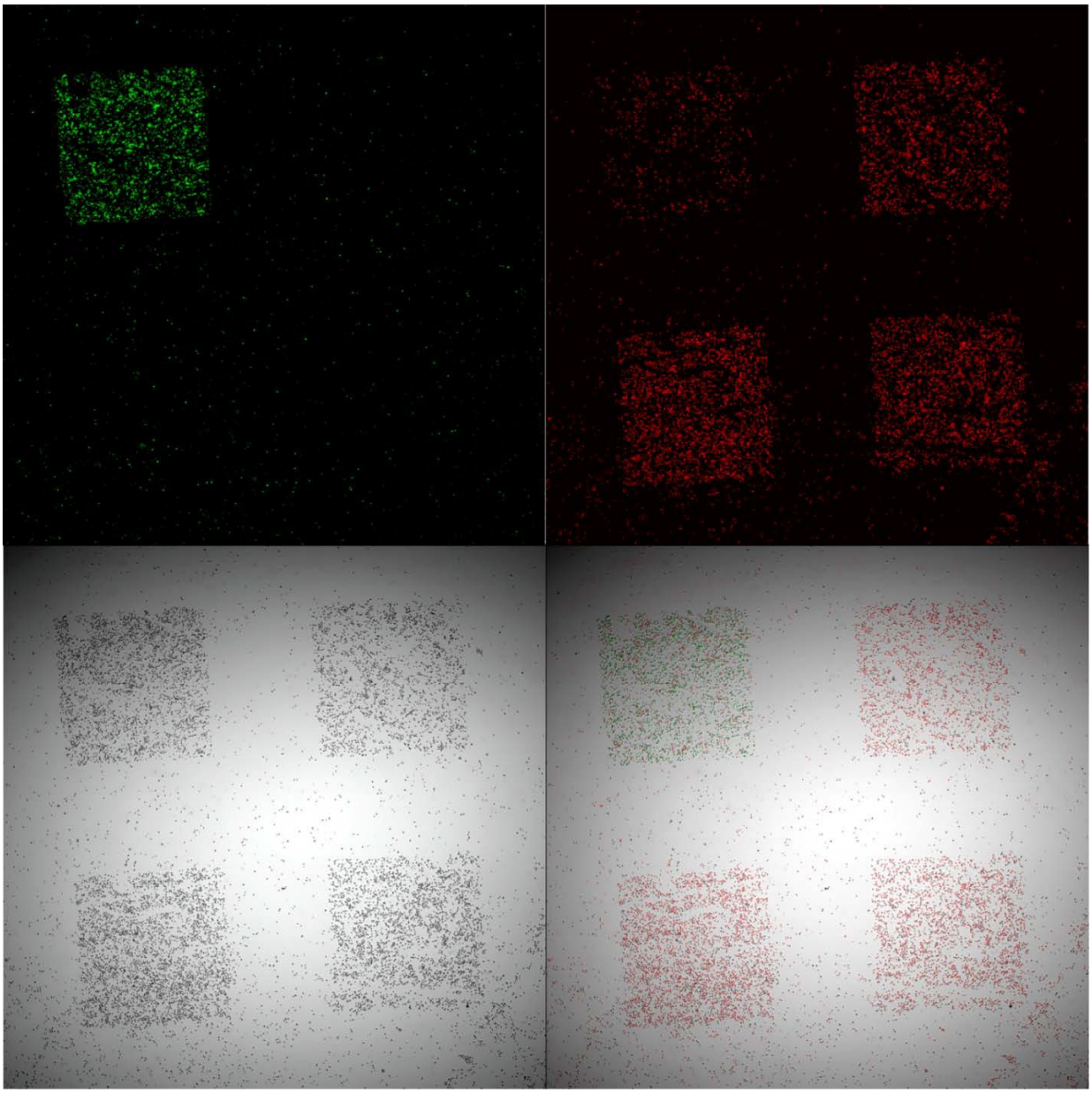

Figure 3.4. A composite image of green and red fluorescent cells patterned together. The microbes patterned in green are patterned with the C2 sequence. The microbes patterned in red are patterned with the polyA sequence. The polyA sequence exhibits cross-hybridization with the C2 sequence but the C2 sequence does not exhibit cross reactivity with the polyA sequence.

We hoped to use this patterning technology to study cellular metabolism and metabolite transfer among patterned microbial communities and see if these aspects translated to insights into how cellular communities behave. Towards this end, *A. vinelandii* cells were patterned on surfaces and incubated in a rich media suitable for rapid growth, Burke's media, or a minimal media where *A. vinelandii* grows slowly (SAV media). A program to distinguish between dividing cells and non-dividing cells in microscopy images was developed using Python software (Figure 3.5, https://github.com/rkwant/Cell-Counting/blob/master/Watershed-SKlearn- explorer.ipynb). To test this program we found the

percent of dividing cells for *A. vinelandii* in minimal SAV media vs. rich Burke's media. No discernable difference between the rates of cell division was observed in minimal vs. rich media (Figure 3.6).

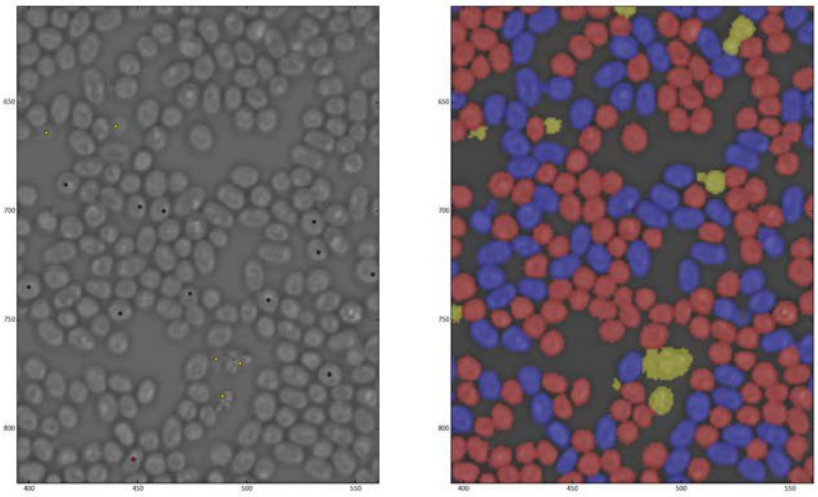

Figure 3.5. Red cells are classified as non-dividing, blue cells as dividing and yellow as cell debris.

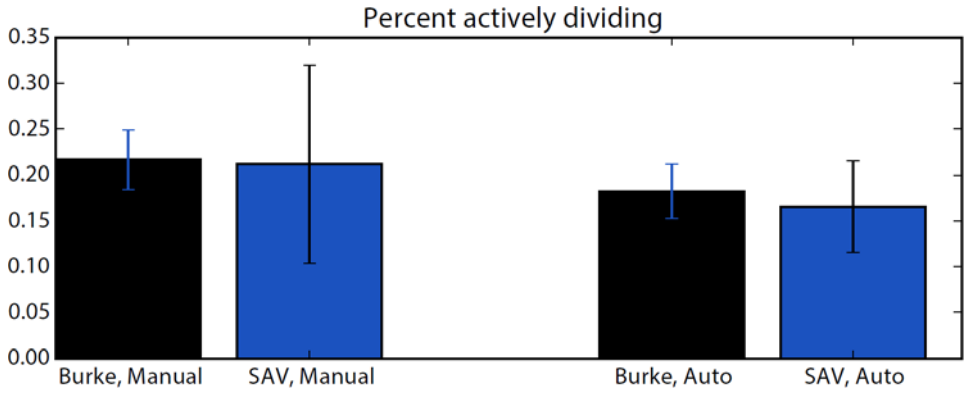

Figure 3.6. Rate of cell division is unaffected by growth media. Dividing *A. vinelandii* cells were counted manually and via a Python program found on GitHub here: https://github.com/rkwant/Cell-Counting/blob/master/Watershed-SKlearn-explorer.ipynb.

The lack of differentiation between minimal vs. rich media for patterned *A. vinelandii* indicated that a different assay was necessary. Furthermore, the difficulty in scaling the photopatterning technique from one patterned DNA sequence to two patterned DNA sequences to three patterned DNA sequences indicates that a different photopatterning method was also necessary.

Electrochemical methods promised the ability to readily detect metabolites and pattern multiple cells in parallel via multiplexed electrodes.

3.3.2. Selection of coupling partners for electrochemical coupling

The spontaneous addition of thiolated biomolecules to gold surfaces is a mainstay technique for accessing biomolecule-modified gold surfaces.[7,30] Although effective, secondary interactions of the molecules with the metal surface complicate the formation of well-defined, homogenous monolayers with consistent coverage. As it has become increasingly apparent that adequate spacing between biomolecules is critical for effective biosensing[29,31] and nanoparticle assembly applications,[32] a growing number of alternative synthetic approaches have been developed for attachment to metal surfaces.[33,34] A major strategy applied to DNA-modified surfaces, mixed monolayers containing chemically active head groups have been pre-formed on a surface, thus removing the secondary interactions of DNA strands from the monolayer formation step.[33] A subsequent 1,3-dipolar cycloaddition of azide groups to alkynes using either copper catalyzed or strain-based versions of this reaction, widely known as "Click Chemistry", provides the most common method for coupling the DNA strands to these surfaces.[29,33,34] While these methods have enabled more control over the spacing between the DNA strands, they either require redox-active catalysts that can damage DNA and complicate electrochemical sensing applications, or they require coupling times of 24 h or more.

We have developed a suite of reactions that enable the rapid bioconjugation of compounds to biomolecules.[2,5,6] These strategies are dependent on the addition of either anilines or protein N-termini to *o*-iminoquinones and *o*-quinones generated *in situ* with a chemical oxidant, such as potassium ferricyanide or sodium periodate. This class of reactions exhibits high chemoselectivity and is compatible with especially low biomolecule concentrations in aqueous media.[2] These reactions have successfully been applied to the attachment of biomolecules to gold nanoparticles.[35] A drawback to the application of aminophenols to this coupling reaction is their instability, necessitating the reduction of an *o*-nitrophenol to the *o*-aminophenol just prior to use.[5] This can be problematic in many cases because of the addition of a reductant.

Initially, we attempted to apply the rapid chemoselective addition of anilines to *o*-iminoquinones by electrochemical activation. Previous work in our group indicated that, in multivalent systems, *o*-iminoquinones are incompatible with placement on the multivalent component (i.e. viral capsids or glass surfaces). Preliminary studies of gold surfaces modified with an *o*-nitrophenol moiety showed irreversible electrochemical signals following chemical reduction to an *o*-aminophenol, followed by electrochemical oxidation. This signal irreversibility is suspected to be due to self-coupling between the active head groups on the surface. Although this issue could likely be solved through sufficient dilution of the *o*-nitrophenols on the gold surface, irreversible signals were observed even with 10% *o*-nitrophenol in the monolayer. Unfortunately, further dilution of the monolayer would yield DNA surface coverages below our detection limits. Thus, we investigated an alternative coupling partner, a catechol that is oxidized to an *o*-quinone.

3.3.3. Catechol-containing monolayers and DNA coupling and quantification

Catechol-containing monolayers were formed through the initial self-assembly of a mixed thiol monolayer on a gold surface composed of mercaptohexanol and a thiol-terminated catechol compound (**S1**, Figure 3.7). Different ratios of mercaptohexanol and **S1** were combined to vary the catechol content of the monolayer. These catechol-containing surfaces were characterized electrochemically, and the electrochemical signal was found to be reversible over multiple electrochemical cycles (Figure 3.7a). The consistent reversibility demonstrates that minimal self-coupling between the *o*-quinones on the surface occurs. Importantly, the final amount of catechol that assembles in a given monolayer is controlled by varying the initial ratio of mercaptohexanol to **S1**, which was quantifiable from the inherent electrochemical signal from the catechol (Figure 3.7b).

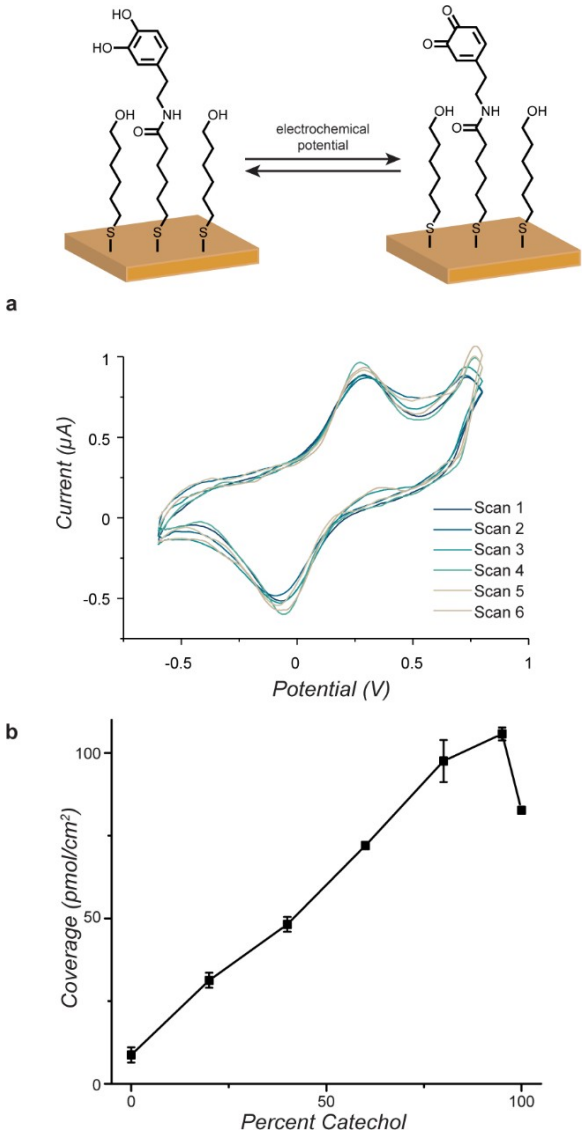

Figure 3.7. Patterning of electrochemically active surfaces. An applied electrochemical potential generates a reactive quinone on the the gold surface. This reaction is reversible (a). Based on the ratio of mercaptohexanol to catechol, the coverage of catechol on the surface can be controlled (b).

Rapid, covalent attachment of biomolecules to surfaces is often difficult due to the sensitivity of biomolecules and the speed of coupling reactions at surfaces. Catalysts and chemical oxidants that can damage biomolecules are often required for efficient coupling to surfaces. **S1** was rapidly electrochemically oxidized, enabling biomolecule coupling in the absence of added reagents (Figure 3.7a). Constant potential amperometry (CPA) was used to activate catechol-modified surfaces to tether DNA. The potential for activation was chosen based on the anodic peak current (310 mV versus AgCl/Ag and 350 mV versus an Ag pseudoreference).

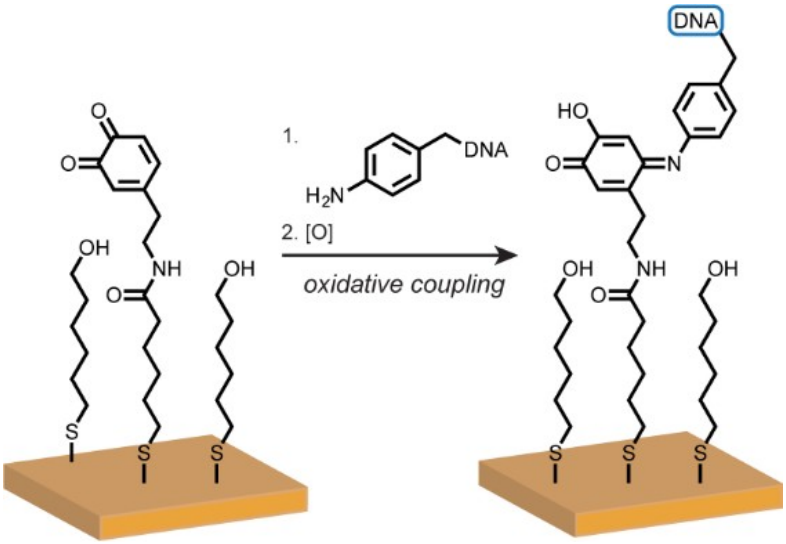

Figure 3.8. Reaction of aniline-DNA with electrochemically-activated quinone on gold surface.

Aniline-modified DNA attachment, shown in Figure 3.8, was optimized for both DNA concentration and the time of applied potential. Low concentrations of DNA yielded efficient coupling, and increasing the concentration past 50 µM did not improve the surface yield (Figure 3.9). DNA was quantified on electrodes using ruthenium hexaamine, which electrostatically interacts with the phosphate backbone of DNA.[29] Quantifying the charge from ruthenium hexamine enabled conversion to a surface coverage of DNA, which is challenging using non- electrochemical methods such as fluorescence or radioactivity. The surface coverage of aniline- modified DNA was proportional to the underlying catechol (Figure 3.10, *red trace*). While anilines are known to react especially rapidly with catechols, both aliphatic amines and thiols also participate in the reaction. The coupling efficiencies of commercially available thiol- terminated and amine-terminated DNA strands were evaluated similarly, and the DNA surface coverage was also found to be proportional to the underlying catechol coverage, albeit at lower overall coverages than aniline DNA.

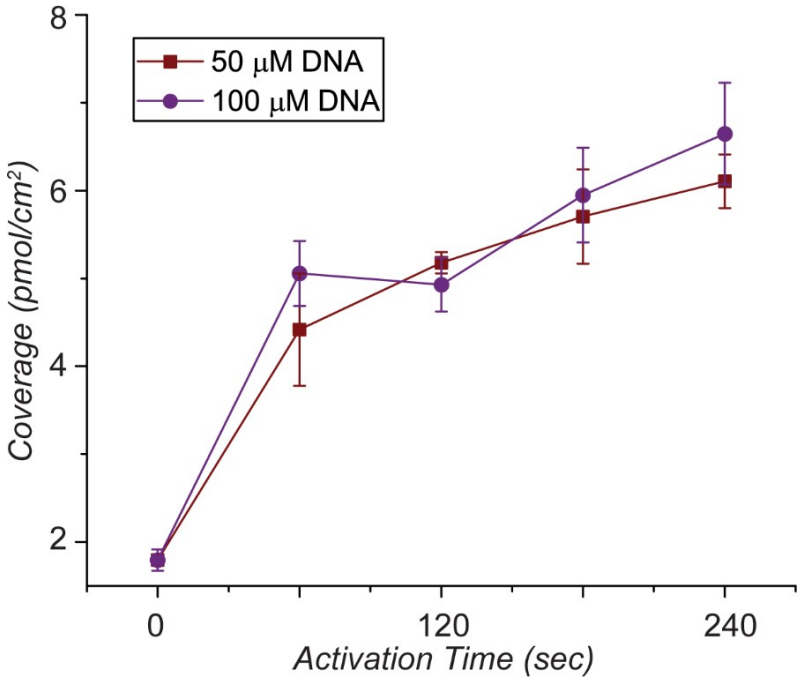

Figure 3.9. The reaction of aniline-DNA with the catechol reaction proceeded quickly at 50 μM DNA.

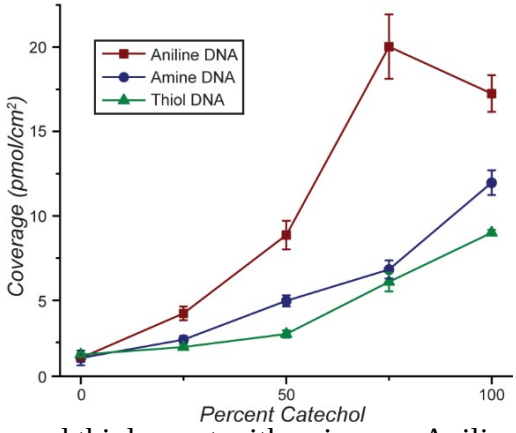

Figure 3.10. Anilines, amines and thiols react with quinones. Aniline reacts the most efficiently under the conditions tested.

The ability to couple DNA specifically to gold surfaces is essential for many techniques, ranging from AFM to SPR to nanoparticle modification.[7,33,35] The most prevalent method of DNA monolayer assembly, thiol self-assembly, yields extremely closely packed DNA monolayers with little control over the final morphology and spacing of the molecules.[34,36] Alternative methods that involve preliminary formation of a monolayer containing reactive head groups generally requires a tradeoff between specificity and control over coupling and necessity of the addition of catalysts or chemical oxidants.[33] We have developed a reagentless coupling method utilizing electrochemical oxidation of catechol-containing monolayers. This method enables control over both the amount of catechol in the monolayer and the final amount of DNA on the surface. Efficient coupling of low concentrations of DNA (50 μM or below) occurs rapidly, within a few minutes, upon application of an oxidizing potential to the electrode surface. The application of DNA to electrodes further enables their direct quantification using the phosphate counting molecule ruthenium hexaamine.

The ability to tune the total amount of DNA on the surface was found to be advantageous for cell adhesion. The efficiencies of cell adhesion through DNA hybridization were found to depend greatly on the surface coverage of DNA, with individual optimization necessary for each situation. We have optimized surfaces for the binding of three non-adherent cell types: Jurkat cells, Ramos cells, and *S. cerevisiae*.

This electrochemically activated coupling method is ideal due to its ease of use, biocompatibility, and reagentless surface activation. DNA monolayer formation was used as a model system with this method and will be useful for the facile formation of multiplexed arrays of DNA sequences. This technique is additionally exciting because of its potential for other biomolecule couplings, including proteins and peptides.

3.3.4. Formation of whole cell thin films on electrodes through DNA hybridization

A major challenge to the study of many types of cells is their lack of innate adhesion to surfaces. DNA hybridization offers a versatile method to pattern cells on a variety of substrates. The exterior of cells were modified with a particular sequence of DNA, and the catechol-containing electrode mixed monolayer was modified with the complementary strand. Utilizing innate DNA hybridization enabled the capture of the cells on the surface of the gold electrode (Figure 3.11a). Different coverages of DNA on gold surfaces formed through electrochemical catechol oxidation were evaluated for their ability to bind non-adherent cells. The non-adherent mammalian cells, Jurkat and Ramos cells, were both tested, as were *S. cerevisiae*. Cells were bound to optically transparent gold electrodes and treated with fluorescein diacetate prior to imaging. Mammalian cells were subsequently fixed on electrode surfaces and imaged by scanning electron microscopy (SEM) (Figure 3.11b). As has been previously reported, the cells maintained their morphology upon binding to electrodes via DNA hybridization.

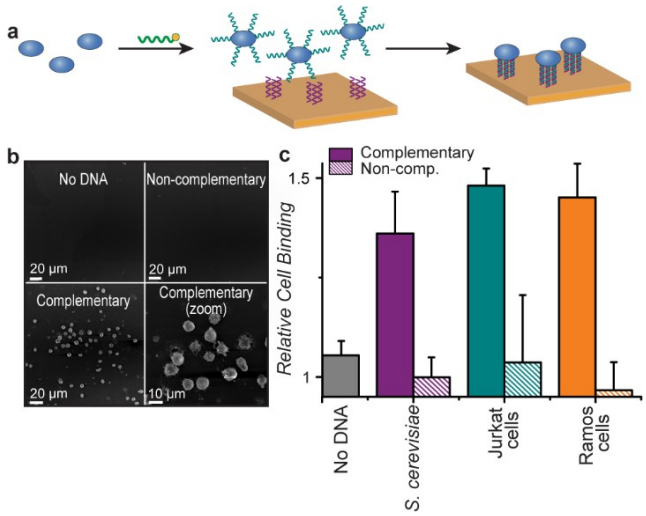

Figure 3.11. DNA-hybridization mediated cell adhesion to a substrate (a). Cells modified with DNA only adhered to surfaces covalently modified with a complementary DNA strand (b,c).

The cells were found to bind specifically to substrates modified with the proper complementary DNA strand. In the absence of DNA (on a catechol-modified electrode) or on an electrode modified with non-complementary DNA, minimal cell binding was observed by both SEM and fluorescence (Figures 3.11b and 3.11c).

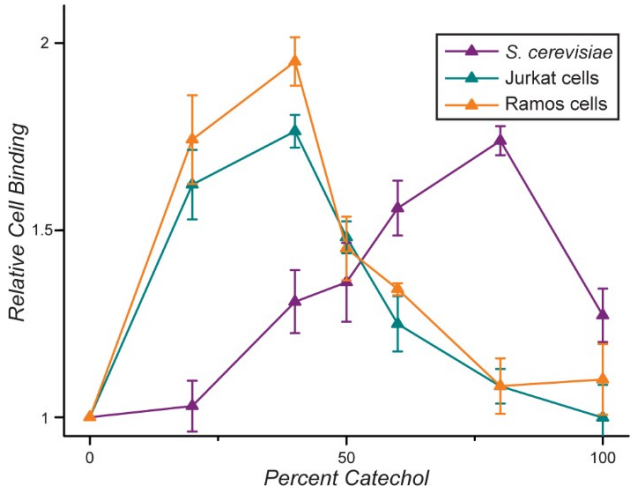

Figure 3.12. Different cell types bind preferentially to surfaces with differing coverages of DNA. *S. cerevisiae* prefers substrates with a higher coverage of DNA. Whereas, the larger Jurkat and Ramos cells prefer mixed monolayers with a lower coverage of DNA.

Interestingly, a correlation was observed between the type of cells applied to electrodes and the optimal DNA density on the surface for their adhesion (Figure 3.12). Both Jurkat and Ramos cells were found to bind optimally to electrodes with an underlying catechol concentration of ~40%. In contrast, *S. cerevisiae* were found to bind optimally to DNA surfaces with underlying catechol concentrations of ~80%.

Electrochemical patterning of DNA enables finer control of DNA coverage to optimize DNA coverage for specific cell types. Furthermore, electrochemical patterning enables rapid patterning of multiple different DNA sequences through the use of a multiplexer. Additionally, electrochemical patterning will enable the detection of interesting metabolites such as quorum sensing molecules like pyocyanin from *Pseudomonas aeurginosa* or even electrical current from a bacterium such as *Shewanella oneidensis*.

3.3.5. *Shewanella oneidensis MR-1* DNA patterning on electrochemical surfaces

To demonstrate one application of DNA patterning on electrodes, we patterned *S. oneidensis* on gold surfaces via our catechol-based patterning technique. *S. oneidensis* can transfer electrons to a solid substrate capable of receiving electrons such as an electrode, though this process typically takes several days to allow for the formation of a *S. oneidensis* biofilm on the electrode surface.[37] Using the DNA-hybridization based patterning approach we can form a dense monolayer of *S. oneidensis* on an electrode surface in several hours without the presence of a biofilm-like matrix (Figure 3.13). We patterned *S. oneidensis* on gold electrodes with a series of 20-mer DNA sequences containing no mismatches, one mismatch or multiple mismatches. Impedance data showed that despite the number of mismatches present, the number of patterned *S. oneidensis* on the electrode surface was largely unaffected (Figure 3.14).

However, the current transferred to the electrode varied considerably depending on the number of mismatches in the 20-mer DNA strand attached to the *S. oneidensis* cell surface, with the largest current corresponding to the well matched 20-mer DNA sequence that does not contain any mismatches (Figure 3.15). This result suggests that when DNA-hybridization is used to attach *S. oneidensis* to an electode, the hybridized DNA enables the transfer of electrons from *S. oneidensis* to the electrode. *S. oneidensis* normally uses its secreted biofilm matrix to assist electron transfer from *S. oneidensis* to electron acceptors outside the cell.[38] In this work, we have demonstrated that DNA patterning can be used to create an alternative means of electron transfer from *S. oneidensis*. DNA hybridization to electrode surfaces enables the study of electron transfer from *S. oneidensis* in a more controlled environment (dense monolayers without a biofilm matrix) and in a manner that is far quicker than is currently possible. Furthermere, this technique could be used in the design of small-scale microbial fuel cells.

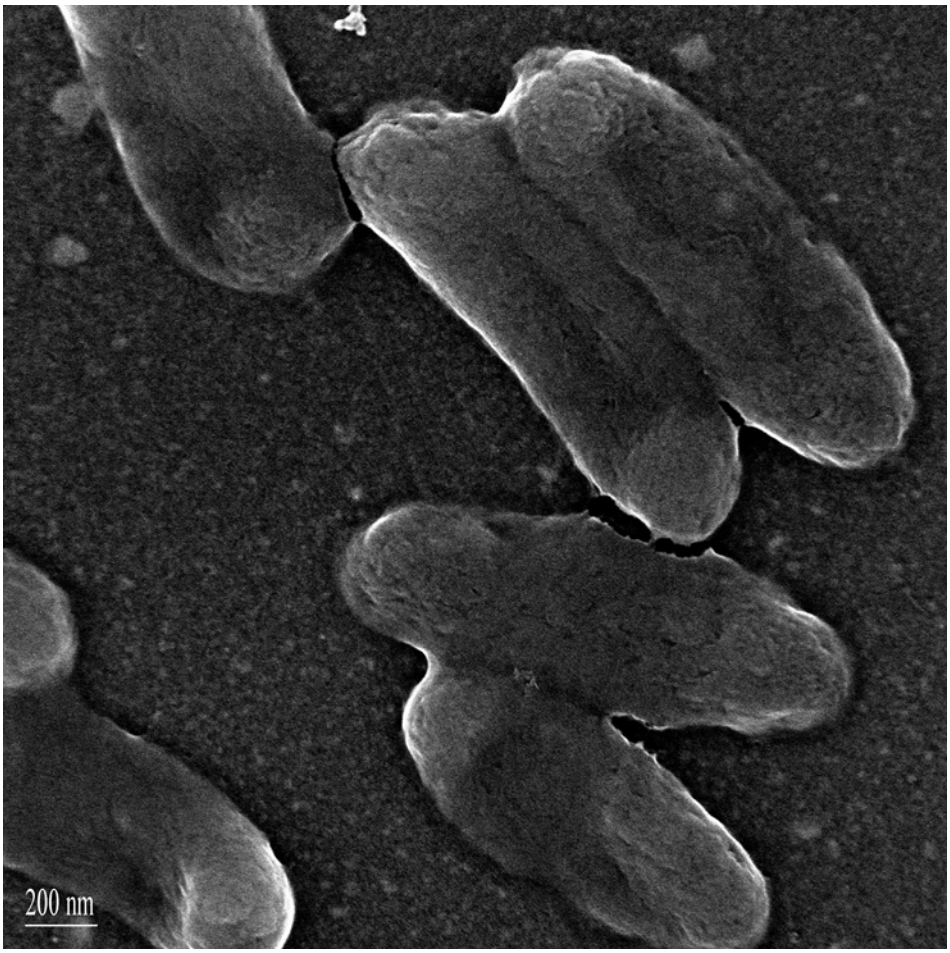

Figure 3.13. Patterned *Shewanella oneidensis* MR-1 imaged with SEM. *S. oneidensis* patterned on gold electrodes via DNA-hybridization do not show indications of a secreted biofilm as seen in the SEM images of *S. oneidensis* MR-1 by Roy et al.[39]

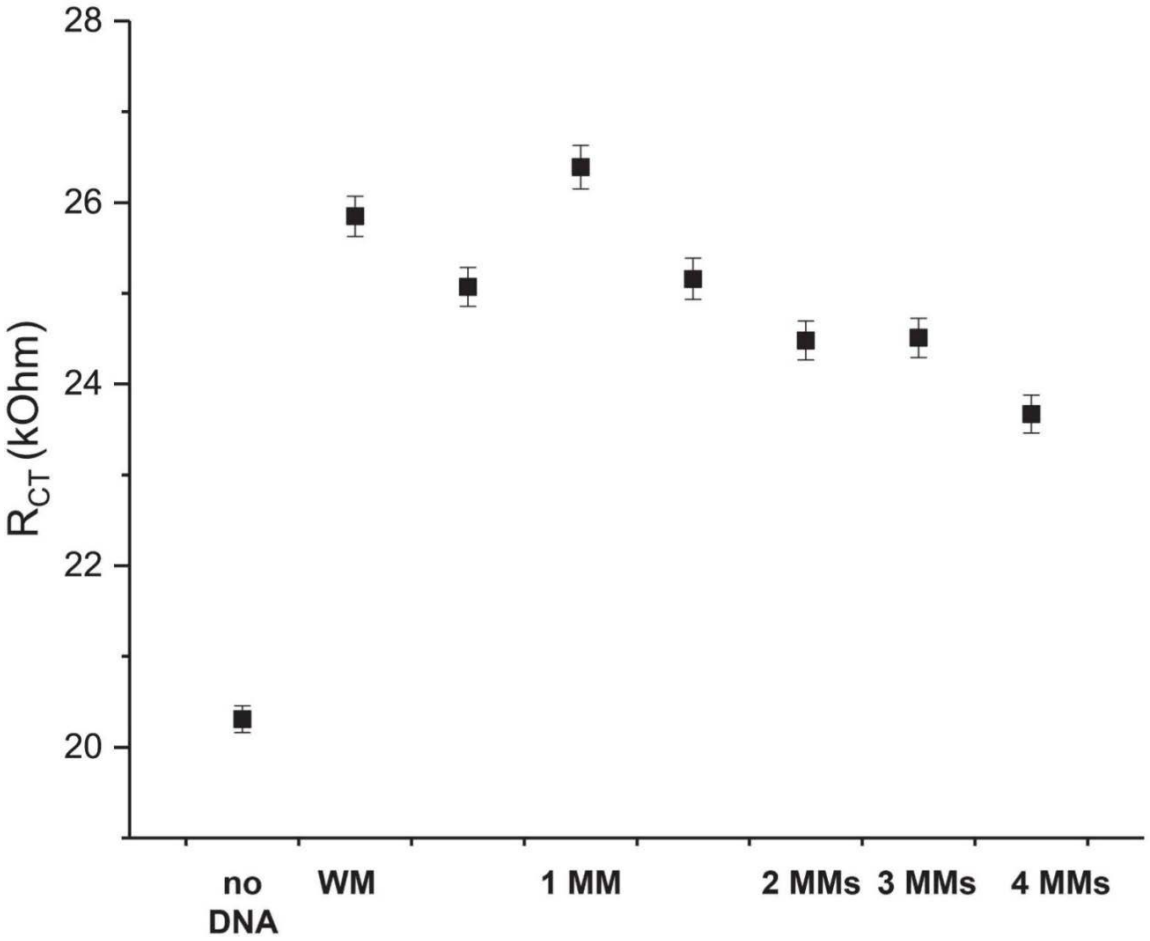

Figure 3.14. Impedance data of patterned *S. oneidensis*. *S. oneidensis* patterned with DNA containing no mismatches (WM) or multiple mismatches show similar impedance values, indicating a similar number of cells patterned onto the electrode surface. MM = DNA mismatch, WM = well-matched DNA

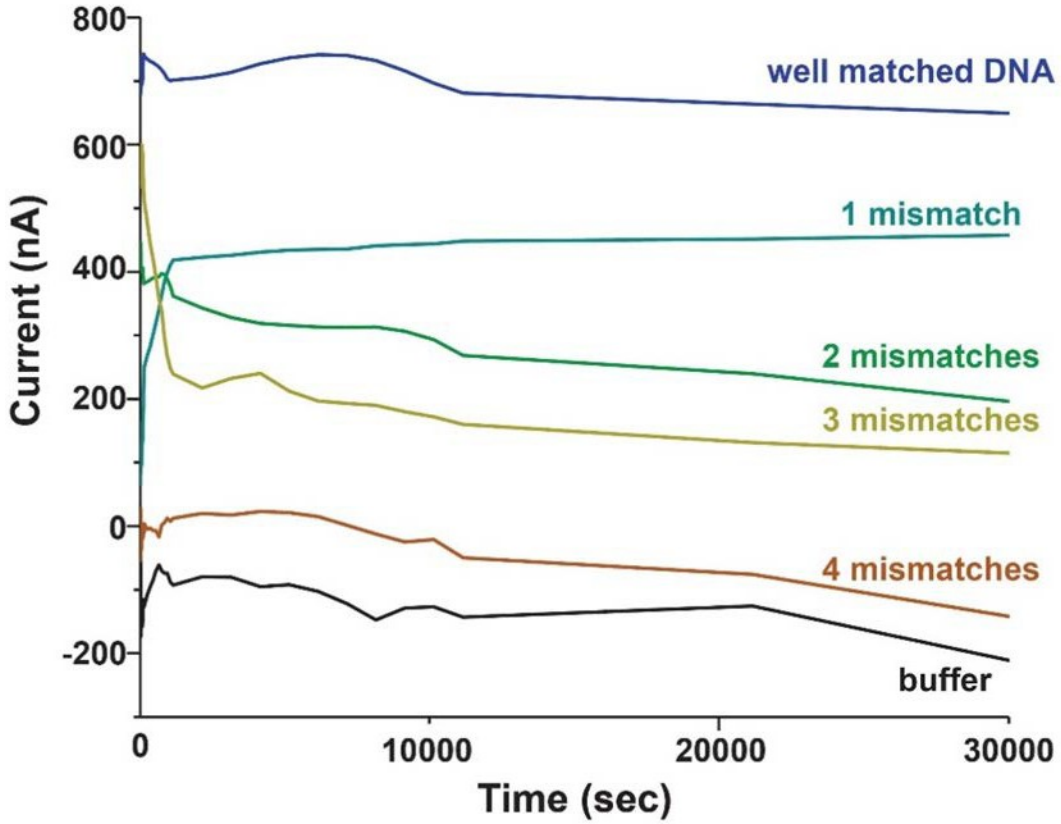

Figure 3.15. Current transferred from *S. oneidensis* DNA-hybridized to an electrode surface via well matched or mismatched DNA. Mismatched DNA results in a lower current being transferred to the electrode.

3.3.6. Enzyme-activated oxidative coupling

An enzyme-activated oxidative coupling reaction could open up new applications for the oxidative coupling reaction, specifically in the selective labeling of a specific cell type in an environment containing many different species. The proposed enzyme-activated oxidative coupling reactions were tested on aniline-modified MS2 capsids (Figure 3.16) and verified via mass spectrometry.

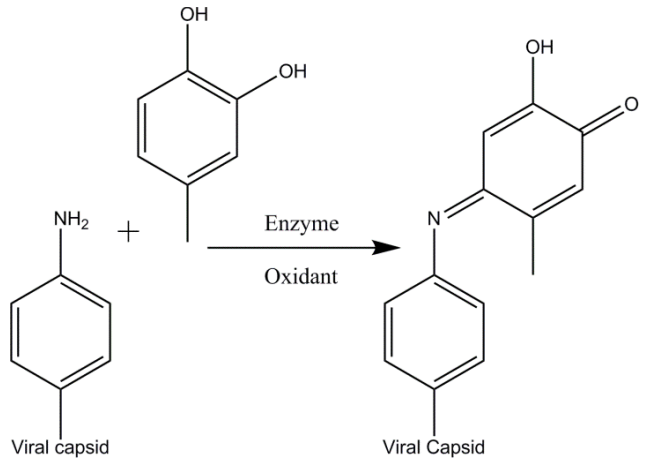

Figure 3.16. The enzyme activated oxidative coupling reaction was tested on aniline-modified MS2 (unnatural amino acid) labeled with 4-methylcatechol.

Mechanistically, horseradish peroxidase seemed an ideal choice to catalyze the oxidative coupling reaciton as it works via a series of 1 electron transfers from an iron metal center. This seemed similar to the use of multiple equivalents of potassium ferricyanide to activate the oxidative coupling reaction. Horseradish peroxidase in the presence of hydrogen peroxide results in complete modification of the MS2 capsid in under 10 min (Figure 3.17). Tyrosinase, another enzyme of interest due to its ability to form catechol substrates, results in multiple modifications (Figure 3.18).

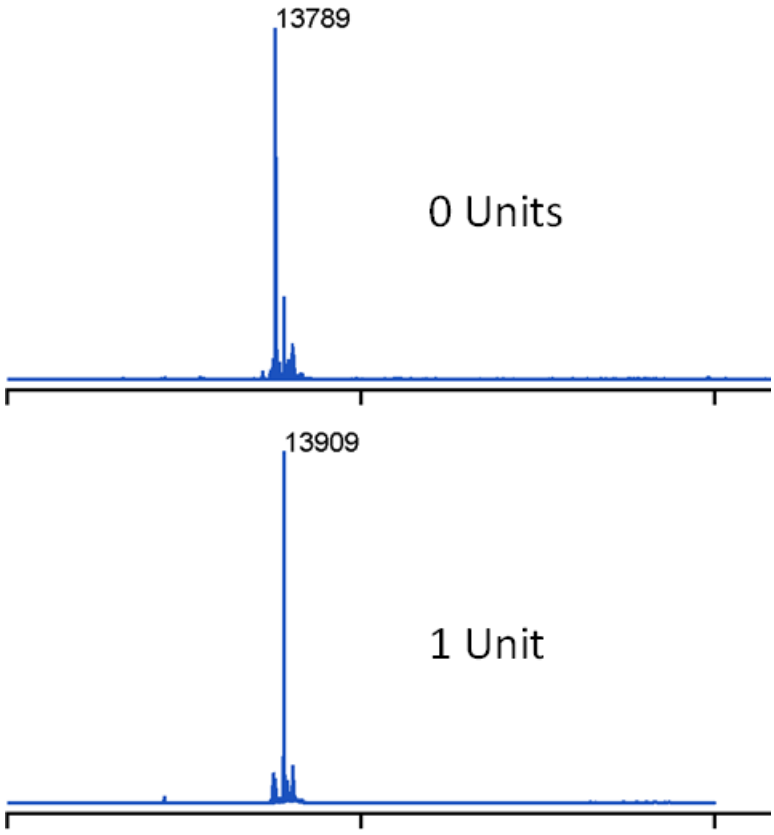

Figure 3.17. Horseradish peroxidase is a promising candidate for catalyzing the oxidative coupling reaction. The reaction was attempted on aniline-modified MS2 viral capsids. Conditions: RT, horseradish peroxidase, 10 min, 1 mM H_2O_2, 20 µM MS2, 40 µM 4-methylcatechol, 50 mM phosphate (pH=6.5). Expected mass: 13909 Da

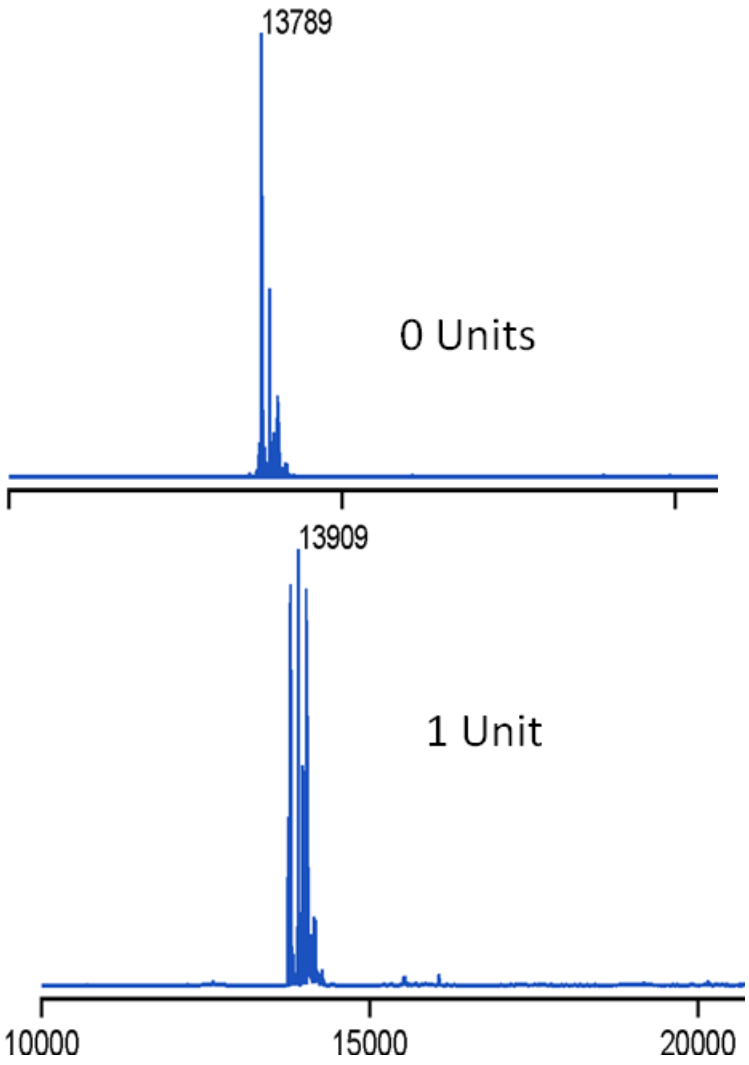

Figure 3.18. Tyrosinase is an oxidative enzyme that is a promising target for enzymatically activating the oxidative coupling reaction. The reaction was attempted on aniline-modified MS2 viral capsids. There is an additionally peak (unlabeled above) at 14029 Da corresponding to a second addition of 4-methylcatechol, possibly to surface tyrosine residues. Conditions: RT, tyrosinase, 10 min, 20 µM MS2, 40 µM 4-mehtylcatechol, 50 mM phosphate (pH=6.5) Expected mass: 13909 Da

Future work will focus on using this work to specifically modify one cell type in a complicated matrix containing many different cell types via, for example, expressing an enzyme on the cell surface of the protein to be labeled.

3.4. Conclusion

The variety of emerging and well-established mass spectrometry, microscopy and genetic techniques that can be used to study patterned microbial cells will enable increasingly complex questions to be asked about biofilm formation, bacterial pathogenesis, the diversity of

the secreted metabolome, and the application of bacterial immobilization for the production of useful products through cocultures. With the development of easier-to-use chemical patterning methods, DNA-hybridization based cell patterning strategies will play an increasing role in elucidating the effects of cell ratio and cell-cell contacts in the behavior of multi-species microbial communities.

3.5. References

(1) Furst, A. L.; Smith, M. J.; Francis, M. B. *J. Am. Chem. Soc.* **2017**, jacs. 7b06385.

(2) Obermeyer, A. C.; Jarman, J. B.; Netirojjanakul, C.; El Muslemany, K.; Francis, M. B. *Angew. Chemie Int. Ed.* **2014**, *53* (4), 1057.

(3) Obermeyer, A. C.; Jarman, J. B.; Francis, M. B. *J. Am. Chem. Soc.* **2014**, *136* (27), 9572.

(4) Behrens, C. R.; Hooker, J. M.; Obermeyer, A. C.; Romanini, D. W.; Katz, E. M.; Francis, M. B. *J. Am. Chem. Soc.* **2011**, *133* (41), 16398.

(5) ElSohly, A. M.; MacDonald, J. I.; Hentzen, N. B.; Aanei, I. L.; El Muslemany, K. M.; Francis, M. B. *J. Am. Chem. Soc.* **2017**, *139* (10), 3767.

(6) El Muslemany, K. M.; Twite, A. A.; ElSohly, A. M.; Obermeyer, A. C.; Mathies, R. A.; Francis, M. B. *J. Am. Chem. Soc.* **2014**, *136* (36), 12600.

(7) Mirkin, C. A.; Letsinger, R. L.; Mucic, R. C.; Storhoff, J. J. *Nature* **1996**, *382* (6592), 607.

(8) Gartner, Z. J.; Liu, D. R. *J. Am. Chem. Soc.* **2001**, *123* (28), 6961.

(9) Twite, A. A.; Hsiao, S. C.; Onoe, H.; Mathies, R. A.; Francis, M. B. *Adv. Mater.* **2012**, *24* (18), 2380.

(10) Hsiao, S. C.; Shum, B. J.; Onoe, H.; Douglas, E. S.; Gartner, Z. J.; Mathies, R. A.; Bertozzi, C. R.; Francis, M. B. *Langmuir* **2009**, *25* (12), 6985.

(11) Chen, S.; Bremer, A. W.; Scheideler, O. J.; Na, Y. S.; Todhunter, M. E.; Hsiao, S.; Bomdica, P. R.; Maharbiz, M. M.; Gartner, Z. J.; Schaffer, D. V. *Nat. Commun.* **2016**, *7*, 10309.

(12) Gartner, Z. J.; Bertozzi, C. R. *Proc. Natl. Acad. Sci. U. S. A.* **2009**, *106* (12), 4606.

(13) Liu, J. S.; Farlow, J. T.; Paulson, A. K.; Labarge, M. A.; Gartner, Z. J. *Cell Rep.* **2012**, *2* (5), 1461.

(14) Dwidar, M.; Leung, B. M.; Yaguchi, T.; Takayama, S.; Mitchell, R. J. *PLoS One* **2013**, *8* (6), e67165.

(15) Connell, J. L.; Ritschdorff, E. T.; Whiteley, M.; Shear, J. B. *Proc. Natl. Acad. Sci. U. S. A.* **2013**, *110* (46), 18380.

(16) Connell, J. L.; Kim, J.; Shear, J. B.; Bard, A. J.; Whiteley, M. *Proc. Natl. Acad. Sci. U. S. A.* **2014**, *111* (51), 18255.

(17) Schaffner, M.; Rühs, P. A.; Coulter, F.; Kilcher, S.; Studart, A. R. *Sci. Adv.* **2017**, *3* (12), eaao6804.

(18) Kim, H. J.; Boedicker, J. Q.; Choi, J. W.; Ismagilov, R. F. *Proc. Natl. Acad. Sci. U. S. A.* **2008**, *105* (47), 18188.

(19) Traxler, M. F.; Watrous, J. D.; Alexandrov, T.; Dorrestein, P. C.; Kolter, R. *MBio* **2013**, *4*(4), e00459.

(20) Hom, E. F. Y.; Murray, A. W. *Science* **2014**, *345* (6192), 94.

(21) Burmølle, M.; Ren, D.; Bjarnsholt, T.; Sørensen, S. J. *Trends Microbiol.* **2014**, *22* (2), 84.

(22) Smith, M. J.; Francis, M. B. *ACS Synth. Biol.* **2016**, *5* (9), 955.

(23) Christensen, B. B.; Haagensen, J. A. J.; Heydorn, A.; Molin, S. *Appl. Environ. Microbiol.* **2002**, *68* (5), 2495.

(24) Haagensen, J. A. J.; Hansen, S. K.; Christensen, B. B.; Pamp, S. J.; Molin, S. *Appl. Environ. Microbiol.* **2015**, *81* (18), 6120.

(25) Zhiyong Suo, †; Recep Avci, *,†; Xinghong Yang, ‡ and; Pascual‡, D. W. **2008**.

(26) Choi, W. S.; Kim, M.; Park, S.; Lee, S. K.; Kim, T. *Biomaterials* **2012**, *33* (2), 624.

(27) Velema, W. A.; van der Berg, J. P.; Szymanski, W.; Driessen, A. J. M.; Feringa, B. L. *Org. Biomol. Chem.* **2015**, *13* (6), 1639.

(28) Twite, A. A.; Hsiao, S. C.; Onoe, H.; Mathies, R. A.; Francis, M. B. *Adv. Mater.* **2012**, *24*(18), 2380.

(29) Furst, A. L.; Hill, M. G.; Barton, J. K. *Langmuir* **2013**, *29* (52), 16141.

(30) Drummond, T. G.; Hill, M. G.; Barton, J. K. *Nat. Biotechnol.* **2003**, *21* (10), 1192.

(31) Soleymani, L.; Fang, Z.; Sargent, E. H.; Kelley, S. O. *Nat. Nanotechnol.* **2009**, *4* (12), 844.

(32) Myers, B. D.; Lin, Q.-Y.; Wu, H.; Luijten, E.; Mirkin, C. A.; Dravid, V. P. *ACS Nano* **2016**, *10* (6), 5679.

(33) Collman, J. P.; Devaraj, N. K.; Chidsey, C. E. D. *Langmuir* **2004**, *20* (4), 1051.

(34) Devaraj, N. K.; Miller, G. P.; Ebina, W.; Kakaradov, B.; Collman, J. P.; Kool, E. T.; Chidsey, C. E. D. *J. Am. Chem. Soc.* **2005**, *127* (24), 8600.

(35) Capehart, S. L.; ElSohly, A. M.; Obermeyer, A. C.; Francis, M. B. *Bioconjug. Chem.* **2014**, *25* (10), 1888.

(36) Hinterwirth, H.; Kappel, S.; Waitz, T.; Prohaska, T.; Lindner, W.; Lämmerhofer, M. *ACS Nano* **2013**, *7* (2), 1129.

(37) Baron, D.; LaBelle, E.; Coursolle, D.; Gralnick, J. A.; Bond, D. R. *J. Biol. Chem.* **2009**, *284* (42), 28865.

(38) Marsili, E.; Baron, D. B.; Shikhare, I. D.; Coursolle, D.; Gralnick, J. A.; Bond, D. R. *Proc. Natl. Acad. Sci. U. S. A.* **2008**, *105* (10), 3968.

(39) Roy, J. N.; Luckarift, H. R.; Lau, C.; Falase, A.; Garcia, K. E.; Ista, L. K.; Chellamuthu, P.; Ramasamy, R. P.; Gadhamshetty, V.; Wanger, G.; Gorby, Y. A.; Nealson, K. H.; Bretschger, O.; Johnson, G. R.; Atanassov, P. *RSC Adv.* **2012**, *2* (26), 10020.